Russian Chemical Reviews **66** (9) 733 – 762 (1997) © 1997 Russian Academy of Sciences and Turpion Ltd

UDC 536.7:541.45

Computer simulation of the structure and properties of non-crystalline oxides

D K Belashchenko

Contents

I.	Introduction	733
II.	Construction of models of oxide systems	733
III.	Main structural characteristics of non-crystalline systems	735
IV.	Models of simple non-crystalline oxides	736
V.	Simulation of homologous series of non-crystalline oxides	743
VI.	Simulation of binary non-crystalline oxide systems	749
VII.	Simulation of multi-component systems	759
VIII.	Simulation of ion transfer processes	760
IX.	Conclusion	760

Abstract. The results of the studies of the structure and properties of non-crystalline (liquid and amorphous) oxide systems obtained using computer simulation methods are summarised. The models of simple oxides, homologous series of non-crystalline oxides and of binary and multi-component oxide systems are considered. The results of the simulation of the ion transfer are discussed. The ionic theory of oxides allows one to predict adequately the structural and thermodynamic properties of oxide systems except for the phosphate oxides and some other systems. The bibliography includes 222 references.

I. Introduction

Studies of the structure and properties of non-crystalline (liquid and amorphous) oxide systems obtained by powerful computer simulation methods, such as molecular dynamic (MD), static relaxation (SR), Monte Carlo (MC), and Reverse Monte Carlo are reviewed in this paper. General aspects of computer simulation have been discussed in detail in a number of reviews (see, for example, Refs 1 – 8) and will not be considered here. We confine ourselves to the analysis of specific applications of the above-mentioned methods to oxide systems.

The results of numerous experimental studies of oxide systems indicate a substantial contribution of ionic bonding to interatomic interactions. This is caused by the high electronegativity of the oxygen atoms. Nevertheless, the account of a covalent component is important in the simulation of structure and properties of the oxides. The covalent interaction is described in terms of three-particle potentials, which significantly increases the computational time required. Since ionic contribution cannot be neglected for oxide systems, the Coulomb interactions have to be considered as well. Construction of a model for an oxide with mixed ion and covalent bonding requires too many force parameters that are extremely difficult to calculate *ab initio*. Therefore, the models have to be simplified. The choice of a model based only on the ionic interactions has significant advantages. Any doubts in the applicability of the ionic scheme were eliminated in a study, in which a purely ionic model of non-crystalline SiO_2 (charge of ions $4+$ and $2-$) was successfully built.[9] The structure and energy of the oxide within this model were in good agreement with the experimental data.

Recently, the ionic model of non-crystalline oxides has found broad applications. Simulation of the properties of many simple and complex oxides as well as of related systems (in particular, oxyfluorides) has been performed. The aim of the present review is to discuss and analyse the results obtained in these studies.

D K Belashchenko Moscow State Institute of Steel and Alloys (Technological University), Leninskii prosp. 4, 117936 Moscow, Russian Federation. Fax (7-095) 237 80 07, Tel. (7-095) 230 46 67
E-mail dkbel@misa.ac.ru

Received 12 March 1996
Uspekhi Khimii **66** (9) 811 – 844 (1997); translated by Ya Zubavichus

II. Construction of models of oxide systems

1. Interparticle potentials in oxides

The applicability of the ionic theory for the construction of models of oxide systems is determined by a significant difference in the electronegativities of oxygen (3.5 according to Pauling) and the majority of metals (0.9 for Na, 1.0 for Ca, 1.5 for Al, *etc.*). For example, in CaO the difference in the electronegativities is ~ 2.5 and the ionicity of Ca – O bond is close to 76%. For SiO_2, the ionicity is $\sim 51\%$. Somewhat simplifying the situation, one may therefore assign a formal charge of $-2e$ (where e is the electronic charge) to oxygen atoms, and $+2e$, $+3e$, $+4e$ to Ca, Al, and Si, respectively. In the case of an ionic bond, the interparticle potential is paired, and it is usually written in the form of the Born – Meyer potential or the Pauling potential (see, for example, Ref. 10). The Born – Meyer potential is written as:

$$u_{ij}(r) = Z_i Z_j \frac{e^2}{r} + B_{ij} \exp\left(-\frac{r}{R_{ij}}\right) - \frac{C_{ij}}{r^6} - \frac{D_{ij}}{r^8}, \qquad (1)$$

where r is a distance between the centres of ions i and j, Z_i, Z_j are the charges of ith and jth ions, respectively (expressed in elementary charge units e), B_{ij} and R_{ij} are parameters accounting for the repulsion of the ionic shells, C_{ij} and D_{ij} are parameters accounting for the dipole-dipole and dipole-quadrupole interactions, respectively. A special form of the potential (1) is the Born – Meyer – Higgins potential (BMH)[10] in which B_{ij} and R_{ij} are expressed through the ion radii r_i and r_j:

$$B_{ij} = b\left(1 + \frac{Z_i}{n_i} + \frac{Z_j}{n_j}\right) \exp\left(\frac{r_i + r_j}{R_{ij}}\right), \qquad (2)$$

where $b = 0.211$ eV, n_i and n_j are numbers of electrons in the outer filled electron shells of the ith and jth ions, respectively (2 for Li, 8 for O, *etc.*). One of the important properties of the potential (1) is that it decreases at small distances for oppositely charged ion pairs. When $r \to 0$, the second term in the expression (2) approaches B_{ij} and the first term approaches $-\infty$. These potentials should be applied with care to prevent a probable collapse of the system (unlimited approach of ions) in the simulations. It was shown[11] that the collapse can occur when B_{ij} is less than a certain critical value ($B_{ij} < B_{ij}^{cr}$). This critical value for a M_mO_n oxide is defined by formula

$$B_{ij}^{cr} = -\frac{Z_i Z_j e^2}{0.5413 R_{ij}}. \quad (3)$$

Usually it is assumed that $R_{ij} = 29$ pm.[9]

However, the collapse may occur even for $B_{ij} > B_{ij}^{cr}$ in the simulations of strongly compressed systems, if the distance between oppositely charged ions becomes less than r_*, which is the position of the maximum of the potential (1) defined as

$$r_*^2 \exp\left(-\frac{r_*}{R_{ij}}\right) = -Z_i Z_j e^2 \frac{R_{ij}}{B_{ij}}. \quad (4)$$

The Pauling potential is written as:

$$u_{ij}(r) = \frac{Z_i Z_j e^2}{r} + \frac{B_{ij}}{r^n} - \frac{C_{ij}}{r^6} - \frac{D_{ij}}{r^8}. \quad (5)$$

Here n is a parameter ranging, as a rule, from 8 to 10. The Pauling potential approaches infinity when $r \to 0$, and hence collapse is impossible.

The values of the BMH and Pauling potentials for systems close to oxides (alkali metal halides) were first determined by Fumi and Tosi.[10,12] The refinement of these parameters was performed according to the known experimental characteristics of the crystalline compounds, such as density, compressibility, and the energy of the system. The precision of the simulations with the BMH potential appeared to be higher than with the Pauling potential. Generally the terms that take into account the dipole-dipole and dipole-quadrupole interactions play a minor role in (1). For instance, the total energy for liquid KCl at 1045 K is -730.2 kJ mol^{-1}, and the contributions of the corresponding interactions are -26.5 kJ mol^{-1} and -4.1 kJ mol^{-1} (see Ref. 13). In oxide systems, these terms are even less important and therefore they are often neglected.

The parameters of the Born–Meyer potentials for crystalline MO oxides (M = Mg, Ca, Sr, Ba) were calculated from the values of cell parameters and dielectric constants.[14] Pair potentials for these oxides and for SiO_2, UO_2, TiO_2, Nb_2O_5, and silicates were considered.[15] The parameters of the interactions in M–O pairs (M = Mn, Fe, Co, and Ni) were also estimated.[16]

Despite their simplicity, the potentials (1) or analogous potentials with the additional terms of the Morse type may be used for a description of crystal structures of quartz, cristobalite, boron oxide, as well as the structures of liquid oxides in systems like $Na_2O-B_2O_3$ and $CaAlSi_2O_8$ (anorthite).[17]

If the simulation does not require calculations of the energy of the system and related characteristics, then the knowledge of the force functions $F(r) = -du/dr$ is sufficient. In a series of studies (see, for example, Ref. 18) Pauling type force functions were applied:

$$F_{ij}(r) = \frac{Z_i Z_j e^2}{r^2}\left[1 + \mathrm{sgn}(Z_i Z_j)\left(\frac{r_i + r_j}{r}\right)^n\right], \quad (6)$$

here the sgn is equal to $+1$ or -1 depending on the sign of the argument (Z_iZ_j) and the parameter n varies in the range from 8 to 10.

More complicated pair potentials similar to the Born–Meyer potentials were proposed for silica.[19] Potential parameters were adjusted to give agreement with the experimental data on the stability of α-quartz, α-cristobalite, coesite, and stishovite crystals.

The interaction potentials for M–O pairs (M = Ca, B, Al, Si, V) were calculated[20] using the 'magic' Mulliken formula,[21] which takes into account the mixed ion-covalent character of bonding. The calculated dependences of the potentials on r were approximated by the Pauling expression:

$$U_{ij}(r) = \frac{Z_i Z_j e^2}{r}\left[1 + \mathrm{sgn}(Z_i Z_j)\left(\frac{r_i + r_j}{r}\right)^n (n+1)^{-1}\right]. \quad (7)$$

For all oxides n was taken to be equal to 10. The calculated formal charges did not agree with the normal oxidation states of the metals:

Oxide	Z_1	Z_2	r_1/pm	r_2/pm
CaO	1.46	−1.46	102.0	133.0
B_2O_3	2.34	−1.56	10.0	140.0
Al_2O_3	2.55	−1.70	42.5	140.0
SiO_2	2.30	−1.15	30.1	120.4
V_2O_5	3.65	−1.46	40.1	133.0

where 1 refers to M and 2 refers to O.

The optimisation of Z_i and r_i according to results of quantum-chemical calculations of ternary systems including Ca, B, Al, Si, V, and O was also performed.[20] In particular, the values of $Z_O = -1.46$, $Z_{Si} = 2.92$, and $Z_V = 3.65$ were obtained. Further, the MNDO quantum-chemical method was applied for calculation of ion-covalent pairwise and three-particle interaction profiles in oxides of silicon, aluminium, phosphorus, *etc.*[22–26] In a number of other studies, the selection of effective ion charges smaller than the standard oxidation state also allowed one to obtain reasonable agreement between the calculated and experimental structural data for non-crystalline oxides in the framework of the pair interaction model, which indirectly takes into account the mixed ion-covalent character of bonding. However, the use of this model of the interpretation of 'intermediate' bonding may prevent calculations of the thermodynamic properties.

The Born–Meyer potentials were used in a simulation of the structure and properties of $LiNbO_3$ and $KNbO_3$ (see Ref. 27). For all ion pairs it was taken that $B_{ij} = 1822$ eV and $R_{ij} = (r_i + r_j)/12.36$. Ionic charges and radii were adjusted to give the best agreement with the experimental phonon spectra. For oxygen atoms in $KNbO_3$, it was necessary to take two r_i values in two different sites in the unit cell. The formal charges Z_O strongly deviate from the common value of -2. For $Li_2O-B_2O_3$ system, the BMH-type pair potentials were used. Ionic radii were chosen equal to 93 (Li^+), 74 (B^{3+}), and 142 pm (O^{2-}); the charges were equal to 1, 3, and -2, respectively.[28]

Interparticle interactions in the covalent bonding model are usually described on the basis of three-particle potentials. The energy of the system is written as

$$U = U_0 + C_2 \sum_i \sum_j \mathrm{u}(r_i, r_j) + C_3 \sum_i \sum_j \sum_k \mathrm{v}(r_i, r_j, r_k), \quad (8)$$

where U_0 is the energy of the ideal crystal,† C_2 and C_3 are coefficients, $\mathrm{u}(r_i,r_j)$ and $\mathrm{v}(r_i,r_j,r_k)$ are bond stretch and angle distortion terms, respectively. The C_2 and C_3 coefficients were chosen to give the best agreement of the simulated and the experimental characteristics of the oxide (vibrational spectra and internuclear distances). The simplest form for $\mathrm{u}(r_i,r_j)$ and $\mathrm{v}(r_i,r_j,r_k)$ functions was suggested by Keating,[29] *viz.*,

$$\mathrm{u}(r_1,r_2) = |\mathbf{r}_1 - \mathbf{r}_2|^2 - d_0^2,$$

where $\mathbf{r}_1$ and $\mathbf{r}_2$ are the radii-vectors of neighbouring ions, and d_0 is the equilibrium bond length, and

† The ideal crystal means the crystal with the equilibrium values for all bond lengths and angles; the equilibrium bond angle depends on the type of the crystal lattice.

$$v(r_i,r_j,r_k) = [\cos\theta(ijk) - \cos\theta_0(ijk)]^2 , \quad (9)$$

where $\theta(ijk)$ is the angle between $i-j$ and $j-k$ bonds, and $\theta_0(ijk)$ is the corresponding equilibrium angle. The summation in (8) is over the nearest neighbours of the central particle. The three-particle potential is especially often used for silicon (see, for example, Ref. 30). In ionic bonding model, the choice of the initial state for a model is of little importance (it could be either a crystal lattice or a random ionic system), but in the 'covalent version', special initial state should be chosen with fixed coordination numbers (for instance, 4 for Si and 2 for O). This selection of the initial state is usually required in simulation of loose systems by the Reverse Monte Carlo method.

For silica [31] the pairwise Mie potential was used.[32]

$$u = a r^{-n} - b r^{-m} ,$$

where $10 \leqslant n \leqslant 12$ and $4 \leqslant m \leqslant 6$; and for a three-particle contribution, the Axilrod–Teller potential was applied, which describes the interaction of three dipoles:[33]

$$v = c(3\cos\alpha \cos\beta \cos\gamma + 1)(r_1 r_2 r_3)^{-3},$$

where r_1, r_2, r_3 are the sides of a triangle formed by dipoles, α, β, γ are its angles, and c is a fitting parameter. The coefficients for low- and high-temperature modifications of cristobalite and quartz were adjusted according to the experimental data for SiO_2. For the Si–Si pairs, the data for pure Si were used and the $u(r)$ potential was chosen in the Lennard–Jones form. A model of pure silicon, which is stable in the diamond lattice, was obtained as a result. For the O–O pairs, the properties of O_2 and O_3 molecules (Lennard–Jones potential) were used. Within this scheme, the dissociation energy of oxygen molecule obtained was in agreement with the experimental data, but the stable configuration for O_3 appeared to be linear rather than triangular. For the Si–O pairs, the Lennard–Jones potential was also used. Other parameters of the model were refined to achieve agreement between the calculated and the experimental results for the properties of the crystalline silica. *Ab initio* potentials were used [34] to describe the lattice parameters and melting points of the MgO, Mg_2SiO_4, and $MgSiO_3$ oxides.

In a number of studies, combined potentials were used that take into account both ionic and covalent contributions in oxides. A combination of the Keating potential (9) for the triatomic combination that included Si and O, and the Lennard-Jones potential for Na–Si and Na–O pairs were used to simulate Na_2O-SiO_2 glasses.[35] A similar approach was utilised to simulate glasses of the $Na_2O-B_2O_3$ type (see Ref. 36). For O–B–O and O–B–B triatomic combinations, the three-particle potential was selected, and for pairs including Na atoms the pairwise Born–Meyer potential (1) was chosen.

Data discussed above show that the choice of the interparticle potential is arbitrary to some extent. After this choice, the values of parameters of the potential can be determined quite accurately from the properties of a crystal or liquid. The more complicated the form of the potential, the more difficult the determination procedure of its parameters and the more specific the potential itself.

2. Specific features of model construction for oxides

If a bulk phase rather than a small cluster is under consideration, the models are placed in the basic cube with periodic boundary conditions, the calculations of the Coulomb terms of the energy and interaction forces is to be done by summing according to Ewald, taking into account all particle pairs in the cube (see, for example, Refs 6, 13, 37, and 38). The procedure of Ewald summation gives high accuracy, but it is time consuming. Thus, some approximations were proposed which described not only spherically symmetrical terms, but also cubic symmetry corrections. For example, the Hansen approximation [39] represents the interaction energy in the form of exponential-polynomial series giving an error of about 0.1%. Attempts to restrict the Ewald sums by spherically symmetrical part of the potential generally lead to substantial losses in accuracy,[40,41] though to more rapid calculations.

For construction of models at temperatures $T > 0$, MD and MC methods are used. Models of amorphous phases at $T = 0$ K can be adequately built with the algorithm of Continuous Static Relaxation (CSR).[42] In this algorithm, the particles are shifted along the overall force by a certain value on each step. The magnitude of the shift is chosen so as to provide an efficient system relaxation. Initial shift may be large (for instance, 50 pm), but as the equilibrium state is approached it gradually decreases to $\sim 0.1-1$ pm. The shift should be decreased in the case when the monotonic decrease in the potential energy of the system ceases. The CSR method has the same disadvantages as MD: it does not guarantee that the global energy minimum is reached, however at low temperatures it allows one to reach substantially more stable states than the MD method.[42]

III. Main structural characteristics of non-crystalline systems

The main structural characteristics of non-crystalline multicomponent systems are partial pair correlation functions (PPCF) $g_{ij}(r)$, which give the probability of occurrence of a pair of i and j particles at a distance r. They are normalised to give $g_{ij}(r) \to 1$ when $r \to \infty$. These functions are directly calculated in MD and CSR methods. The distribution of azimuthal θ(BAC) angles for B–A–C three-atomic systems in which B and C atoms are the closest neighbours of the central A atom can be also calculated. These distributions are especially informative for loose systems with chain or network structures. Construction of Voronoi polyhedra[43,44] for loose systems is of little interest due to their high diversity; none of the polyhedra type is more abundant in these systems.

Analysis of polymerisation processes is performed by building up bound groups, which allows one to reveal complex ions such as SiO_4^{4-}, $Si_2O_7^{6-}$, *etc.*, which are formed in silicates as time-stable moieties. In the search for the bound groups, the Si–O distance (r_c) should be defined. This distance determines the closest neighbours of the central particle and usually coincides with the first minimum position of the corresponding PPCF. The cyclic part of the structure can be found and the distribution of rings along the overall structure can be calculated in a similar way. The cycle included only neighbouring particles at distances not longer than r_c.

Topological looseness of a system can be characterised by two parameters, *viz.*, ρ_1 and s.[45] The parameter ρ_1 is defined as the mean height of the first peaks in the PPCF.

$$\rho_1 = \frac{\sum X_i X_j r_1(ij)}{d_0} , \quad (10)$$

where X_i and X_j are the ionic parts for the ith and jth particles, respectively, $r_1(ij)$ is the position of the first maximum in the PPCF of the ij pairs, summation is done over all pairs of particles, and $d_0 = (V/N)^{1/3}$, N is a number of particles in the volume V. Topologically dense systems (simple liquids, liquid and amorphous metals, non-crystalline alkali metal halides, *etc.*) have $\rho_1 = 1.08 \pm 0.02$ and loose systems have $\rho_1 < 1.05$. For the loosest systems, such as amorphous carbon, the ρ_1 value is 0.608.[46]

The second parameter is defined by ratio $s = g_1/g_{1d}$, where g_1 is a mean value of the first maxima heights of the PPCF and g_{1d} is the corresponding value for a dense system calculated according to the widths of the first maxima of the PPCF.[45] Topologically dense systems have $s \approx 1$, while for loose systems $s > 1$.

There are a number of other physicochemical characteristics of the systems considered, which are often studied by computer simulations. They include self-diffusion coefficients of particles, viscosity, autocorrelation functions of velocities, flows, *etc.*, which allow calculations of vibrational spectra and their comparison with the experimental data on elastic and inelastic scattering of

radiation. Studies of this kind for oxide systems are relatively rare (see, for example, Refs 1–6).

The role of Coulomb interactions in the structure formation and its influence on some properties of non-crystalline ionic systems were investigated.[47,48] LiCl–KCl eutectics were analysed[47] with Coulomb interactions 'switched on' and 'switched off' (the BMH potentials were used). It was demonstrated that for a neutral system the positions of the first maxima of the PPCF for all pairs depend on the particle size and increase on going from Li to K. Taking account of the Coulomb interactions (for the same volume) results in a drop of pressure and a decrease in self-diffusion coefficients by a factor of 2–5 and an increase in lifetime of the first coordination spheres of Li and K by a factor of 1.5–3.

Gradual changes in the structure and the thermodynamic properties of a liquid on going from the ideal gas state to the ionic model state of an MO oxide were considered.[48] The density of a system corresponded to that of liquid MgO. Particle interactions were described by Eqn (1) with the variables $B_{ij} = B$ and $Z_1 = -Z_2 = Z$. The influence of these parameters on the shape of PPCF, coordination numbers (CN), topological characteristics, and thermodynamic properties was considered. It was established that the growth of B leads to a monotonic increase in the PPCF peak heights. If $B < 600$ eV and $Z = 0$, the structure of the liquid appeared to be loose ($\rho_1 < 1.01$). On going from the ideal gas state to an MO system with neutral particles at constant volume and temperature, the entropy decreased by $3.43Nk$ (where N is the number of particles in the model, k is the Boltzmann constant). On further transition to the ionic system with $Z = 2$, it decreases additionally by $1.76Nk$. Therefore, the Coulomb interactions give a somewhat smaller contribution to the entropy of a liquid than the repulsion of ionic shells.

IV. Models of simple non-crystalline oxides

M_2O and MO oxides do not form glasses on ordinary cooling of liquids. Diffraction studies (hereinafter, X-ray and neutron diffraction methods are meant) of these liquid oxides, to our knowledge, have not been performed. Oxides of M_2O_3 (B_2O_3, Al_2O_3), MO_2 (SiO_2, GeO_2), M_2O_5 (P_2O_5, Nb_2O_5, Ta_2O_5), and MO_3 (WO_3) types have been intensely studied by the methods mentioned. The number of studies of silica and boron oxide is especially large.

1. Models of silica

According to diffraction data,[49–51] liquid and amorphous SiO_2 have the structure of a tetrahedral network with the coordination number for Si–O pairs $z(\mathrm{Si-O}) = 4$. The structural element of the network is a nearly tetrahedral complex SiO_4^{4-}, the adjacent tetrahedra are attached to each other through the shared vertices so that oxygen atoms have coordination numbers $z(\mathrm{O-Si}) = 2$. The most serious defects in this structure are silicon atoms with coordination number $z(\mathrm{Si-O}) = 3$.[52]

The first ionic model of SiO_2 that used the Born–Meyer pair potentials was constructed in 1976.[9] The charges of Si and O were equal to 4 and −2, respectively. The model contained 162 ions in the basic cube with periodic boundary conditions. The MD method with Ewald's account for the Coulomb interaction was applied. The B_{ij} parameters of the potential (1) for Si–Si, Si–O, and O–O pairs were equal to 2055.4, 1729.5, and 906.5 eV, respectively. First, heating of the system up to 6000 K was simulated in order to accelerate the diffusion of particles. After relaxation, cooling of the system to 300 K was simulated. In this way, a model of glass-like silica was obtained. The PPCF for a model of SiO_2 obtained with similar potentials[53] are shown in Fig. 1. The position of the first peak for Si–O pairs is ∼162 pm, which is in accordance with the experimental data.[49–51] It is noteworthy, that the energy‡ of the model (−12 240 kJ mol^{-1} relative to ions at infinite distance) is very close to the real value (−13 300 kJ mol^{-1}). This means that the ionic model describes the real situation adequately.

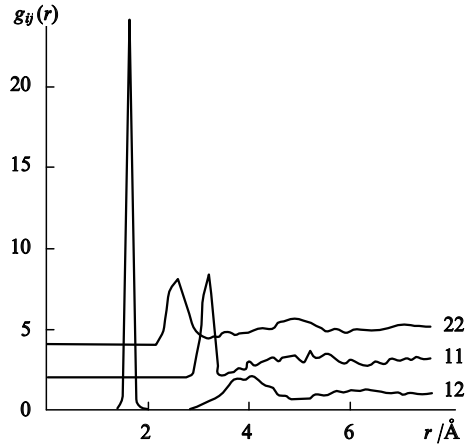


Figure 1. Partial pair correlation functions for the models of amorphous silica at 0 K (CSR method).
The curves are shifted along the ordinate axis; numbers denote pairs of ions (1 states for Si, 2 for O).

Ion models containing 375 and 3000 ions in the basic cube were constructed.[54,55] Simple force functions in the form (6) were applied. Values of $Z_1 = +2.272$ and $Z_2 = -1.136$ had to be chosen to achieve agreement with the diffraction data. First, relaxation of liquid SiO_2 at 3000–7000 K was simulated by the MD method. Subsequent cooling to ∼1500 K resulted in a glass-like state with the structure of a tetrahedral network. Model PPCF were in good agreement with the X-ray data on the peak positions. It was demonstrated that at 300 K the distribution of O–Si–O azimuthal angles has a maximum at 109.5±10° and that of Si–O–Si at 151±18°. The structure of SiO_2 is loose and contains cavities (pores) with a mean radius of 93 pm. Jumps in heat capacity, pressure, and self-diffusion coefficient observed for the model at ∼1500 K were attributed to a glass transition.

An autocorrelation function of velocities and, from this function, density of vibrational states, were calculated for amorphous silica.[55] However, no agreement with the experimental data on neutron scattering was achieved. It was found[56] that the Keating potential (9) matches best to a reconstruction of the vibrational spectrum. Good agreement with the experimental data was also obtained for a model with 750 particles.[57] The calculated vibrational spectra for Si^{4+} and O^{2-} ions[58] differ somewhat from the measured ones.

The statistics of pore distribution and the character of their aggregation into the bigger cavities ('trees') in amorphous silica were investigated on a model composed of 648 atoms.[59,60] Pore radii appeared to be in the range of 18–183 pm. A series of overlapping pores was considered to be a tree. It was demonstrated that the number of 'trees' decreases rapidly with the increase in a pore number (N) in a 'tree' ($N = 3$–20). The longest trees have approximately linear shape.

The presence of pores in the structure of silica plays an essential role. Ionic admixtures occupying these pores may enlarge their sizes and affect density fluctuation of the silicon-oxygen network. The appearance of a first sharp diffraction peak in structural factor of silica at magnitude of the scattering vector of $K \simeq 15$ nm^{-1} was explained by the presence of pores.[61] This assumption was examined[62] by the MD simulation of $(MO)_x(SiO_2)_{1-x}$ (M = Li, Na) solutions with $x = 0.18$–0.67. Each model contained 216 Si particles. Admixture atoms occupied the pores of the silicon-oxygen network. The intensity of the first sharp diffraction peak increased linearly as the Li atoms concentration increased and decreased on addition of sodium. This

‡ Hereinafter the following notations will be used in the discussion: E, E_{coul}, E_{kin}, E_{sh}, which stand for the total, Coulomb, and kinetic (thermal) energies and energy of repulsion of electron shells, respectively.

behaviour is due to the ratio of neutron scattering lengths on pores and impurity atoms.

A model of amorphous SiO_2 (246 ions) was also constructed by the CSR method.[63] Later, models of liquid and amorphous silica containing 498 ions each in the basic cube were constructed.[53,64–66] The pair potentials (1) were used (without the two last terms) with the values of $B_{11} = 0$, $B_{12} = 1729.5$, $B_{22} = 1500$ eV, and $R_{ij} = 29$ pm. Coulomb interactions were taken into account by the Ewald–Hansen method. First, a heating of the system up to 6000–9000 K was simulated to reach the equilibrium structure and then the temperature was lowered to 2000 K. The length of MD-sweeps was 500–1000 time steps (one time step is 2.04 fs). The values of the total energy for models of SiO_2 with different numbers of particles (n) at $T = 0$ K obtained in different studies (scaled for equal B_{ij} coefficients) are compared below.

$-E$ /kJ mol^{-1}	n	Ref.
12245	162	9
12487	246	63
12414	498	53

For the two last models, the energy differs by only 0.58%, which exceeds insignificantly the computational error. In another study,[9] the energy is higher by ~ 200 kJ mol^{-1}, *i.e.* this model is less stable. The differences may be caused not only by the different number of particles, but also by a different degree of approach of the system to the equilibrium.

Table 1 shows the characteristics of silica calculated at 0 K and 2000 K and those found experimentally at 300 K. It is clearly seen that the ionic model of SiO_2 with the potentials (1) and (2) allows one to obtain altogether reasonably good agreement with the experimental results. Coordination numbers of Si^{4+} ions are distributed as follows:

z(Si–O)	3	4	5
Number of Si^{4+} ions	7	152	7

Thus, $\sim$8.4% of silicon atoms have a coordination number (CN) equal to 3 or 5, but the majority of Si atoms are surrounded by four oxygen atoms. In the real non-crystalline silica the number of 'defective' silicon ions is much less. Coordination numbers of 4 and 2 were determined by Della Valle and Andersen.[67] The mean value of O–Si–O angle in the models is close to the tetrahedral (109.5°). Therefore, the structure of silica is a tetrahedral network. According to the values of the topological parameters ρ_1 and s, this structure is rather loose. If a volume of silica is contracted by a factor of $\sim$2.5, then the ρ_1 value becomes equal to 1.08 and the structure turns dense, similar to the structure of metal glasses.[11]

Models of liquid silica at temperatures of 2100 K and 6000 K and densities 2.2–4.0 g cm^{-3} were constructed.[68] Coulomb interactions were taken into account by the Ewald summation. The $p-V$ isotherms, structural characteristics, self-diffusion coefficients of ions, density of vibrational states, and IR absorption spectra were calculated. A study of SiO_2 structure at 6000 K and pressures up to 35 GPa by the MD method indicated[69] an increase in ordering of the melt structure and in the coordination numbers with the increase in pressure. It was demonstrated that compression of the glass noticeably changes the ring statistics.[70]

Table 1. Calculated and experimental parameters for ionic models of silica.

Parameter	Calculation[53]		Experiment[49,50] 300 K
	0 K	2000 K	
r_1(Si–Si) /pm	319	317	312
r_1(Si–O) /pm	161	162	162
r_1(O–O) /pm	257	259	265
θ(O–Si–O) /deg	109.2 ± 12.9	109.1 ± 14.6	109.5
θ(Si–O–Si) /deg	154.8±14.7	152.7±14.5	147.0±16.0
ρ_1	0.892	0.882	–
s	1.59	1.39	–

The existence of a close correlation between ρ_1 and s parameters and the trend of the system to glass formation was proposed.[11,53] Indeed, the looser the system, the more difficult the crystallisation process (even merely for geometrical reasons). The factors governing the glass transition are evidently kinetic ones. There is also a thermodynamic aspect associated with the driving force of the crystallisation (difference in the Gibbs energies of non-crystalline and crystalline phases). However, for a number of loose structures with $\rho_1 < 1.0$ there is a regularity, which states that a decrease in ρ_1 results in easier glass formation. In particular, low value of ρ_1 (~ 0.9) is the reason for easy glass formation by silica on ordinary cooling in air.

In order to investigate the size effects, big models of amorphous silica with numbers of ions 648, 5184, and 41 472 and density of 2.2 g cm^{-3} were constructed using the MD method.[71] Pair potentials of the Pauling type, but with shielded Coulomb interactions and including ion polarisability, were used. In addition, the three-particle interactions were introduced by the method of Stillinger and Weber.[72] As a result, 19 potential parameters had to be adjusted. Heating of β-cristobalite up to 12 000 K and its gradual cooling to 300 K were simulated. The calculated structural factor (SF) of the model was in very good agreement with the data on neutron scattering. The agreement for PCF was also good. It was demonstrated that the size of the system does not affect the PPCF shape of the model, although structural factors differ slightly in the region of the scattering vectors of 15–55 nm^{-1}. The height of the first distinct peak of SF at the scattering vector $K = 15$ nm^{-1} increases slightly with increase in the size of the system (from 1.25 to 1.48) and for $N = 41\,472$ it is in excellent agreement with the experimental value. The density of vibrational states in SiO_2 was calculated [71] by diagonalisation of the dynamic matrix.[73]

Destruction of amorphous and crystalline silica have been simulated.[74] Models of porous silica with different densities were also investigated.[75]

2. Models of boron oxide

According to diffraction analysis data,[49,51,76,77] amorphous B_2O_3 has a layered structure with average CN of B–O pairs equal to 3. The first peak of the total PCF (TPCF) for X-ray radiation, which corresponds to B–O pairs, is located at 137–138 pm. The second peak corresponds to O–O pairs (237 pm). An isosceles triangle with sides of 138, 138, and 237 pm contains the obtuse angle of *ca.* 120°. Therefore, BO_3 groups have to be almost planar triangles. These triangles are fused by shared vertices (oxygen atoms). In the glass-like boron oxide, the presence of boroxol B_3O_3 rings with angles inside the ring of $\sim$120° was proposed.[50] Addition of Na_2O to B_2O_3 leads to an increase in coordination number of boron from 3 to 4 and to a decomposition of the initial structure.[49]

The structure of the B_2O_3 glass was also investigated by NMR method using ^{11}B isotope (see Ref. 78). Boron sites of two types with ratio 2:1 were observed. The first type was assigned to boroxol rings and the second one to BO_3 groups; and these structural elements are present in equal ratios. O–B–O angles for these two configurations are similar. However, the chemical shifts for the sites of two types are different due to the longer B–O bonds in the rings as compared to BO_3 groups.

Basing on NMR data and model calculations of the correlation functions, it was shown [79,80] that the B_2O_3 glass can contain more extended elements of local ordering than the BO_3 groups and boroxol rings, in particular, B_3O_7, B_3O_8, B_4O_9, B_5O_{10}, B_5O_{11}, and B_5O_{12} in which the boron atoms may have CN of 3 and 4. In this case, simulations give a glass density close to the experimental value which could not be achieved using purely boroxol model.

It should be taken into account that nanometer-scaled structural inhomogeneities revealed in real glasses or melts by, for example, small angle scattering cannot be reproduced on relatively small models with the basic cube edge of $\sim$ 2 nm. Using this

method, structures of B_2O_3 (200 – 270 °C) and of a series of alkali borates and silicates systems were studied.[81,82] In the case of B_2O_3, domains with an average size of ~ 1.5 nm and with densities lower than in the surrounding matrix, were found. In alkali borate glasses the inhomogeneities are due to several reasons, *viz.*, thermal density fluctuations, structural inhomogeneities, supercritical concentration fluctuations, and peculiarities of the fusion of high-alkali structural complexes.

Models of amorphous boron oxide were constructed.[18,83–86] Force functions (6) were introduced for the boron oxide description.[18,83,84] The parameters were adjusted to obtain the structure with planar triangular BO_3 fragments. The models composed of 320 ions were relaxed during 1000 steps at 6000 K. The diffusion processes in the system occurred very slowly. This could be accelerated by decreasing the ion charges. Two experiments with the models composed of 192 and 1920 ions were carried out. For both models, the temperature was gradually decreased from 2000 to 300 K at constant volume. The energy and pressure decreased during the cooling, and the temperature dependencies of both characteristics could be represented in the form of two linear regions. If the intersection point is identified as the glass transition point and its actual value (~ 540 K) is taken into account, the estimates for the effective charges are $Z_1 = +1.125$ and $Z_2 = -0.75$.

Analysis of the models demonstrated that the values of the azimuthal O–B–O angle lie in the range 119±6° and of the B–O–B angle, in the range 154±20°. The rings composed of six and more B atoms predominated in the structure and the boroxol rings B_3O_3 were absent. Almost ideal, centred BO_3 triangles linked through the vertices form an infinite system of layered elements and twisted ribbons.

An attempt to decrease the width of the B–O–B angle distribution in the model of B_2O_3 using a special algorithm was undertaken.[87] To this end, the values of B–O and B–B bond lengths were fixed at 138 and 239 pm ($239 = 138\sqrt{3}$), respectively. The model comprised 1680 ions. A decrease in temperature from 6000 to 300 K was performed in 5000 steps, 1 fs each. At 300 K, the energy was equal to -2950 kJ (g-at.)$^{-1}$ instead of -2975 kJ (g-at.)$^{-1}$ without fixing the bond lengths. The heat capacity of the model with the fixed bond lengths was equal to 10.3 J (g-ion K)$^{-1}$ instead of 24.5 J (g-ion K)$^{-1}$ with the usual algorithm. The final structure of the glass did not contain the six-membered boroxol rings. Therefore, the mere fixation of B–O–B angles (120°) does not lead to the formation of these rings. The structure of boron oxide is a result of a fusion of BO_3 triangles by shared vertices. The planes of neighbouring triangles are non-coplanar, and the most probable angle between them is 90°. It was shown [85] that a decrease in the rate of cooling in the simulation by six orders of magnitude leads to an increase in the glass density, but it hardly affects the ordering of the structure.

Models of liquid and amorphous B_2O_3 were also constructed.[64,88] The models comprised 500 ions in the basic cube. The potentials (1) with the account for the Coulomb interactions according to Ewald–Hansen[39] were applied. The potential parameters were as follows: $Z_1 = +3$, $Z_2 = -2$, $B_{11} = 0$, $B_{12} = 800$ eV, $B_{22} = 1500$ eV, and $R_{ij} = 29$ pm. Characteristics of B_2O_3 calculated for 0 K and 2000 K and the experimental values are shown in Table 2.

Partial pair correlation functions for the model of liquid B_2O_3 at 1473 K are depicted in Fig. 2. Simulated $r_1(ij)$ distances are in very good agreement with the experimental data. Coordination numbers were the same as in Ref. 18: $z(B-O) = 3$ and $z(O-B) = 2$ (with the closest neighbour sphere radius of 200 pm). The distributions of the O–B–O and B–O–B azimuthal angles are Gaussian (116±10.3° and 154.2±12.2°) and are similar to those found earlier.[18] Structural characteristics of the liquid oxide at 2000 K differ only slightly from those calculated at 0 K (see Ref. 64). Topological characteristics of the models indicate the looseness of the structures of both liquid and amorphous boron oxide. It is less dense than the structure of silica. The basic

Table 2. Calculated and experimental parameters of B_2O_3.

Parameter	Calculation [64,88]		Experiment [49]
	0 K	2000 K	300 K
V /cm^3 mol^{-1}	38.43	45.80	38.6
P /GPa	~0	~0	~0
E_{coul} /kJ mol^{-1}	−21718	−21665	–
E_{tot} /kJ mol^{-1}	4417	4332	–
$r_1(ij)$ for pairs			
B–B	267	267	(270)
B–O	139	138	138
O–O	235	239	237
ρ_1	0.830	0.787	–
s	2.21	3.16	–

structural elements are almost planar BO_3 groups fused through shared vertices. In the model of liquid B_2O_3 four four-membered, five six-membered, and seven eight-membered rings were found.

The molar volume for the model of amorphous B_2O_3 is close to its actual value. However, the calculated atomisation energy for the model is 1383.1 kJ mol^{-1}, while the experimental value [89] for B_2O_3 crystals is 2737.1 kJ mol^{-1}. The difference between these values is 7.8% of the total energy and can not be attributed to the amorphisation energy of crystal. Probably, it indicates the greater contribution of covalent bonding in boron oxide. The value of energy at 300 K (−14 875 kJ mol^{-1})[87] is substantially higher than that found in other studies.[64,88]

New interparticle potentials for boron oxide were proposed;[90] their parameters were adjusted using the method of linear programming. For better description of the properties of various crystal phases, terms depending on CN were included. This method allowed one to predict new stable polymorphous forms of crystalline B_2O_3 with a high content of the boroxol rings (up to 100%). These potentials were applied for the construction of a B_2O_3 glass model with an increased concentration of these rings.[91] Seven different potentials (including three-particle ones) were used [92] for construction of an MD model of B_2O_3 (424 particles). Structures of the models proposed appeared to be similar to each other and were close to the real one. Nevertheless, the dynamic properties of the system (vibrational modes) were reproduced correctly only in the case when the three-particle contributions were taken into account.

A process of glass formation in boron oxide and some borates on cooling from a liquid state was investigated using MD method.[93] The properties of the phase were described with Prigogine–Defay parameter (γ), which establishes the correlation between the glass transition point and the ordering parameters.[94] For the system studied $\gamma > 1$. It was shown, that the formation of B_2O_6 groups results in a decrease of γ, and the formation of groups

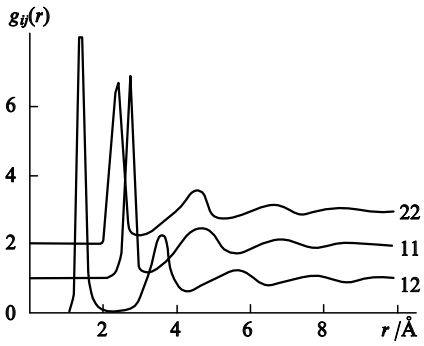


Figure 2. Partial pair correlation functions for the model of liquid B_2O_3 at 1473 K.
The curves are shifted along the ordinate axis; numbers denote pairs of ions (1 states for B, 2 for O).

with terminal oxygen ions (which have only one neighbouring boron atom) results in an increase of γ.

3. Models of non-crystalline Al_2O_3

The structure of liquid Al_2O_3 has not been studied experimentally due to its high melting point. In the bulk, alumina does not form glass. Amorphous oxide is formed only as thin films (for example, in anodic oxidation of the aluminium). Data by different authors on the structure of Al_2O_3 are only in partial agreement. An electronographic study of films obtained by anodic oxidation in boric acid-containing electrolyte was reported.[95] Peak positions in the total PCF (TPCF) were equal to 175, 275, and 320 pm. The first peak corresponds to Al—O pairs, the second one to O—O, and the third one to Al—Al pairs. Similar films with a thickness of 5 nm were studied[96] at the maximum scattering vector $K = 185\ nm^{-1}$. Peak positions in the TPCF were 182, 310, and 420 pm. The mean CN were as follows: $z(Al—O) = 6$ and $z(O—Al) = 4$. Therefore, virtually all aluminium atoms were in an octahedral environment.

For a film with thickness of 150 nm (after separation),[97] the peak positions were at 180 and 320 pm, and $z(Al—O) = 5.5$. Such an arrangement of particles is typical of γ'-Al_2O_3 crystal modification. An approximate interpretation gave the following results:

Pair	Al—Al	Al—O	O—O	Al—O(2)
$r(ij)$ /pm	315	180	261	345
CN	10.3 ± 0.2	5.4 ± 0.1	12.0 ± 0.1	9.1 ± 0.2

The notation Al—O(2) relates to the second peak of the Al—O pairs. These data are close to the results of another study.[95]

The following groups: AlO_4, AlO_5, and AlO_6 were found in a transitional amorphous phase α-Al_2O_3 using NMR ^{27}Al (see Ref. 98).

A model of amorphous Al_2O_3 incorporating the structural data[96] has been constructed.[99] The model contained 150 particles in a sphere with a diameter of $\sim$150 pm. First, the particles were arranged in a quasirandom order with limitations on the minimum interparticle distance, CN, azimuthal angles, and the type of neighbours. Further relaxation of the model was performed by the Reverse Monte Carlo method. In the structure obtained, the distribution of the Al—O—Al angles had maxima at 60, 80–100°, and 120–130°, and the maxima of distribution of the O—Al—O angles were at 80–100°, 130–140°, and 150–160°. Taking into account the small size of the model, the authors concluded that its structure was similar to that of α-Al_2O_3. A model of amorphous oxide composed of 120 particles was constructed analogously[100] revealing a layered structure and the formation of clusters of 5- or 6-membered spatial rings in the layers.

An MD model of liquid oxide at $T = 2560$ K with ion charges $Z_1 = +2.55$ and $Z_2 = -1.70$ was constructed.[101] The Al—O and O—O distances appeared equal to 185 and 273 pm, *i.e.* slightly longer than the actual values, with $z(Al—O) = 5.2$.

In a simulation (500 particles) of liquid (overcooled) oxide at 2000 K and of amorphous oxide at 0 K by MD and CSR methods the potentials (1) were applied.[88] The following parameters were chosen: $Z_1 = +3$, $Z_2 = -2$, $B_{11} = 0$, $B_{22} = 1500$ eV (the same as for models of silicates[65]). The parameter $B_{12} = 1479.86$ eV was adjusted to make the molar volume of corundum at $P = 0$ equal to the actual value. Coulomb interactions were taken into account according to the Ewald–Hansen method.[39] The difference between the calculated energy for the ionic model and the energy of the real crystal was only 3.1%, and therefore an interpretation of corundum as the ionic compound is quite reasonable. In a simulation of the amorphous phase at 0 K, the initial CSR step was 50 pm and then it was gradually diminished to 1–2 pm.[88] About 250 steps were necessary to complete relaxation. The model built had the following parameters:

V /cm^3 mol^{-1}	31.2	r_1 /pm for pairs	
P /GPa	1.65	Al—Al	312
E /kJ mol^{-1}	−15289	Al—O	175
		O—O	268

The difference in energies of amorphous Al_2O_3 and crystalline corundum, equal to 274 kJ mol^{-1}, is the heat of crystallisation of amorphous Al_2O_3. The heat of crystallisation of liquid alumina at 2300 K is 109 kJ mol^{-1} (see Ref. 89). These values are in reasonable agreement taking into account the difference in temperatures. The molar volume of amorphous Al_2O_3 is closer to the molar volume of γ-Al_2O_3 crystal (spinel type, 27.83 cm^3 mol^{-1}) rather than of α-Al_2O_3 (25.57 cm^3 mol^{-1}). The real density of amorphous oxide films, to our knowledge, have not been measured. The volume of γ-Al_2O_3 increases by $\sim$ 12% upon amorphisation.

Structural characteristics of models of amorphous alumina are in good agreement with the experimental data.[95] However, $g_{ij}(r)$ functions determined in independent studies[88,101] differ substantially. This is mainly due to the difference in the pair potentials used. Mean CN for the models[88] are as follows: $z(Al—O) = 4.47$ and $z(O—Al) = 2.98$. These values exceed the normal atom valences by factor $\sim$1.5, and therefore an assumption of the presence of a continuous random bond network in the structure of amorphous alumina may be rejected. The value of $z(Al—O)$ is slightly lower than in the γ-Al_2O_3 crystal lattice ($0.7 \times 6 + 0.3 \times 4 = 5.4$), which is typical of dense non-crystalline structures.

Distributions of CN in the amorphous oxide are rather broad. Their calculation with the radius of the closest neigbour sphere of 240 pm gave the following results:

Number of neighbours	1	2	3	4	5	6	7
Number of Al^{3+} ions	–	–	8	102	78	12	–
Number of O^{2-} ions	–	42	222	36	–	–	–

Most of Al^{3+} ions have four and five O^{2-} neighbours, and most of oxygen atoms have three Al^{3+} neighbours. These data do not confirm the suggestion of the existence of such structural elements as the AlO_3 trigonal pyramid.

A model of liquid (overcooled) Al_2O_3 was constructed[66] using the MD method with the same parameters as in Ref. 88. Coulombic interaction was taken into account according to the Ewald–Hansen method.[39] The model contained 500 ions. The calculated molar volume of the liquid oxide at $P = 0$ (34.3 cm^3 mol^{-1}) was very close to the actual value (34.3 cm^3 mol^{-1} at 2300 K, see Ref. 102). The Al—Al, Al—O, and O—O distances were found to be equal to 313, 174, and 286 pm, so the heating by 2000 K affected noticeably only the O—O pairs. Mean CN of Al—O pairs was equal to 4.50 and their distribution was still very broad. Both at $T = 0$ K and $T = 2000$ K, the system had a relatively small number of aluminium ions with octahedral coordination; the predominant values were $z(Al—O) = 4$ and 5.

The topological characteristics of the Al_2O_3 structure were calculated (see Refs 66 and 88).

T /K	0	2000
ρ_1	1.051	1.056
s	1.16	1.13

Consequently, the structure of non-crystalline alumina lies on the lower boundary of the area of topologically dense systems. This accounts for difficult glass formation in the ordinary cooling of a liquid; ρ_1 and s values contradict the assumption of a layered structure of the oxide.

4. Models of non-crystalline Fe_2O_3

Fe_2O_3 oxide has not been obtained in an amorphous state, and in the liquid state it is unstable and readily decomposes to FeO and oxygen. However, Fe^{3+} ions are present in complex oxides in various concentrations depending on the oxidation potential of the medium. Models of non-crystalline Fe_2O_3 oxide were constructed using MD and CSR methods at 0 K and 2000 K.[103–106] The models contained 500 ions in the basic cube. The pair

potentials (1) with parameters $B_{11} = 0$, $B_{22} = 1500$ eV, $R_{ij} = 29$ pm were applied, the value of $B_{12} = 2114.2$ eV was calculated

Table 3. Calculated parameters of the models of non-crystalline Fe_2O_3.[103]

Parameter	0 K	2000 K
V /cm^3 mol^{-1}	39.0	40.2
E /kJ mol^{-1}	−14418	−14168
$r_1(ij)$ /pm for pairs		
Fe−Fe	331	327
Fe−O	191	190
O−O	298	291
z(Fe−O)	4.7	4.7
ρ_1	1.07	1.05
s	1.21	1.18

according to the actual density of the crystal with the corundum lattice. The models were constructed in a way similar to that for Al_2O_3. Table 3 shows the parameters of the models for Fe_2O_3 at 0 K and 2000 K.

The Fe−O distance of 190 pm can be compared with the diffraction data for $Fe_2O_3 \cdot 4(Na_2O \cdot 2SiO_2)$ (see Ref. 107) and $CaO \cdot Fe_2O_3$ (see Ref. 108) glasses where it lies in the range of 196–203 pm. In order to elongate the Fe−O distance to 198 pm, the B_{12} parameter was increased to 2453.0 eV.[104–106]

These data show that the structures of Fe_2O_3 and Al_2O_3 are close to each other. At 0 K, 64 out of 200 iron ions have four neighbours, 105 ions have five, and 31 ions have six O^{2-} neighbours.[103–106] A relatively big Fe^{3+} ion cannot arrange a rigid group of oxygen ions around it, as takes place in B_2O_3, and the network of bonds is not created. Slightly increased value of the s parameter is due to the presence of big pores. According to the value of ρ_1, the structure of non-crystalline oxide is rather dense.

The hysteresis effects in Fe_2O_3 are small. Construction of a model of amorphous oxide at 0 K using the CSR method, an increase in the temperature up to 2000 K using the MD method and consequent cooling back to 0 K led to a decrease in the energy relative to the initial value by only 0.05%.

5. Models of UO_2

Models of crystalline and liquid UO_2 have been constructed (see Ref. 109). A model of rigid ions with charges +4 and −2 has been used. The parameters of the potential (1) were as follows: $B_{11} = 0$, $B_{12} = 869.98$ eV, $R_{12} = 42.7$ pm, $B_{22} = 11272.6$ eV, and $R_{22} = 13.63$ pm for $r < 120$ pm, while at longer distances the potential $u(r)$ was represented in a polynomial form. All potentials were cut off at 520 pm. In addition, the dipole-dipole interactions were included in a potential for U−O pairs.

A model of UO_2 crystal (96 ions in the basic cube) gave a good fit with the experimental data on elastic constants and the dielectric properties. It was shown that the self-diffusion coefficient of O^{2-} ions in the temperature range of 2500–3300 K, while the system is still solid, is of the order of 10^{-5} cm^2 s^{-1}, which is typical of liquids, *i.e.* the oxide under these conditions is a superionic conductor. In the liquid state (at 3200–4200 K), the self-diffusion coefficient of oxygen changes from 7×10^{-5} to 1.4×10^{-4} cm^2 s^{-1}, which is 3–4-fold greater than that for the uranium ions. The structure of the oxide has not been described.[109]

6. Models of non-crystalline P_2O_5

Phosphate slags are important in metallurgy. Phosphate glasses attract considerable attention due to their prospective use in optoelectronics. P_2O_5 easily forms glasses. It possesses the high viscosity, and its use as an additive allows preparation of glasses with variable composition. The properties of phosphate glasses have been reviewed.[110–113] Hysteresis of the properties, *i.e.* their dependence on the prehistory of a sample, is a typical feature of the phosphate glasses.

Experimental data on the structure of phosphate glasses obtained by diffraction methods are rather numerous. Crystalline P_2O_5 is built up either of isolated P_4O_{10} molecules or of infinite layers of tetrahedral PO_4 groups (see Ref. 112). One of bonds between pentavalent phosphorus and oxygen atoms is double. The distance r_1(P−O) determined for a $NaPO_3$ glass [114] is equal to 155 pm. The structure of this oxide is represented by long chains of PO_4 tetrahedra linked with other chains through sodium ions. X-ray studies of $[M(PO_3)_2]_n$ (M = Zn, Cu, Mn, Ca, Mg) [115] gave the value of r_1(P−O) of 155 pm, which was virtually independent of the composition. However, the magnesium derivative behaved abnormally. Its density is higher than that calculated from a general linear correlation on the number of the M element in the Periodic Table (2.45 instead of the interpolated value 2.25 g cm^{-3}), and the interionic M−O distance is reduced (190 pm for Zn, 195 for Cu, 220 for Mn, 250 for Ca, and 190 for Mg). The first SF peak for magnesium phosphate appears at $K = 15.5$ nm^{-1} (instead of 17.0 for the other compounds) and is also abnormally high. It was supposed [115] that the anomalies of magnesium phosphates are due to the formation of phosphate rings in this glass.

The structure of glasses with a composition $M(PO_3)_2$ (M = Zn, Mg, Ca, Sr, Ba) were investigated by neutron scattering method.[116] O−O, P−O, and M−O pairs give the principal contributions into the TPCF (with shares of ~47%, 28%, and 15%, respectively). Separation of the TPCF into partial contributions is ambiguous. Nevertheless, for all glasses it was found that z(P−O) ≃ 4, [z(Ca−O) ≃ 4 as well]. The most reliable results are those for the P−O and O−O pairs:

Parameter	Zn	Mg	Ca	Sr	Ba
r_1(P−O) /pm	154	153	154	154	154
z(P−O)	3.9	4.0	4.0	4.0	4.2
r_1(O−O) /pm	251	250	248	252	252
z(O−O)	4.5	4.7	4.3	3.8	4.5

PO_4 tetrahedra are linked to each other *via* two bridging oxygen atoms forming presumably non-straight chains.[116] Cations are placed between the chains and are surrounded by different numbers of oxygen ions. One of the oxygen atoms in the tetrahedron is doubly bound to the phosphorus atom. However, the computational accuracy is not sufficient to differentiate bonds of phosphorus with bridging and terminal oxygen particles.[116]

The applicability of the ionic model to P_2O_5 is not obvious. The electronegativities of oxygen and phosphorus atoms (according to Pauling) are equal to 3.5 and 2.1, respectively. From their difference of 1.4, the degree of the P−O bond ionicity is only 39%, which is substantially lower than for silica (51%).

Computer models of non-crystalline P_2O_5 were constructed using the MD and CSR methods.[117] The Born–Meyer pair potentials (1) with ion charges +5 and −2 were applied. The interaction parameters B_{12} and B_{22} were determined using the experimental data on $Ca(PO_3)_2$ (with $B_{11} = 0$). The r_1(P−O) was adjusted to 155 pm in a model of glassy oxide by varying the B_{12} parameter. The B_{22} parameter for the model of $Ca(PO_3)_2$ at 300 K was adjusted to reproduce the actual volume 8.40 cm^3 (g-ion)$^{-1}$ (see Ref. 118). Models of glasses were obtained by rapid cooling from 2000 K to 0 K within the CSR method with a 2 pm step; one typical run included 500 iterations. In the simulation of cooling under isobaric conditions (P close to 0), both the r_1(P−O) distance and the volume of the system changed slightly (by 1–3 pm and 1%–3%, respectively). Therefore, the parameters were corrected and MD-relaxation at 2000 K followed by cooling to 0 K was performed again. This cycle was repeated until the calculated parameters conformed with the experimentally established values for r_1(Ca−O) and molar volume of $Ca(PO_3)_2$ glass. Finally, the values of $B_{12} = 1847.66$ eV and $B_{22} = 1009.98$ eV

were obtained. The latter is substantially less than that proposed for silicates (1500 eV).[65]

The B_{ij} values found for $Ca(PO_3)_2$ oxide were used in order to construct models for P_2O_5 at 2000 K and 0 K using the MD and CSR methods. All models relaxed in 1000 steps at 6000 K (2.04 fs per step), then the system was cooled to 2000 K and annealed for two runs of 1000 steps each. A model of the glass at 0 K was obtained by switching from the MD to the CSR method (with 2 pm shifts) using models for liquid oxide after a molecular dynamic run of 1000 steps at 2000 K.

For the model of pure P_2O_5 at 2000 K and 0 K, the molar volumes were 46.2 and 45.6 $cm^3\ mol^{-1}$, which is substantially less than the molar volume of the real glass (55.0 $cm^3\ mol^{-1}$, see Ref. 118). In part, this discrepancy may be explained by a difference in the properties of real glasses prepared by different ways

Table 4. Distribution of CN for models of P_2O_5 at 2000 K.

CN	P−O (O−P)	O−O	CN	P−O (O−P)	O−O
1	(2)	–	6	18	96
2	(352)	–	7	–	165
3	(1)	1	8	–	65
4	19	–	9	–	23
5	105	3	10	–	2

(the transition from the MD to the CSR method implies an exclusively high cooling rate). Interionic distances for the P−P, P−O, and O−O pairs at 2000 K appeared to be equal to 313, 158, and 228 pm, respectively. The mean CN for P−O pairs was 4.99. Table 4 shows the distributions of CN in the model of P_2O_5 at 2000 K.

Similar results were obtained at 0 K. Distributions of CN for P−O pairs had a maximum at $z(P-O) = 5$. About 74% of phosphorus ions occupy centres of 5-vertex trigonal bipyramids, however a noticeable part of P^{5+} ions are surrounded by four or six O^{2-} ions ($\sim$13%−14% both). Virtually all O^{2-} ions in the P_2O_5 models have two P neighbours bridging PO_n groups. A bound group analysis indicate complete polymerisation of the structure.

Distribution of the O−P−O and P−O−P angles is as follows: $\theta(O-P-O) = 106.5\pm25.8^\circ$, $\theta(P-O-P) = 157.4\pm11.8^\circ$. Hence, the PO_5 bipyramids are linked through shared vertices, and the P−O−P angles are close to the Si−O−Si angles in silica.

The presence of a ring component of the structure was also analysed. A P−O pair with a distance between the ions less than 175 pm was considered as a link. In models of P_2O_5 at 2000 K and 0 K the 6- and 8-membered rings were found; and almost all particles of the model were included in the rings. The following topological parameters of P_2O_5 models at 2000 K were found: $\rho_1 = 0.931$ and $s = 1.51$. These values imply that the structure of P_2O_5 is rather loose and close in this sense to the structure of silica. According to these parameters, the tendency to glass formation also should be high, which is in agreement with the experimental data.

In the simulation of P_2O_5 at 0 K with the actual molar volume of 55.0 $cm^3\ mol^{-1}$ by the CSR method, the interionic distances for the P−P, P−O, and O−O pairs were 323 pm, 161 pm, and 239 pm, respectively. The pressure was found to be about −30 GPa, CN of the P−O pairs decreased to 4.9, *i.e.* the tetrahedral configuration was still little represented (19% of the phosphorus ions). Distributions of azimuthal angles and topological parameters of the model were practically unchanged.

It is difficult to compare the real structure and the models of P_2O_5 at 2000 K due to the absence of experimental data. However, for amorphous P_2O_5, the deviations from the real glass were significant; especially in CN of the P−O pairs. A model of ionic bonding with the use of the potential (1) with ion charges +5 and −2 does not provide the dominant tetrahedral coordination of phosphorus particles in pure P_2O_5. Better agreement with the experimental data may be achieved either by decreasing ion charges or taking into consideration three-particle interactions typical of covalent bonding. As it will be demonstrated below, the tetrahedral coordination of phosphorus ions in the glass may be obtained within the framework of the pair interaction by selecting lower effective ion charges.

7. Models of non-crystalline V_2O_5

The oxide V_2O_5 forms a glass upon ordinary cooling of the liquid. Glasses with the composition V_2O_5 — (Li_2O, Ag_2O, BaO, SiO_2) were prepared by quenching between rotating cylinders.[118]

The structure of liquid V_2O_5 was studied by X-ray diffraction at 953 K and 1173 K.[51] According to these data, the position of the first peaks in the PPCF at 1000 K for the V−V, V−O, and O−O pairs were at 345, 180, and 256 pm, respectively. The mean CN value of V−O was 5.2. The temperature practically did not affect the structure of the melt, and this is believed to be similar to the structure of a crystal built of zigzag chains of oxygen bipyramids with vanadium ion at the centre, which are linked to each other through remote oxygen ions into a continuous network.[51] Addition of lithium, potassium, calcium, and lead oxides to V_2O_5 results in a decrease in the V−O distance (to 168 pm at 25 mol.% of PbO). However, the V−V, V−O, and O−O distances determined by X-ray and neutron diffraction of V_2O_5 were equal to 336, 170, and 276 pm, respectively, and CN of V−O pairs was 3.6.[119] A model in which vanadium atoms occupy centres of VO_4 tetrahedra and every three vertices of the tetrahedron are common for neighbouring tetrahedra was suggested.[119] In a liquid state, large clusters of tetrahedra have to decompose into constituents, and some vanadium atoms in the centres of tetrahedra may be substituted by oxygen atoms.

In a $V_2O_5 \cdot 4.4TeO_2$ glass, two V−O distances were found by neutron diffraction: 161 pm (CN 1.0) and 199 pm (CN 4.0).[120]

The structure of liquid V_2O_5 was simulated.[121–123] An MD-model of the oxide at 1050 K with the effective ion charges of +3.95 and −1.58 was described.[121] The model contained 560 particles in the basic cube. The V−O distance was 178 pm, and CN for V−O was 6.1; the pressure of the system was $\sim$30 GPa. A model of liquid oxide with the actual molar volume 78.4 $cm^3\ mol^{-1}$ at 1000 K was constructed.[122] The model contained 336 ions in the basic cube, ion charges were +5 and −2. The value of B_{12} (2970.0 eV) was determined from the lattice parameter of the crystalline oxide. For this model, the energy of the ionic V_2O_5 crystal appeared to be higher than the actual value (−38 314 kJ mol^{-1}) by $\sim$13%. This difference is probably due to a significant contribution of covalent bonding in the real oxide. Besides, the model did not take into account van der Waals contributions to the total energy.

From the model, V−O distance was 180 pm, CN was 4.94, and the pressure was $\sim$2 GPa. It was concluded that the structure of the V_2O_5 melts is loose and built up of oxygen bipyramids with vanadium ions in the centres and CN of V−O pairs close to 5.[122] It was established that the CN distribution is rather narrow, and more than 92% of vanadium ions have five oxygen neighbours. The distribution of O−V−O azimuthal angles has an intense peak at 90° and a small peak at 155°. These angles are typical of a distorted trigonal bipyramid with the vanadium atom in the centre. Distribution of the Voronoi polyhedra also confirms the pyramidal structure.

A series of models for oxides with a general formula M_2O_5 was constructed using the potentials (1) at zero pressure.[123] The number of particles in all models was 497. For the model corresponding to V_2O_5 (with $B_{12} = 2970$ eV), the calculated energy was −33 160 kJ mol^{-1} at 2000 K and −33 390 kJ mol^{-1} at 1000 K (the difference between them is less than 0.4%).[122] However, molar volumes for these models differed by 23% (62.3 and 78.4 $cm^3\ mol^{-1}$, respectively). Checking with the use of the same programme demonstrated that each model is rather stable

during MD-relaxation for hundreds of steps (~ 1 ps). Thus, in this case two rather stable oxides with different prehistory and structures were found. Probably, this effect is analogous to the compacting of silica (by 10% – 15% in volume), which had been reproduced earlier by MD method.[9]

Calculated [122, 123] V – V, V – O, and O – O distances were 350, 180, and 257 – 259 pm, respectively. They are close to the experimental values [51] but differ noticeably from the results of another study.[119] The CN values for V – O pairs change from 4 to 6, where $\sim 70\%$ of vanadium ions have the CN = 5, and the mean CN is equal to 4.9 – 5.0.[123] For the models of liquid V_2O_5, the values of topological parameters are as follows: $\rho_1 = 0.885$ and $s = 2.71$.[122] Therefore, the structure of oxide is rather loose.

Taking into account the discrepancy in diffraction data, it is difficult to discuss the correctness of the models of vanadium pentoxide. A covalent component may give a substantial contribution to the interaction of particles in this oxide.

8. Models of non-crystalline WO_3

Diffraction data on the structure of non-crystalline tungsten oxides are scarce. For amorphous films of WO_3, the electronographic study gave the values of W – W and W – O distances of 378 pm and 188 pm and the corresponding CN 5.7±0.4 and 5.8±0.2.[124] A structure of bulk WO_3 glass was studied by anomalous X-ray scattering.[125] For the W – O pair two distances were found: 182 (W = O) and 220 pm (W – O); the mean distance is equal to 196 pm (CN 5.2). It was shown that for the O – O pairs the distance is 287 pm (CN 7.0) and for the W – W pairs, 372 pm (CN 4.2). Therefore, the results of the two studies [124, 125] are in some disagreement. A study of $2Na_2O \cdot WO_3$ and $Na_2O \cdot 2WO_3$ glasses gave W – O distance close to 180 pm and CN 4.7 and 5.2, respectively.[126]

The potential (1) with the parameters $B_{11} = 0$, $B_{22} = 1500$ eV, and $R_{ij} = 29$ pm was applied in models of liquid and amorphous WO_3 oxide composed of 500 ions.[127, 128] The B_{12} parameter was determined provided the W – O distance was taken to be 180 pm, and was found to be 3400 eV. First, a CSR model at 0 K and zero pressure was constructed. Then the increases in temperature up to 2000 K were simulated by the MD method. After the relaxation, the system was cooled again to 0 K using the CSR method to check it for probable hysteresis effects. The molar volume of the amorphous oxide at 0 K was found to be equal to 28.7 $cm^3\ mol^{-1}$ and to 28.9 $cm^3\ mol^{-1}$ for the liquid one at 2000 K. The molar volume of the crystal at 300 K is 31.3 – 32.2 $cm^3\ mol^{-1}$ (see Ref. 129), which exceeds that of the amorphous oxide by 9% – 12%. The reason for this effect is a rather loose structure of the crystal.

The adequacy of a purely ionic bonding approximation may be estimated for WO_3. The atomisation energy of WO_3 was calculated using the Born – Haber cycle.[130] The sum of the first six ionisation potentials found in this way was 193.33 eV, and the actual sum is 193.7 eV. Therefore, the ionic bonding approximation is reasonable, and the higher ionisation energy of tungsten atoms is compensated by the Coulomb energy of ion interactions.

The mean thermal expansion coefficient for WO_3 models in the range of 0 – 2000 K is very small ($3.1 \times 10^{-6}\ K^{-1}$). This is explained by the small ratio of the thermal energy at 2000 K to the total energy (0.0044). By the same reason, the low thermal expansion coefficient of SiO_2 (E_{kin}/E is 0.006) may be explained. Structure of WO_3 does not change substantially on heating, and the mean heat capacity is close to its classical limit $3R = 24.9$ J (g-ion K)$^{-1}$.

The values of W – W, W – O, and O – O interionic distances were equal to 352, 179, and 238 pm at 2000 K and to 351, 179, and 236 pm at 0 K, respectively.[127] They very little depend on temperature. The W – O distance is in good agreement with the diffraction data. The first PPCF peak of the W – O pairs is isolated. The mean CN of the W – O pairs is 5.98; CN distributions of the W – O and O – W pairs were identical and rather narrow at 2000 K and 0 K.[127, 128]

CN	1	2	3	4	5	6	7
Number of W ions	–	–	–	–	11	107	7
Number of O ions	4	371	–	–	–	–	–

Thus, $\sim 86\%$ of tungsten ions have 6 neighbouring oxygen atoms and are in the octahedral environment. Other tungsten atoms have 5 or 7 neighbours. Tetrahedral coordination was not observed in the models. This is at variance with the approximate structure interpretations.[126]

It is noteworthy, that the content of W^{6+} ions with CN 6 in the WO_3 oxide is somewhat less than the content of Si^{4+} with CN 4 in silica (92%). Therefore, the first coordination sphere of W^{6+} ions is less rigid. due to the larger size of the tungsten ions and strong repulsion of the six surrounding O^{2-} ions.

The topological characteristics of WO_3 models are as follows:[127, 128]

T/K	0	2000
ρ_1	0.979	0.972
s	1.55	1.42

The structure of the oxide is loose, but the values of ρ_1 are not very low. Pure WO_3 does not form glasses,[118] but on sufficiently rapid cooling (quenching between rotating cylinders) it is possible to obtain a glassy oxide.[131] Hence, the values of $\rho_1 = 0.97 – 0.98$ lie on the very limit of glass formation for the MO_3 oxides.

9. Models of non-crystalline Na_2O

Pure sodium oxide does not form glasses on cooling of a liquid. Diffraction data for sodium silicates have been reviewed.[132] According to these data, the Na – O interionic distances at 300 – 1373 K are 233 – 240 pm and CN for the Na – O pairs lie in the range of 4 – 6. The molar volume of the liquid oxide at 1673 K is 33.0±4.6 $cm^3\ mol^{-1}$ (see Ref. 133).

Models of liquid and amorphous Na_2O were constructed with the pair potentials (1).[103, 127, 134, 135] For the O – O pairs, the value of B_{22} was taken to be equal to 1500 eV, as for silicates. For the Na – Na pairs, the calculations gave $B_{11} = 842.2$ eV.[10,12] The B_{12} coefficient can be calculated from the molar volume of the crystalline oxide. Taking into account only two first terms in (1), the value of $B_{12} = 1601.9$ eV ($R_{ij} = 29$ pm) was obtained.[103,134] However, if the B_{11} value is chosen as 0, then $B_{12} = 1814.5$ eV. Since the interaction of the Na – Na pairs gives a small contribution to the energy, the value of $B_{11} = 0$ was chosen.[127]

MD-models were constructed with account for Coulomb interactions according to Ewald – Hansen.[39] The molar volume of the non-crystalline oxide appeared to be equal to 27.6 to 28.6 $cm^3\ mol^{-1}$ at 0 K and 33.0 – 36.0 $cm^3\ mol^{-1}$ at 2000 K. Interpolation to 1673 K gives the value of ~ 34.6 $cm^3\ mol^{-1}$, which is in good agreement with the experimental results. The Na – O distance is 222 pm at 0 K (see Ref. 134) and 228 pm at 2000 K.[64] In another study[127] the value of 222 pm was found at 2000 K. The deviations from r_1(Na – O) in silicates (233 to 240 pm) is reasonable, since this distance in a $Na_2O - SiO_2$ system increases with increase in the silica content.[134] The mean CN for the Na – O pairs is 2.9, which is less than the CN in the antifluorite crystal (4.0). This value is close to the lowest limit of the range of diffraction data for sodium silicates. The distribution of CN shows that only half of Na^+ ions have exactly four neighbours.

z(Na – O)	3	4	5
Number of sodium ions	48	88	30

TPCF of the oxide contains only distinct first peaks attributed to the Na – O and Na – Na pairs, which precludes the interpretation of the structure from the diffraction data.[135]

The topological characteristics of the Na_2O model at 0 K and 2000 K ($\rho_1 = 1.062$ and 1.018, $s = 1.06$ and 1.01) show that the oxide has a rather dense structure in both amorphous and liquid states. The fact that the structure of amorphous oxide is dense explains the low tendency of Na_2O towards glass formation.

V. Simulation of homologous series of non-crystalline oxides

1. Models of non-crystalline oxides in the M_2O series

The description of oxides with a definite stoichiometry and using the potential (1) with B_{12} as the only variable parameter allows one to construct a series of models differing in the $r_1(M-O)$ interionic distances, which is equivalent to changes in the ion radius of the M ion. If real oxides are satisfactory described by the potentials (1) with constant R_{ij}, B_{11}, and B_{22}, then the properties of the oxides can be calculated by an interpolation of data obtained for other members of the series. In that case, the efficiency of computational methods enhances substantially.

This idea was proposed in studies devoted to oxides of $2MO \cdot SiO_2$ series [136–139] and then extended to other oxides. Two series of models for M_2O at 0 and 2000 K with the pair potentials (1) and the values of B_{12} ranging from 545.3 to 9999.0 eV, $B_{11} = 0$, $B_{22} = 1500$ eV, and $R_{ij} = 29$ pm, were considered.[135] Each model contained 249 ions. Estimates made from the molar volume of antifluorite-type crystals at $p = 0$ gave $B_{12} = 626.67$ eV for Li_2O, 3844.1 eV for K_2O, and 5320 eV for Rb_2O (the structure of Cs_2O is more complex). Coulomb interactions were taken into account by the Ewald–Hansen method.[39] The period of the basic cube was adjusted so that the pressure was close to zero. Due to fluctuations in the pressure, the molar volume of the models was determined with an error of 0.2%–0.3% at 0 K and 2%–4% at 2000 K.

Figure 3 shows the dependence of parameters of M_2O models on B_{12} at 2000 K. The adequacy of the potentials used can be checked by comparing the molar volumes for the models with the experimental data. An interpolation using the data from Fig. 3 for Li_2O with $B_{12} = 626.67$ eV gives the molar volume at 2000 K 7.9 cm^3 $(g\text{-ion})^{-1}$ and at 1673 K 7.75 cm^3 $(g\text{-ion})^{-1}$.[135] The actual value at 1673 K [6.47±0.83 cm^3 $(g\text{-ion})^{-1}$] (see Ref. 133) is less by 16%. For Na_2O at 2000 K the calculated molar volume was 12.0 cm^3 $(g\text{-ion})^{-1}$ at $B_{12} = 1601.94$ eV. The actual volume 11.0±1.5 cm^3 $(g\text{-ion})^{-1}$ at 1673 K (see Ref. 133) is close to the calculated value. For the K_2O model at 2000 K, the molar volume appeared to be equal to 15.5 cm^3 $(g\text{-ion})^{-1}$, which is also in accordance with the experimental value of 17.2± 2.2 cm^3 $(g\text{-ion})^{-1}$ at 1673 K.[133] As it is clearly seen from Fig. 3, the $r_1(M-O)$ distance depends almost linearly on $\ln B_{12}$. The $r_1(M-M)$ and $r_1(O-O)$ distances depend monotonically on B_{12}.

Calculation of the TPCF for liquid oxides at 2000 K for X-rays showed that in the case of Li_2O, the M–M pairs do not contribute significantly due to a small scattering amplitude of Li atoms. For sodium and potassium oxides, the contribution of the M–M pairs is greater. The highest TPCF peak is due to the M–O pairs. However, because of the mutual interference of the PPCF oscillations the corresponding TPCF are close to unity already at distances longer than 0.5 nm.

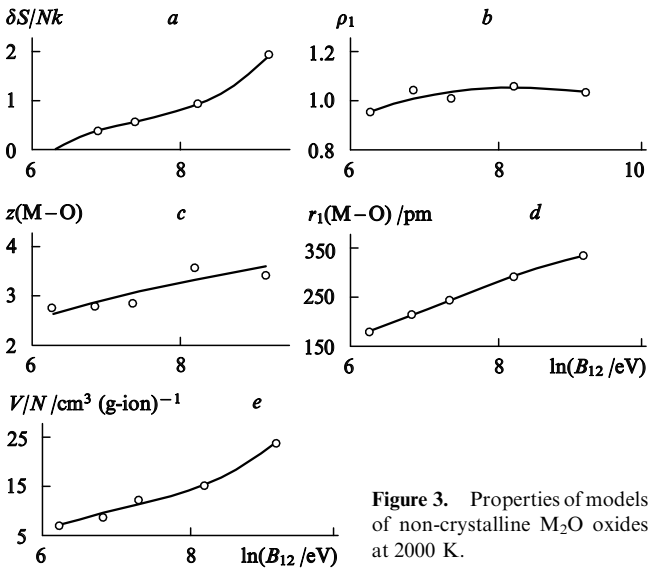


Figure 3. Properties of models of non-crystalline M_2O oxides at 2000 K.

The mean CN for the M–O pairs also increase as B_{12} increases, *i.e.* with an increase in size of M^+. In crystals, $z(M-O)$ is equal to 4, and melting or amorphisation is accompanied by a decrease in the CN of the M–O pairs. For the entire M_2O series, the range $2.6 < z(M-O) < 3.6$ is typical. Distributions of $z(M-O)$ become broader with the increase in B_{12}.

$z(M-O)$	2	3	4	5	6
Number of ions at					
B_{12} = 545.3	81	85	–	–	–
1601.9	48	88	30	–	–
3844.1	6	63	85	11	1
9999.0	8	71	76	10	1

For a broad distribution of CN, it is impossible to isolate any stable element of the structure, and the system should resemble more or less dense packing of spheres with different diameters. The broad distributions of O–M–O and M–O–M azimuthal angles also point to this fact.

Temperature only slightly affects the structure of the oxides. The $r_1(M-O)$ distances change insignificantly, but for the M–M and O–O pairs they increase noticeably with heating due to the thermal expansion. The ratio of molar volumes $V_{2000\ K}/V_{0\ K}$ for $B_{12} = 545.3$ eV is equal to 1.08 (for Li_2O), 1.16 (for Na_2O), and 1.12 (for K_2O). An important role of the temperature is due to the fact that E_{kin} at 2000 K makes a noticeable part of E (from 2.6% for Na_2O up to 4.1% for K_2O).

The topological coefficient ρ_1 increases from 0.95 to 1.06 as B_{12} increases (see Fig. 3), while the s coefficient decreases from 1.17 to 1.00. Therefore, structures of the oxides with $B_{12} >$ 1600 eV (including Na_2O, K_2O, Rb_2O) are close to the dense one. That is why it is difficult to prepare these compounds in a glass state.

If M–O distance in non-crystalline M_2O oxides is suggested to be equal to the sum of ion radii and usual values are taken for M^+ ions (*viz.*, 68 pm for Li^+, 98 pm for Na^+, 133 pm for K^+, and 149 pm for Rb^+), then the radius of O^{2-} appeared to be 118±7.7 pm, which is in agreement with the estimates of its crystallographic radius on the fluoride scale (121–128 pm).[140] Thus the approximate value of the radius is 120 pm.

Analysis of the thermodynamic properties of the oxide models was performed.[135] Comparison of experimental values for total energy of M_2O crystals with the results of simulations at $B_{11} = 0$ and $B_{22} = 1500$ eV (taking account of only Coulomb interactions and electron shell repulsion) demonstrated that the difference is 12% for Li_2O and gradually decreases to 4% for Cs_2O.

Oxide	Li_2O	Na_2O	K_2O	Rb_2O	Cs_2O
$-E$ (calc.) /kJ $(g\text{-ion})^{-1}$	1020.1	852.9	770.5	740.2	695.7
$-E$ (exp.) /kJ $(g\text{-ion})^{-1}$	910.8	788.2	738.0	692.4	667.4

The deviations are probably caused by the fact that the R_{M-O} parameter for light ions differs from the conventional value of 29 pm. In principle, the agreement between the experimental and simulated results may be improved by adjusting the R_{ij} values specifically for each oxide. A contribution of covalent interactions to the potential, which decreases for heavier Group I cations and which was not taken into account in the simulation, may be another reason for the deviations.

Amorphisation energies ΔE_{am} for the models decrease from 40 kJ $(g\text{-ion})^{-1}$ for Li_2O to 14 kJ $(g\text{-ion})^{-1}$ for Cs_2O (see Ref. 135). Heats of melting [from 19.7 kJ $(g\text{-ion})^{-1}$ to 6.4 kJ $(g\text{-ion})^{-1}$] are 1.6–3.4-fold less than ΔE_{am} and also gradually decrease as B_{12} increases. The ratio of volumes of amorphous and crystalline phases also changes analogously. Amorphisation of a model of a Li_2O crystal at 0 K is accompanied by an increase in the volume by 34%, and for model of Cs_2O by 4%. These features of amorphisation are due to structural changes. Amorphisation of Cs_2O is accompanied by a decrease

in the mean CN for the M−O pairs from 4 to 3.6; for Li_2O, the CN for the M−O pairs decreases to 2.5.

The change in the Gibbs energy along the homologous series may be calculated using the expression [138]

$$\delta G_y = \int_{y_1}^{y_2} \langle U_{12} \rangle \mathrm{d}y \,, \tag{11}$$

where $y = \ln(B_{12})$, y_1 and y_2 refer to the initial and final states, $\langle U_{12} \rangle$ is the mean equilibrium value of energy of electron shell repulsion of the M−O pairs. In (11), the integration is performed at constant pressure and temperature. Using the values of $\langle U_{12} \rangle$ obtained from the molecular dynamic experiments, the value of δG_y may be calculated. Further, taking into account that $\delta G = \delta E + p\delta V - T\delta S$, the change in entropy δS for each member of the series may be determined. The change in $\delta S/Nk$ is shown in Fig. 3: as B_{12} increases, the configurational entropy of the oxide (at a constant mass of M^+ ion) increases monotonically, *i.e.* gradual disordering of the structure takes place, which is manifested particularly in the broadening of CN distributions. The maximum change in entropy for the system considered is $\sim 2Nk$.

The term δS_y represents only the configurational part of the change in entropy. If the mass of m_i ion is changed to m_j on going from one oxide to another, then the contribution

$$\delta S_m = \tfrac{3}{2} Nk X_M \ln(m_j m_i^{-1}) \,,$$

has to be added to the value of δS_y, where $X_M = 2/3$ is the ionic contribution of the M^+ ion.

2. Models of non-crystalline oxides in the MO series

MO series includes such important components of industrial slags and glasses as MgO, CaO, SrO, BaO, and probably BeO, FeO, MnO, PbO, *etc*. The first model of CaO composed of 216 ions was constructed using MD and CSR methods with the pair potentials (1) and the following parameters: $B_{11} = 0$, $B_{12} = 3283$, $B_{22} = 1500$ eV, and $R_{ij} = 29$ pm.[65] The value of B_{22} was adjusted so as the O−O distance in the models of calcium and iron silicates was close to the values determined by diffraction methods (~ 323 pm, see Ref. 141). For the Ca−O pairs, the parameter $B_{12} = 3283$ eV was from the density of crystalline CaO. The electrostatic energy appeared to be -4037 kJ mol^{-1}, and the energy of electron shell repulsion was 483 kJ mol^{-1}. The total energy (not accounting for zero vibrations) was equal to -3554 kJ mol^{-1}, which is in reasonable agreement with the experimental value[65] of the energy of the crystal (-3378 kJ mol^{-1}); the difference being 5.2%. The modulus of bulk compressibility was 171 GPa compared to the experimental value of 115 GPa. Therefore, the Born–Meyer potentials are not quite precise, but they can be used for construction of models.

An investigation of models of non-crystalline MO oxides (composed of 216 ions) was performed.[103, 142] The Coulomb interactions were taken into account using the Ewald–Hansen method.[39] The models with $B_{12} = 400-800$ eV describe hypothetical oxides with very small M^{2+} ions. Models corresponding to MgO, FeO, CaO, SrO, and BaO have B_{12} equal to 1441.4, 1900.0, 3283.0, 4744.1, and 8885.1 eV, respectively. The B_{12} values were determined from the experimental lattice parameters. The calculated values of energy of the crystals using the Born–Meyer potential was lower than corresponding experimental values by 2.2%–5.8%. This difference indicates a certain inaccuracy of the potentials (1).

A model of amorphous phase at 0 K was constructed using the MD method starting from a random initial state.[103, 142] Then the temperature was increased up to 2000 K by the MD method and the system was relaxed during several hundreds steps to reach the equilibrium state. Some models were constructed with the use of the previous ones with other B_{12} values. The amorphisation energies [45–65 kJ (g-ion)$^{-1}$] were calculated as differences between energies of the amorphous phase and the crystal. Their ratios to the heats of melting of the corresponding oxides increased from 1.18 to 1.84 on going from MgO to BaO. The amorphisation was accompanied by a substantial increase in a volume of crystal (by 17% for BaO and 38% for MgO).

Dependencies of V/N, $r_1(ij)$, mean CN z(M−O), ρ_1, and $\delta S/Nk$ on B_{12} are shown in Fig. 4. An increase in B_{12} results in a monotonic increase in the M−M and M−O distances, while the O−O distance changes non-monotonically. The volume of oxides passes through a minimum at $B_{12} = 800-1900$ eV.

The reason for the appearance of the minimum can be understood when the change in the CN of M−O pairs is considered. As it is seen from Fig. 4, if $B_{12} \leqslant 500$ eV then CN equals 2 and the system has a chain structure. The O−M−O and M−O−M azimuthal angles at 2000 K are close to 160° and correspond to the zigzag −M−O−M−O− arrangement of the ions. Analysis of distribution of CN demonstrated that when $B_{12} \leqslant 500$, virtually all M^{2+} ions have two neighbours (O^{2-} ions) and vice versa. The distance r_1(M−O) is 110-120 pm. In the case of M^{2+} ion with the smallest size (Be), the distance is 180 pm in the crystal and 151 pm in the amorphous oxide. Therefore, models with $B_{12} \leqslant 500$ eV are hypothetical.

An abrupt decrease in the molar volume when the value of B_{12} approaches 800 eV is caused by a rapid increase in the CN of the M−O pairs from 2 to 3. When CN is 3, a layered trigonal structure appears. The O−M−O and M−O−M angles are 108–112°, *i.e.* the closest neighbours of M(or O) ions occupy vertices of strongly flattened trigonal pyramids. The contribution of ions with z(M−O) = 2 or 4 is relatively small (< 30%), thus oxides with $B_{12} = 800$ eV have rather ordered structures.

The transition to $B_{12} \geqslant 1900$ eV results in a substantial broadening of distribution of CN for the M−O pairs, and the mean CN approaches the value of 6, typical of the MO crystal lattice. In the range of $B_{12} = 1441-1900$ eV, the CN is almost constant [z(M−O) = 4.14–4.90], and consequently the molar volume changes only slightly. This is probably due to the high stability of the structure with $z = 4$ and a tetrahedral coordination of ions. However, this coordination is observed only as a mean value since the distributions of CN z(M−O) in MgO and FeO models are rather broad.

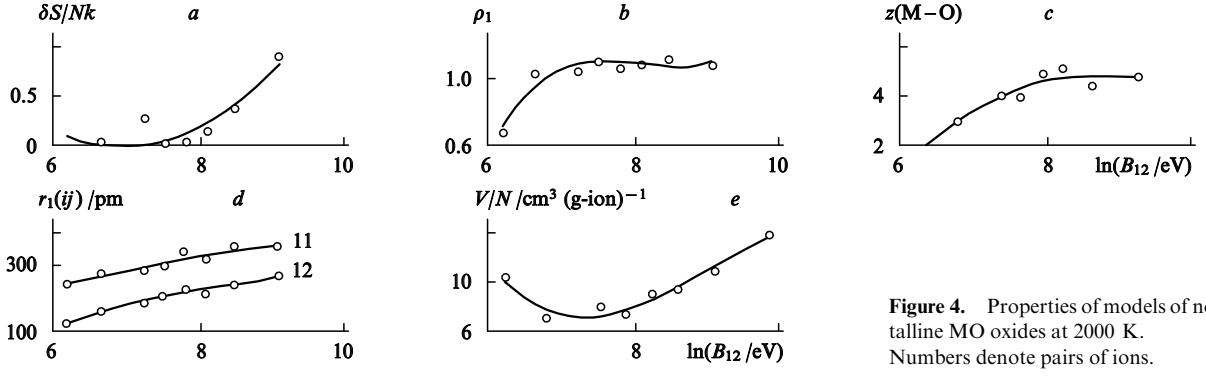


Figure 4. Properties of models of non-crystalline MO oxides at 2000 K.
Numbers denote pairs of ions.

z(M–O)	3	4	5	6	7
Number of M ions					
for a model of MgO	12	74	22	–	–
for a model of FeO	1	26	61	19	1

Temperature affects the structure of oxides relatively little, since even at 2000 K the thermal energy is only 1.0% – 1.7% of the total energy. The mean heat capacity for all models [19.8 – 26.6 J (g-ion K)$^{-1}$] is close to the classical value $3R$ = 24.9 J (g-ion K)$^{-1}$.

The value of the topological parameter ρ_1 is low for models with $B_{12} \leqslant 800$ eV (see Fig. 4), *i.e.*, the corresponding structures are rather loose. The s parameter is 2.68 for B_{12} = 500 eV and even 4.00 for B_{12} = 400 eV. However, the MgO model already has a quite dense structure (ρ_1 = 1.04 at 2000 K and 1.05 at 0 K). Other models have ρ_1 = 1.07 – 1.08 and s = 1.00 – 1.07. These structures are topologically dense, which accounts for the difficulty in obtaining the real MO oxides in a glassy state.

The properties of models with $B_{12} \leqslant 800$ eV vary with a substantial hysteresis.[142] A model constructed with B_{12} = 500 eV from a random initial state by the CSR method gave a molar volume of only 5.85 cm^3 (g-ion)$^{-1}$ and an energy of −2394.4 kJ (g-ion)$^{-1}$. Its annealing (2000 K) is accompanied by an increase in the volume up to 11.2 cm^3 (g-ion)$^{-1}$. For simulation of this process, more than 1000 steps of the MD method were required. After cooling to 0 K using the CSR method and subsequent relaxation, the volume was equal to 11.4 cm^3 (g-ion)$^{-1}$. The energy of this state is 18.3 kJ (g-ion)$^{-1}$ lower that that of the initial state. At higher B_{12} values, the hysteresis effects are almost unnoticeable. They are typical of loose structures and their nature is similar to the processes that occur in the compacting of silica.

Changes in the Gibbs energies and entropies on moving along the MO series were calculated as for M_2O.[142] This required that the integration of repulsion energies $\langle U_{12} \rangle$ was performed according to the equation (11). It was demonstrated, that the configurational entropy of oxides at 2000 K virtually does not change in the range $500 \leqslant B_{12} \leqslant 2550$ eV and begins to increase when $B_{12} >$ 2550 eV. This growth is caused by broadening of distributions of CN and azimuthal angles and by the increase in the degree of disordering on going from loose to the topologically dense systems.

3. Models of non-crystalline oxides in the M_2O_3 series

A series of models for amorphous and liquid M_2O_3 oxides was constructed with the potentials (1) and parameters B_{12} = 580 – 5000 eV. The value of 800.0 eV corresponds to boron oxide, 1479.86 to Al_2O_3, 2114.2 and 2453 to Fe_2O_3; other models correspond to hypothetical oxides. Data for the three above-mentioned compounds have already been discussed. A collapse in this series occurs when B_{12}^{cr} = 550 eV; the lowest value of 580 eV only slightly exceeds the critical one.

All models contained 500 ions in the basic cube. The edge length of the basic cube was selected so as to give the pressure close to zero. Fig. 5 shows the characteristics of the models in the M_2O_3 series at 2000 K. The r_1(M–M) and r_1(M–O) distances depend almost linearly on lnB_{12}. The molar volume of the oxide has a deep minimum at $B_{12} \simeq 1480$ eV. The first members of the series have the mean values of CN equal to 3. This value increases monotonically up to ~ 5.9 when B_{12} = 5000 eV. As in the case of the MO series, the minimum of the molar volume is due to a rapid increase in the CN and a rearrangement of the structure in the range 1150 – 1480 eV.

Distributions of CN for the M–O and O–M pairs are the most narrow when B_{12} = 590 and 800 eV and rapidly broaden at larger B_{12} values. Boron oxide is the most ordered in the configurational sense. The value of z(M–O) = 4 can be obtained for an oxide with B_{12} = 1195 eV. In such an oxide, the values of z(O–M) equal to 2 and 3 have to occur in the ratio 1 : 2, which does not allow one to provide as good ordering of the oxygen subsystem as in boron oxide, where z(O–M) = 2.00.

Data on CN are confirmed by the character of the distributions of azimuthal angles. At 2000 K, these distributions are as follows:

B_{12} /eV	θ(O–M–O) /deg	θ(M–O–M) /deg
580	121.7 ± 14.9	160.1 ± 10.1
800	119.3 ± 10.2	153.2 ± 19.2
1480	106.9 ± 23.3	121.1 ± 18.6
2453	105.4 ± 26.9	113.1 ± 19.6
5000	98.8 ± 28.0	108.4 ± 23.5

The O–M–O angle approaches 90° at higher B_{12} values, which roughly corresponds to an octahedral packing of the closest neighbours. In this case, z(M–O) ≃ 6 and z(O–M) ≃ 4, *i.e.* the surrounding of the oxygen atom by the metal atoms is almost tetrahedral. This is in keeping with the mean M–O–M angle (109°), which is therefore close to that of the ideal tetrahedron.

Taking into account that the effective radius of the O^{2-} ion for non-crystalline oxides is ~ 120 pm (see above), the radii of the M^{3+} ions can be calculated for B_{12} from the plot of r_1(M–O) depicted in Fig. 5. The model with B_{12} = 3500 eV corresponds to the oxide with the ionic radius of 92 pm. The radii of Y^{3+} and Tl^{3+} ions (93 and 95 pm, respectively) are close to this value. A system with B_{12} = 5000 eV corresponds to an ion with a radius of 108 pm, which is close to the radius of La^{3+} (115 pm). Further increase in B_{12} results in a region of unreal hypothetical large cations.

The topological characteristics (ρ_1 and s) in the M_2O_3 series indicate a noticeable looseness of the models with B_{12} = 580 eV (0.695 and 3.50, respectively) and with 800 eV (0.787 and 2.34). Nevertheless, the model of Al_2O_3 is almost dense (ρ_1 = 1.056 and s = 1.16). On further movement along the series the structure of oxides remains topologically dense.

The changes in the configurational Gibbs energy and entropy were calculated for the M_2O_3 series according to the equation (11). Dependence of $\delta S/Nk$ on B_{12} is shown in Fig. 5. When $B_{12} >$ 2453 eV, the entropy is virtually constant and δS_y = 9.6±0.9 J (g-ion K)$^{-1}$. A decrease in B_{12} to 800 eV and transition to a more ordered layered structure of boron oxide is accompanied by a decrease in the configurational entropy. Further decrease in B_{12} results in a slight increase in the entropy due to

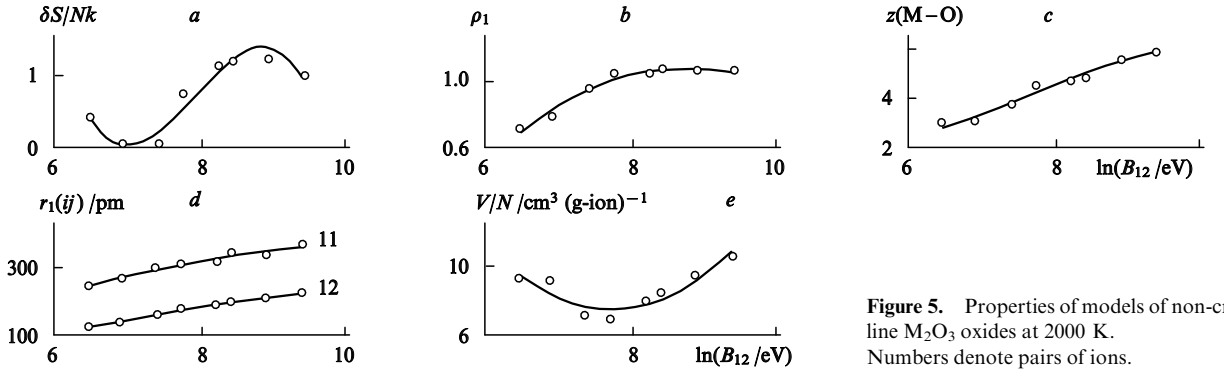


Figure 5. Properties of models of non-crystalline M_2O_3 oxides at 2000 K.
Numbers denote pairs of ions.

greater disorder because of the broadening of CN distributions mentioned above.

4. Models of non-crystalline oxides in the MO_2 series

Non-crystalline oxides of the MO_2 series include silica and a glass-forming GeO_2 oxide. It is also possible to obtain glassy TeO_2 by quenching it between rotating cylinders.[131] Such oxides as TiO_2, SnO_2, and ZrO_2 do not form glasses on ordinary cooling of a liquid.[143]

Glassy SiO_2 and GeO_2 have been intensely studied by diffraction methods. The $r_1(ij)$ distances for GeO_2 were determined using anomalous X-ray scattering: $r_1(Ge-Ge) = 310-320$ pm, $r_1(Ge-O) = 160$ pm, $r_1(O-O) = 280$ pm.[144] The following r_1 distances for glassy GeO_2 were reported:[143] 315–345 pm for Ge–Ge pairs, 170–174 pm for the Ge–O pairs, and 283–285 for the O–O pairs. The mean CN for the Ge–O pairs lies in the range of 3.9–4.0. The mean Ge–O–Ge azimuthal angle is 133° (see Ref. 145). In an $Na_2O \cdot 4GeO_2$ glass, the Ge–O distance is 180 pm.[146] For pure TeO_2, no diffraction data were found. For a glass of composition $V_2O_5 \cdot 9TeO_2$, neutron diffraction gave the Te–O distances of 192 pm ($z = 2.71$) and 216 pm ($z = 0.85$ pm).[120] In a SiO_2-TiO_2 glass (< 10 mol.% of TiO_2), the Ti–O distance appeared to be equal to 189–191 pm.[146]

Models for MO_2 oxides composed of 498 ions in the basic cube were constructed using the MD and CSR methods at 0 K and 2000 K.[53] The pair potentials (1) were applied with the following parameters: $Z_1 = +4$, $Z_2 = -2$, $B_{11} = 0$, $B_{22} = 1500$ eV, $R_{ij} = 29$ pm. Since for this series $B_{12}^{cr} = 734$ eV, the values of B_{12} were chosen in the range of 850–8000 eV; the values $B_{12} = 1729.5$ eV and 1848 eV were proposed for silica and for simulations of the Si–O pairs in silicates, respectively.[84]

Figure 6 shows the characteristics of MO_2 models as the function of B_{12}. The distance of $r_1(M-O)$ depends linearly on $\ln B_{12}$. The M–M and O–O distances also increase with increase in B_{12}. When $B_{12} = 850$ eV, $z(M-O) = 3.70$. Extrapolation of the curve in Fig. 6*c* to the stability limit gave $z(M-O) = 3.5$, *i.e.* CN of 3 and 4 are equiprobable.

Distributions of CN for the M–O pairs in the models have the following form:

z(M–O)	3	4	5	6	7	8	9	Mean CN
Number of M^{4+} ions								
at B_{12} = 850.0	50	116	–	–	–	–	–	3.70
1729.5	7	152	7	–	–	–	–	4.00
3500.0	–	12	58	80	15	1	–	5.61
8000.0	–	–	1	47	86	30	1	6.91

The increase in B_{12} (*i.e.* the increase in the size of an M^+ ion) is accompanied by a increase in the mean CN for the M–O pairs and broadening of its distribution. The MO_2 structure rearranges in the range $750 < B_{12} < 1000$ eV, when the trigonal structural elements are replaced by tetrahedral ones. A small minimum of the molar volume near $B_{12} = 1250$ eV (see Fig. 6*e*) is due to the rearrangement. A similar process is typical of oxides of the MO series in the range $800 < B_{12} < 1440$ eV (see above).

The next rearrangement of the structure occurs in the range $2000 < B_{12} < 3000$ eV. Here, $z(M-O)$ increases abruptly up to 6 (see Fig. 6*c*), the distribution of $z(M-O)$ becomes substantially broader, and the elements of the tetrahedral networks typical of silica disappear. Further increase in B_{12} does not lead to any new structural rearrangement.

These results agree with the results of analysis of the azimuthal angle distribution. When $B_{12} \leqslant 1848$ eV, the mean O–M–O angle is close to the tetrahedral one, and the θ(M–O–M) angle is 156–160°. Similar distributions were obtained for silica (see above). Further increase in B_{12} is accompanied by a decrease in the mean value of O–M–O and M–O–M angles, but their distributions broaden by a factor of 2–3. The values of topological parameters ρ_1 (see Fig. 6*b*) and s indicate that the structures of oxides in the MO_2 series are loose when $B_{12} < 3500$ eV and close to the dense one when $B_{12} \geqslant 5000$ eV.

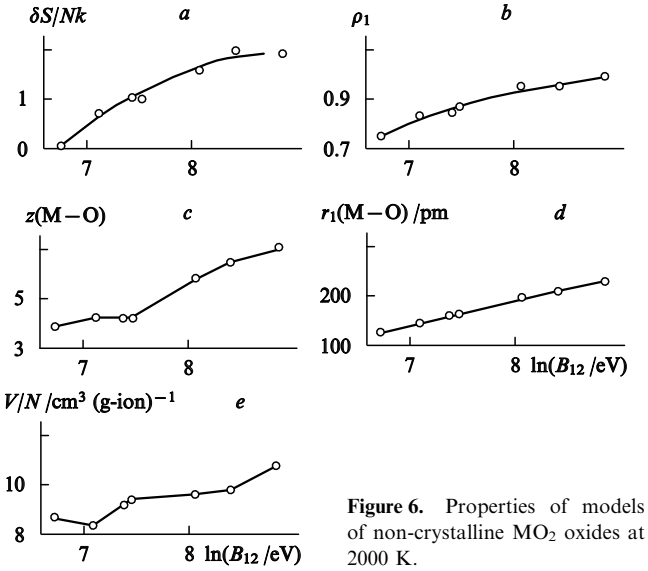


Figure 6. Properties of models of non-crystalline MO_2 oxides at 2000 K.

Comparison of the models with the real oxides in respect of $r_1(M-O)$ distances and M^{4+} ion radii was performed.[53] Oxides with $B_{12} < 1700$ eV are hypothetical. The value of $B_{12} = 2080$ eV corresponds to GeO_2, 2940 eV to TiO_2, and 3410 eV, to TeO_2. A model with $B_{12} \simeq 3500$ eV corresponds to ZrO_2 and with, $B_{12} \simeq 5000$ eV to UO_2. An intermediate value (between 5000 and 8000 but closer to 5000 eV) corresponds to CeO_2.

An increase in temperature from 0 to 2000 K affects insignificantly the structure of the models. Positions of TPCF peaks do not virtually shift and their heights decrease only slightly. Coordination numbers for the M–O pairs also insignificantly depend on temperature. This is due to the fact that even at 2000 K the thermal energy of the oxides is very small compared to their total energy (0.5%–0.7%). The thermal expansion coefficient is also very small and almost equal to zero when $B_{12} = 8000$ eV.

The changes in the Gibbs energy and entropy along the MO_2 series were calculated [53] using the equation (11). The magnitude of $\delta S/Nk$ increases monotonically as in the M_2O and MO series (see Fig. 6*a*).

The relation between the topological looseness of oxide structures and their tendency to glass formation has been discussed above. Since SiO_2 and GeO_2 readily form glasses on ordinary cooling of a liquid, and TiO_2, SnO_2, and ZrO_2 do not form glasses, the value $B_{12} \simeq 2500$ eV may be selected as the limit of glass formation. The $\rho_1 = 0.92$ and $s \simeq 1.25$ coefficients correspond to this point. An estimate of ρ_1 from the plot (see Fig. 6*b*) for TeO_2 gives $\rho_1 = 0.94$ at $B_{12} \simeq 3410$ eV, which only slightly exceeds this limit (0.92). This is in accordance with the fact that pure TeO_2 does not form a glass on ordinary cooling of a liquid but does form it on quenching between rotating cylinders.

5. Models of non-crystalline oxides in the M_2O_5 series

Non-crystalline oxides of the M_2O_5 series include such compounds as P_2O_5 and V_2O_5 along with As_2O_5, Nb_2O_5, Ta_2O_5, etc. Among these oxides, only P_2O_5 and V_2O_5 form glasses on ordinary cooling of a liquid, and niobium and tantalum oxides do not form glasses even on quenching between rotating cylinders.[131] The properties of P_2O_5 and V_2O_5 models were described above. There are very few diffraction data on the structures of melts and glasses containing M_2O_5 oxides. The structure of an $Nb_2O_5 \cdot 2B_2O_3 \cdot 2K_2O$ glass was studied by XRD; the values of 190, 311, 317, and 385 pm were obtained for the Nb–O, Nb–B, O–O, and Nb–Nb distances, respectively.[147] The mean CN for the Nb–O pairs is ~ 6.0. The structure of the oxide contains a network of cyclic elements with six- and four-membered groups, such as NbO_6, BO_3, and BO_4.[147]

Thus, the data on the structure of non-crystalline oxides of this series are quite fragmentary. There have been only a few studies on their thermodynamic properties. The Physicochemical properties of the non-crystalline M_2O_5 oxides were studied[123] using MD method. The potentials (1) were used with the following parameters: $Z_1 = +5$, $Z_2 = -2$, $B_{11} = 0$, $B_{22} = 1500$ eV, and $R_{ij} = 29$ pm. The dipole-dipole and dipole-quadrupole interactions were not taken into account. The critical value $B_{12}^{cr} = 918$ eV, so the models were constructed for the range of $B_{12} = 950-8000$ eV.[123] Spherically symmetrical potentials provide the equivalence of all M–O bonds, which is typical of non-crystalline oxides. Each model comprised 497 ions. The Coulomb interactions were taken into account using the Ewald–Hansen method.[39] The edge length parameter of the basic cube was adjusted to maintain the pressure close to zero.

In order to examine the presence of hysteresis phenomena in the oxides, after heating of the system up to 2000 K its cooling to 0 K was simulated. The calculated energy appeared to be somewhat lower than the corresponding value for the initial models constructed using the CSR method (by $\sim 0.5\%$). It was shown that temperature insignificantly affects the properties of the oxide models. At zero pressure, the volume of the system increases by not more than 2% when the temperature changes from 0 K to 2000 K. In this respect, M_2O_5 oxides are similar to the MO_2 oxides. Positions of the TPCF peaks do not shift when the temperature is increased but the peaks become broader and less intense. The values of CN for the M–O pairs also change only slightly, as well as the position of the centres and widths of the O–M–O and M–O–M azimuthal angle distributions. The thermal energy is only 0.4%–0.6% of the total energy.

Figure 7 shows the dependences of the simulated characteristics for M_2O_5 oxides on B_{12}. The molar volume has a deep minimum at $B_{12} = 1500$ eV. The mean CN for the M–O pairs increases from 3.6–4.0 at $B_{12} = 950$ eV to 7.4–7.9 at $B_{12} = 8000$ eV. Such changes of the characteristics indicate a substantial structural rearrangement in the range of B_{12} values from 950 eV to 2500 eV. The structure of the first oxide ($B_{12} = 950$ eV) is intermediate between continuous random network with $z(M-O) = 4$ and layered trigonal [$z(M-O) = 3$] structures. Distributions of $z(M-O)$ in the M_2O_5 oxides are as follows:

z(M–O)	3	4	5	6	7	8	9	10
Number of M^{4+} ions								
at B_{12} = 950	59	83	–	–	–	–	–	–
1500	–	76	63	3	–	–	–	–
2500	–	20	98	24	–	–	–	–
3500	–	11	93	38	–	–	–	–
5000	–	–	24	76	36	5	1	–
8000	–	–	–	17	61	49	14	1

When $1500 \leqslant B_{12} \leqslant 3500$ eV, the distributions of $z(M-O)$ are limited by 4–6, but at $B_{12} \geqslant 5000$ eV their distribution becomes noticeably broader and shifts towards the greater values. A trigonal bipyramid with $z(M-O) = 5$ dominates as a structural element only in the range of B_{12} values from 2500 eV to 3500 eV.

Comparison of the models constructed with the real M_2O_5 oxides can be performed by the analysis of the $r_1(M-O)$ distances. For liquid V_2O_5, this distance is close to 180 pm. The curve on Fig 7 *d* allows one to estimate the value of B_{12} as ~ 2980 eV. An estimate made from the density of the crystal at 0 K and $p = 0$ gives a close value (2970 eV). A radius of 120 pm may be taken for O^{2-} ion. In this case, the difference $r_+ = r_1(M-O) - 120$ pm indicates that B_{12} is ~ 1800 eV for P_2O_5, 2400 for As_2O_5, 3360 for Sb_2O_5, 3940 for Nb_2O_5, 3940 for Ta_2O_5, and 4230 eV for Bi_2O_5. Therefore, the range of B_{12} from 1800 to 4230 eV corresponds to the real M_2O_5 oxides. And consequently, models with $B_{12} \leqslant 1500$ or $B_{12} \geqslant 5000$ eV are hypothetical. For models of real oxides, the distributions of $z(M-O)$ are such that the ordering type can not be described by an alternation of certain elements, a like trigonal bipyramid or an octahedron as it was suggested for V_2O_5.[51] An

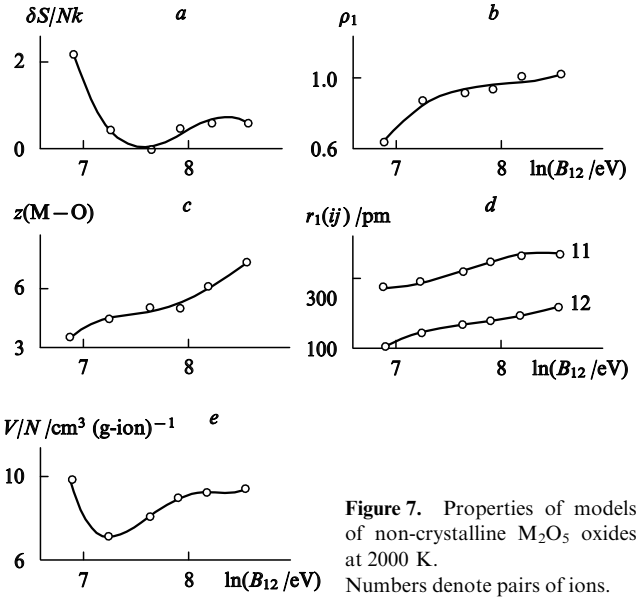


Figure 7. Properties of models of non-crystalline M_2O_5 oxides at 2000 K.
Numbers denote pairs of ions.

oxide with $B_{12} = 2500$ eV (the closest real oxide is As_2O_5) occupies the best position: for this oxide the distribution is almost symmetrical relative to $z(M-O) = 5\%$ and 69% of M^{5+} ions have exactly five O^{2-} neighbours.

It should be kept in mind that distributions of CN of the M–O pairs in real oxides may be more narrow than in the corresponding models. In general, relatively small models of non-crystalline substances composed of several hundreds or thousands particles contain more 'defects' per atom than the real substances. This fact has been established for amorphous silicon and germanium but it also holds for other oxides. The reason for the higher defectiveness is boundary conditions in the basic cube. Presumably, the same reason causes very slow (compared to the real oxide) decrease in the self-diffusion coefficients in the models on cooling.

According to the values of ρ_1, all M_2O_5 oxides have loose structures, especially in the cases when $B_{12} < 5000$ eV (see Fig. 7 *b*). This is typical of all real M_2O_5 oxides. The reason for the looseness is presumably the unfavourable stoichiometry (seven atoms per molecule), which cannot exist in more or less regular networks.

Substantial complication of the oxide structures with an increase in B_{12} is accompanied by a small decrease in the mean value of the O–M–O azimuthal angle (from 110 to 100°). However, the width of distribution of this angle increases from 18 to 31°. The value of M–O–M angle changes along the series much more strongly (from 165 to 116°), and the distribution width is doubled. In well-ordered network structures of B_2O_3 and SiO_2, the widths of angle distributions obtained in computer simulations were usually 8–10°. This feature also does not permit reliable conclusions on the presence of distinct structural elements in M_2O_5 oxides.

The looseness of structures is clearly seen in the visual study of spatial models constructed from balls of different diameters with the coordinates taken from the results of computer simulations of the oxides. For instance, large irregular pores situated between such groups as MO_4, MO_5, or MO_6 linked through shared vertices, can be seen in a spatial model built based on a calculation for $B_{12} = 2500$ eV. The surface of the pores is formed by oxygen ions and their repulsion stabilises the shape of pores. The packing of O^{2-} ions does not contain any linear or layered elements.

The maximum pore size was 163 pm, *i.e.* a positive ion or a neutral atom of a relatively large size may easily occupy the pore. In the model, six pores with radii > 140 pm, six pores with radii between 130 and 140 pm, *etc.* were found. These results, in particular, allow one to estimate the solubility of noble gases in

the oxides. An analysis of bound groups showed that all M_2O_5 oxides are completely polymerised (in terms of the polymer theory of slags).

According to Fig. 7*b*, for V_2O_5 with $B_{12} = 2970$ eV, $\rho_1 \simeq 0.96$, and for Nb_2O_5 and Ta_2O_5 with $B_{12} = 3940$ eV, $\rho_1 \simeq 1.00$. Thus, the glass formation limit for the M_2O_5 oxides lies in the range $0.96 < \rho_1 < 1.00$ (ρ_1 0.97) that is slightly higher than for the MO_2 oxides. This shift is due to a more complex structure of the M_2O_5 oxides. Therefore, P_2O_5, V_2O_5, As_2O_5, and Sb_2O_5 should readily form glasses but liquid Bi_2O_5 should not form a glass on ordinary cooling in air, since the estimate of ρ_1 for this oxide is $\sim 1.0-1.1$.

The changes in the configurational entropy along the M_2O_5 series were calculated using the equation (11). The entropy initially decreases with the increase in B_{12} and then goes through a shallow minimum at $B_{12} \simeq 2500$ eV (see Fig. 7*a*). This minimum is due to the fact that the distribution of CN for the M–O pairs is rather narrow and almost symmetrical with its centre close to 5.0 for $B_{12} = 2500$ eV. When $B_{12} < 2500$ eV, the structure of oxide becomes more complex, since $z(M-O) = 4$ and 5 are almost equally probable. At $B_{12} > 3500$ eV, the CN distribution width rapidly increases, resulting in the increase in entropy. When $B_{12} \geqslant 5000$ eV, the width of CN distribution and the configurational entropy remain almost unchanged.

6. Models of non-crystalline oxides in the MO_3 series

Oxides of the MO_3 series include such components of glasses and metallurgic slags as CrO_3, MoO_3, and WO_3. Pure MoO_3 and WO_3 form glasses on ordinary cooling of melt,[143] as well as on flattening.[131] There are very few diffraction data on the structure of the MO_3 oxides. Thus, the structural information on complex oxides should be used. The study on the structure of Na_2O-WO_3 glass [126] was already cited.

A series of computer models for MO_3 oxides at 0 and 2000 K was constructed using the MD and CSR methods.[130] All models contained 500 ions in the cube. The potentials (1) with the following parameters were applied: $Z_1 = +6$, $Z_2 = -2$, $B_{11} = 0$, $B_{22} = 1500$ eV, $R_{ij} = 29$ pm. The critical value of B_{12} for this series is 1101 eV. Therefore, the values of B_{12} were chosen in the range of 1150–9999 eV. The models were constructed in a way similar to other M_mO_n series. The Coulomb interactions were taken into account using the Ewald–Hansen method.[39] The edge length of the basic cube was adjusted to maintain the pressure close to zero.

A model with $B_{12} = 1150$ eV was in a special position. The pressure in the system remains positive at 2000 K and at any volume, which means that the system was in the state of a strongly compressed gas. In vacuum, this gas contains the MO_3 molecules with ionic bonding in the form of centred regular triangles. Visual analysis of a spatial model constructed on the base of results of computation with $B_{12} = 1150$ eV demonstrated that the oxide is composed of separate MO_3 groups, which represent almost planar triangles with the M^{6+} ions in their centres. The planes of the triangles are randomly oriented, however there is a tendency on a rotation of one of the vertices towards the centre of the neighbouring triangle. This arrangement gives a gain in energy. Many large pores and cavities were found in the model. The MO_3 groups are aggregated into clusters of 4–5 groups, and the clusters are relatively remote from each other.

The dependencies of the characteristics for the MO_3 models on B_{12} are shown in Fig. 8. The $r_1(ij)$ values increase monotonically with increase in B_{12}, the molar volume goes through a minimum at $B_{12} \simeq 3400$ eV. As in the case of other oxides, this minimum is due to a rapid increase in CN for the M–O pairs from 3.00 at $B_{12} = 1150$ eV to ~ 6 at $B_{12} = 3400$ eV and further up to ~ 8.0.

At $B_{12} = 3400$ eV, the M–O distance is 179 pm, which almost coincides with the W–O distance in tungstenate glasses. So far, this model can be attributed to WO_3 oxide. In fact, in addition to $r_1(M-O)$, the mean CN for the M–O pairs (6.0) also coincides with the experimental data.[126] However, the distribution of $z(M-O)$ reveals that CN equal to 5 and 7 are also present in the models, though the value 6 (octahedral arrangement) dominates.

$z(M-O)$	4	5	6	7	8	9	10
Number of M^{6+} ions							
with $B_{12} = 1850$	41	66	17	–	–	–	–
3000	–	27	93	5	–	–	–
4800	–	13	97	15	–	–	–
9999	–	–	5	31	59	26	4

When $3000 \leqslant B_{12} \leqslant 4800$ eV, the majority of O^{2-} ions have two neighbouring M ions and they play a role of bridging particles linking two neighbouring MO_n groups. Only at $B_{12} = 9999$ eV, do the majority of O^{2-} ions have three M neighbours. As regards the $z(ij)$ distribution, the oxide structure with $B_{12} = 4800$ eV is the most ordered.

Distributions of CN for the O–O pairs have specific features. When $B_{12} \geqslant 3400$, they have an usual form with a maximum near $z(M-O) = 8-9$. However, when $B_{12} \leqslant 1850$ eV, these distributions exhibit two maxima at $z = 3-4$ and $6-7$. The first maximum is especially high for the model with $B_{12} = 1150$; it is attributed to the above-mentioned configuration, in which a vertex of one of the MO_3 triangles is directed towards the centre of another triangle. The first maximum is assigned to O^{2-} ions that do not link the two triangles. The second maximum is assigned to the bridging O^{2-} ions. An increase in B_{12} results in a gradual smearing of the structural elements and the system turns into the dense one. This can be seen from the values of the topological parameters ρ_1 and s. At $B_{12} = 1850$ eV, $\rho_1 = 0.780$ and s 2.0; increase in B_{12} is accompanied by an increase in ρ_1 to 1.05 and a decrease in s to ~ 1.0, which indicates the appearance of a dense structure. When $B_{12} \leqslant 4800$ eV, all models have loose structures.

Distributions of the O–M–O azimuthal angles are very broad (the standard deviations up to $25-30^\circ$) for all models besides the model with $B_{12} = 1150$ eV. Distributions of M–O–M angles are more narrow, their standard deviations increase from 9.2 (at $B_{12} = 1850$ eV) to 24.8° (at $B_{12} = 9999$ eV).

Taking account of ionic radii, the models were identified as follows:[130]

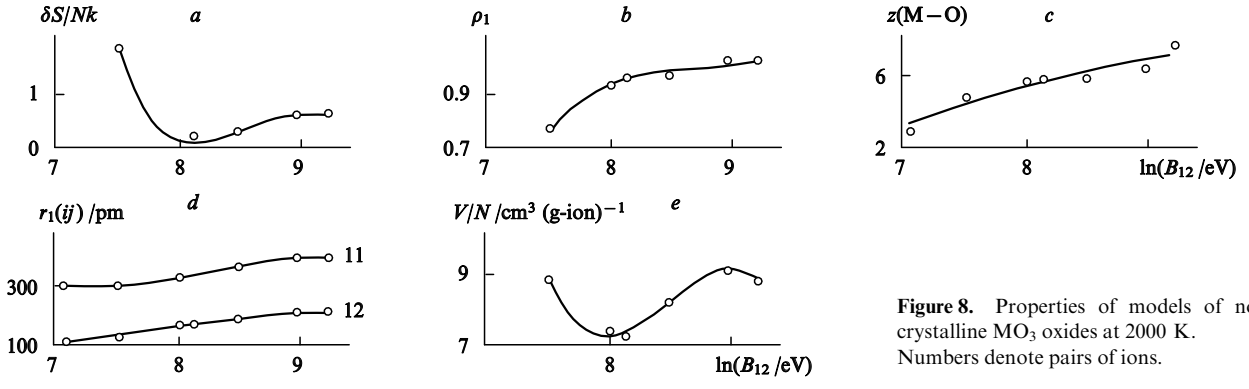


Figure 8. Properties of models of non-crystalline MO_3 oxides at 2000 K. Numbers denote pairs of ions.

MO_3	CrO_3	ReO_3	TeO_3	MoO_3	WO_3
B_{12} /eV	2300	2800	2930	3260	3400

Therefore, real MO_3 oxides form a rather narrow group corresponding to a small region $2300 \leqslant B_{12} \leqslant 3400$ eV in the homologous series. Other models are hypothetical.

For models of the MO_3 oxides, thermal energy at 2000 K is 0.5% of the total energy. Thus, temperature has little effect on their structure. The average heat capacity C_p is close to the classical value $3R = 24.9$ J (g-ion K)$^{-1}$.

Change in the configurational entropy δS along the series [130] (see Fig. 8 *a*) has a rather deep minimum at $B_{12} \simeq 3000$ eV, and is almost constant at higher B_{12}. Again, the entropy behaviour may be explained by structural effects, although in the interval corresponding to the real oxides the entropy changes insignificantly.

VI. Simulation of binary non-crystalline oxide systems

1. Simulation of non-crystalline silicate systems

a. Models of systems of M_2O-SiO_2 type

Numerous studies are devoted to silicate systems due to their practical importance. Structural data for silicates [141] and $M_2O \cdot 2SiO_2$ bisilicates [132] were reviewed. Lithium bisilicate does not form a glass on ordinary cooling of a melt, for sodium bisilicate the glass formation is difficult, and potassium bisilicate readily forms a glass.[143] However, it was stated [148] that a lithium bisilicate glass was prepared by ordinary cooling of a melt. Negative deviations from the ideal thermodynamic state of M_2O were observed in M_2O-SiO_2 systems.

Experimental data on the structure of alkali metal silicates were obtained by X-ray and neutron scattering. It was established that the Si–O distance almost does not depend on the composition and temperature of oxide and is close to 161 pm, and $z(Si-O) \simeq 4.0$. For the M–O pairs (M = Li, Na, K), the M–O distance and the mean CN increases in the series Li → K. Data given by different authors disagree. For Li, the M–O distances lie in the range of 190–260 pm, for Na in the range of 222–248 pm, and for K in the range of 265–275 pm. The CN for the Li–O pairs varies from 3 to 4, for the Na–O pairs, from 4 to 6, and for K–O and Cs–O pairs, from 5 to 7.5.

It should be noted that the structural data for lithium silicates are unreliable. The contribution of the Li–O pairs to the total PCF is very small both for X-rays and neutrons, and thus this peak is almost indistinguishable in the TPCF above the background of false oscillations due to the Fourier transformation of the structural factor.

Structural studies of Na_2O-SiO_2 glasses with 19 mol.%–35 mol.% of Na_2O showed that the Na–O Si–O, Si–Si, and O–O distances are 235, 162, 320, and 264 pm, respectively; $z(Si-O) = 4.0$ and $z(Na-O) \simeq 6$.[149,150] For potassium silicates with 14 mol.%–20 mol.% of K_2O, the CN for the K–O pairs was $\sim 10 \pm 1$.[150] It was established that Na^+ and K^+ ions occupy pores formed by the silicon-oxygen network.

Structures of $M_2O \cdot 2SiO_2$ bisilicates (M = Li, Na, K), and of $(Li_{0.63}Na_{0.37})_2 \cdot 2SiO_2$ were investigated using scattering of a pulsing neutron beam.[151] Contributions of the Li–O pairs appeared insignificant. An approximate interpretation gave the following values of the interionic distances:

Pair	Li–O	Na–O	Si–O	O–O
$r_1(ij)$ /pm	~200	~240	161–163	263–265
$z(ij)$	–	–	3.9–4.0	4.4 (Li), 4.9 (Na)

Data on computer simulations of binary systems such as Li_2O-SiO_2,[152–155] Na_2O-SiO_2,[35, 83, 134, 153, 154, 156–161] K_2O-SiO_2,[153, 154, 161, 162] as well as oxides in the $M_2O \cdot 2SiO_2$ series (see Ref. 132) have been published. Different potentials were applied in the simulations. In many studies,[131, 134, 152, 153, 155, 162] the potentials (1) with accurate account of the Coulomb interactions using the Ewald–Hansen method [39] were used. An accelerated computational scheme was developed [153] in which the Ewald sums were calculated for the sublattice of one basic cube octant on initial steps and the interpolation was performed for all intermediate points. In [154] the Ewald sums were truncated. A combination of the Keating's three-particle potential for three-atom combinations of silicon and oxygen particles, with the Lennard–Jones potentials for interactions of sodium particles with the other particles was applied [35] for the Na_2O-SiO_2 oxides. In the majority of simulation studies, only structural aspects were carefully explored, and little attention was paid to the thermodynamic properties.

Models for M_2O-SiO_2 systems (M = Li, Na, K) comprising 800 ions in the basic cube were constructed.[154] Concentration of M_2O varied from 1.47 mol.% to 23 mol.%. Generally, reasonable agreement between simulation and diffraction data for melt structures was achieved.[151] However, the Si–O distance appeared to be somewhat shorter (157 pm instead of 161–162 pm). No clustering of M^+ ions was observed. The addition of an M_2O oxide does not affect the basic structure of silica and leads only to the appearance of non-bridging O^{2-} ions (*i.e.* particles with CN for the O–Si pairs differing from 2). The mean Si–O–Si angle was somewhat larger than the actual value ($\sim 155^\circ$ instead of $\sim 143^\circ$). This deviation can be explained by the contribution of covalent bonding to the interparticle interactions in real oxides that has not been taken into account in the model.[154] It was found that a change in the molar volume affects substantially the azimuthal angles and CN for the M–O pairs. Vibrational frequencies for various ions were also estimated.[154]

Structural differences of sodium and potassium silicate glasses are due to the different degrees of nanoscale inhomogenities in the distribution of terminal oxygen ions (which have only one silicon neighbour) and the alkali metal ions bound to them. These inhomogenities were considered [161] to be a specific feature of alkali-silicate glasses.

Models of a melt (1000–4000 K) and glass (300 K) of $2Li_2O \cdot SiO_2$ were constructed using the MD method and with accounting for Coulomb interactions using the Ewald method.[152, 155] The density for the model of glass was taken to be equal to the actual value. The models comprised 576 ions; the Born–Meyer potentials were used. Charges of lithium, silicon, and oxygen ions were +1, +4, and −2, respectively. Values of 160 and 186–193 pm were obtained for Si–O and Li–O distances; the mean CN for these pairs were 4.0 and 3.5, respectively. The calculated interionic distances were compared with the experimental results [151] (see below).

Pair	Li–O	Li–Li	O–O	Li–Si	Si–Si
$r_1(ij)$ /pm					
calculation	186–193	248–260	258	306–310	320
experiment [151]	223(?)	–	263–265	–	320

The agreement between these data is moderate, although the experimental estimates for the Li–O pairs are hardly accurate. Monomeric and dimeric structural groups SiO_4^{4-} (43 groups) and $Si_2O_7^{6-}$ (18 groups) were found along with SiO_3^{2-} chains. The mean CN for the Li–O pairs in the models lie in the range of 3–4 (the experimental value is 3.1, see Ref. 151).

The following values of self-diffusion coefficients (D) were calculated from the slope of the regression line for ion shifts *vs.* time:

Ion	Li^+	Si^{4+}	O^{2-}
$10^5 D$ /cm^2 s^{-1}			
melt (3000 K)	21.5	1.88	2.23
glass (1000 K)	1.09	0.184	0.283

As could be expected, the diffusion of lithium ions is rather fast, while for silicon and oxygen the values of self-diffusion coefficients are close to the limits of the MD calculations.

Having revealed in the models the O^{2-} ions with 2 (bridging), 1 (terminal), and 0 (free) closest Si neighbours, the authors calculated the equilibrium constant for the reaction $2O^- = O^0 + O^{2-}$ in terms of the polymer theory of slags.[155]

The constant for the $2Li_2O \cdot SiO_2$ glass at 300 K was 0.0032, which implies that almost all the oxygen atoms belong to the SiO_4^{4-} monomers.

Models of melts (2000 K) and glasses (605 K) with composition of $2M_2O \cdot SiO_2$ (M = Li, Na, K) were also constructed.[153] According to a more recent publication,[163] these models contained 110–120 ions in the cube. For the Li–O pairs, the distance of 260 pm was obtained. This value is definitely overestimated, since the sum of the ionic radii is 74 + 120 = 194 pm. Self-diffusion coefficients of ions at 1010 K were also calculated in this study. The following values were obtained:

Ion	Li^+	Na^+	K^+	Si^{4+}	O^{2-}
$10^5 D$ /cm^2 s^{-1}	15	3.3	2.3	0.98	2.0

The MD method was used[156] to construct a model of $Na_2O \cdot 2SiO_2$. The repulsion of ions was described by the Pauling formula (6) with the power coefficient $n = 10$. The basic cube contained 3000 ions. Interionic distances and CN were as follows:

Pair	Na–Na	Na–Si	Si–Si	Na–O	Si–O	O–O
$r_1(ij)$ /pm	~310	335	312	228	162	262
$z(ij)$	–	5.1	?	5	4	–

These results are in agreement with diffraction data[151] for the Si–O and O–O pairs.

Models of sodium silicates containing 4.846 mol.% to 30.1 mol.% of Na_2O were constructed;[157] the models comprised 700–900 ions. The size of the basic cube was chosen taking into account the actual density of a melt. The pair potentials (1) with parameters adjusted to the properties of α-quartz were used. The relaxation was performed in the sequence 6000–3000–1500–293 K for 10 000 steps at each temperature. The results obtained agreed well with the diffraction data. A difference in bond lengths between the silicon atom and the bridging (165 pm) and terminal (< 156 pm) oxygen atoms was observed. It was found that the portion of bridging oxygen ions with $z(O–Si) = 2$ decreases from 95% to 65% with increase in the Na_2O content, while the portion of terminal ions increases from 5% to 35%. The models were inhomogenous on a nanometer scale, so that the sodium atoms were clustered around non-bridging oxygen atoms.

Models of amorphous (0 K) and liquid (2000 K) bisilicates $M_2O \cdot 2SiO_2$ with the Born–Meyer potentials were constructed using the CSR and MD methods.[132] The following values of B_{ij} were selected: 0 for the M–M and M–Si pairs, 2055.4 (Si–Si), 1729.5 (Si–O), 1500 eV (O–O), and 545.3, 925.1, 1601.94, 3844.1, and 9999.0 eV for the M–O pairs in five different models. The third and the fourth models related to sodium and potassium bisilicates, respectively. The distance in the M–O pairs depends almost linearly on $\ln B_{13}$ (atom numbering is as follows: 1 for M, 2 for Si, and 3 for O). As B_{13} increases, the M–Si and M–O distances increase monotonically, the M–M distance changes non-monotonically, and the Si–Si, Si–O and O–O distances remain almost unchanged. At $B_{13} = 626.7$ eV in the model that corresponds to lithium silicate, $r_1(M–O) = 181$ pm. Diffraction data give the higher value (186–193 pm). For sodium and potassium silicates, the agreement between the corresponding values is substantially better. All model distances for sodium silicate obtained in[132, 156] agree well with the experimental data.

The adequacy of the models constructed may be examined by comparing the calculated and actual molar volumes at 2000 K and zero pressure.

Oxide	$Li_2O \cdot 2SiO_2$	$Na_2O \cdot 2SiO_2$	$K_2O \cdot 2SiO_2$
V/N /cm^3 (g-ion)$^{-1}$			
calculation	9.73	10.2	11.6
experiment[133]	8.1	9.5	11.6

For lithium bisilicate, the difference between the results of simulation and experimental data reaches 20%, but for sodium and potassium bisilicates it does not exceed 4%–6%. For rubidium bisilicate, the interpolation of V/N at $B_{13} = 5320$ eV gives the value 11.9 cm^3 (g-ion)$^{-1}$, while the experimental value (extrapolated to 2000 K) is 12.0.[133]

The reason for the deviations observed is probably the more distinct manifestation of hysteresis phenomena on going from Na to Li. At a pressure of 4 GPa and 673 K, the density of lithium silicates increases by 6%–9% in 15 min, while that of sodium trisilicate, by 3.2%, and of potassium trisilicate, by 0.2%.[118] Overestimated molar volume for models of lithium bisilicate may be due to their metastability. Furthermore, it is also possible that the Born–Meyer potentials are poorly applicable for the description of lithium oxide.

It is noteworthy that model M–O distances[132, 152, 155] are shorter than those obtained from diffraction studies, while the molar volume for the models is larger than that of the real oxides. This contradiction might be explained assuming that the diffraction data for the Li–O pairs are inaccurate and the PPCF peak for the Li–O pair in the total PCF is attributed incorrectly.

For MD simulation of lithium silicates, the values $B_{13} = 1443$ eV and $R_{13} = 29$ pm were selected.[154] The calculated M–O distance (200 pm) was close to that obtained from diffraction data. However, with this value of B_{13} the molar volume of a model Li_2O crystal was equal to the actual value [4.974 cm^3 (g-ion)$^{-1}$] only at a pressure of 98 GPa. Thus, the assumption on overestimated Li–O distances obtained from diffraction studies seems reasonable.

The CN values for the M–O pairs in the models of bisilicates[132] were as follows:

B_{12} /eV	545.3	925.1	1601.9	3844.1	9999.0
z(M–O)					
2000 K	2.48	3.36	4.97	5.41	6.10
0 K	2.20	2.54	3.59	5.21	7.15

In M_2O crystals, the CN for the M–O pairs is 4.0. Melting or amorphisation are accompanied by a decrease in the CN. On going from a simple oxide to bisilicate, the CN increases substantially and when $B_{13} \geqslant 1601$ eV it already exceeds 4. For sodium bisilicates, the agreement between z(M–O) obtained from the simulation (4.97 at 2000 K) and diffraction (5.8 at 1373 K, see Refs 51, 141) is quite reasonable.

An increase in CN for the M–O pairs on going from simple oxide to bisilicate at $B_{13} \geqslant 1601$ eV is partially due to an abrupt decrease in the molar volume, although the formation of a silicate network is another important factor. In the case of M^{n+} ions with $n \geqslant 2$ (for example, Ca^{2+}), the transition from MO to $MO \cdot 2SiO_2$ leads to a relatively small change in the CN for the M–O pairs (from 5.1 in CaO to 5.6 in bisilicate). This can be explained by the fact that ions with charges $\geqslant 2$ form a coordination sphere around O^{2-} ions, and its structure is almost independent of the composition of the complex oxide.

Interparticle distances for the O–O pairs may be compared with those obtained from the diffraction analysis. In real lithium, sodium, and potassium silicates, r_1(O–O) = 263-266 pm.[141, 151] This distance in the models is 259–262 pm.[132, 156] Small deviations are probably due to the use of different computational schemes. The experimental values for z(O–O) appeared equal to 5.6 for all bisilicates,[141] while the model CN gradually decrease from 5.75 at $B_{13} = 545.3$ eV to 4.89 at $B_{13} = 9999$ eV.[132] The agreement of these results may be regarded as good, since the PPCF peaks of the Na–O and K–O pairs overlap with the peaks of the O–O pairs, which makes accurate calculations of partial CN difficult. In this sense, the simulation gives more precise results.

Analysis of the shape of TPCF for bisilicates at 2000 K (for X-rays) obtained from simulations demonstrated that peaks assigned to the Li–Li, Li–Si, and Li–O pairs are totally absent due to the small scattering factor of lithium atom. For potassium silicate, K–O and Si–O peaks do not overlap. Comparison of these data with the diffraction data[141] showed that the assignment of peaks[141] is in accordance with the results of simulation only in the case of potassium bisilicate. When $r > 500$ pm, the TPCF are

virtually equal to the asymptotic value of 1.00 due to a mutual interference of oscillations of six PPCF.

Comparison of the experimental data with the results of simulations shows that in diffraction studies of multi-component systems a correct interpretation can be made, in the best case, only for one or two first TPCF peaks. Consequently, the computer simulation of these systems is of special importance.

Additional information on the structure of compounds considered may be extracted from the $z(O-O)$ distributions in bisilicates. The distributions exhibit two maxima at CN equal to 3 and 6. For instance, the CN distribution for binary $Na_2O \cdot 2SiO_2$ oxide has the form:[132]

$z(O-O)$	2	3	4	5	6	7	8	9	10
Number of Na^+ ions	–	64	23	9	118	48	11	1	–

The value 3 is typical of isolated SiO_4^{4-} tetrahedra and CN 6 is typical of two linked tetrahedra with a shared vertex. In the model of SiO_2 at 2000 K, $z(O-O)$ lies in the range from 5 to 12 with a strong maximum at 6–7, and the mean CN is 7.14. Therefore the presence of values $z < 5$ in bisilicates indicates partial decomposition of an oxygen-silicon network and the appearance of unshared vertices. Oxygen ions occupying these vertices, according to the polymer theory of slags, are called terminal O^- ions. If the radii of the closest spheres for the O–O and O–Si pairs were identical, the number of terminal O^- ions would be equal to the number of O^{2-} ions with $z(O-Si) = 1$.

For the M–O pairs, the distributions of CN are very broad (for instance, in sodium bisilicate the CN values lie in the range from 2 to 8, and for potassium bisilicate, in the range from 3 to 11). Hence, ions with charge +1 cannot form a rigid coordination sphere around them. Small ions with large charge, such as Si^{4+}, can do this: 100 out of 110 Si^{4+} ions have exactly four O^{2-} neighbours. Spatial distribution of neighbours around Si^{4+} ions is approximately tetrahedral, the O–Si–O azimuthal angles are $109\,^\circ \pm (11-13\,^\circ)$. The mean value of the O–Si–O angle is close to the ideal tetrahedral value, but this distribution is rather broad. The values of M–O–M angles vary from Li to Cs over a wide range, although their mean value is almost constant ($93-97\,^\circ$).

The topological characteristics of the above models are as follows:

B_{13} /eV	545.3	925.1	1601.9	3844.1	9999.0
ρ_1	0.886	0.930	0.959	0.962	0.988
s	2.05	1.77	1.42	1.60	1.42

It is seen that the structure of alkali metal bisilicates is loose, and when $B_{13} \leqslant 925$ eV the values of ρ_1 are even lower than for pure silica (0.93). The addition of M_2O oxide with small M^+ ions (such as Li^+) results in the increase in the looseness of the system and in the appearance of large cavities (pores) therein.

The thermodynamic properties of liquid and amorphous bisilicates were simulated.[132] It was established that the increase in B_{13} leads to a gradual increase in the molar volume. The ratio of molar volumes $V_{2000\ K}/V_{0\ K}$ is close to 1.00 at $B_{13} = 545.3$ eV and increases to 1.12 for $B_{13} = 9999$ eV. The mean heat capacity C_p of the oxides is close to $3R$. Changes in volume in the formation of one mole of a complex oxide from the simple ones is positive for $B_{13} \leqslant 1602$ eV and negative for $B_{13} \geqslant 3844$ eV. The change in energy in the formation of one mole of bisilicate is negative for all values of B_{13} and lies in the range from -27 kJ mol^{-1} to -118 kJ mol^{-1}. Therefore, negative deviations from the ideality should be observed for these oxides. The values of ΔE_{form} found are very close to the experimental heats of formation of the corresponding crystalline lithium, sodium, and potassium bisilicates. Thus, the ionic model of complex oxides works adequately in respect of their thermodynamic properties. Even selection of a very simple form of the pair potentials (1) leads to agreement with the experimental data.

Changes in the Gibbs energy and entropy along the $M_2O \cdot 2SiO_2$ series were calculated according to the equation (11).[132] It was established that the increase in B_{13} is accompanied by a decrease in ΔG_{form} (formation of a complex oxide from the simple ones). These results are not only in qualitative, but (for lithium and sodium bisilicates) also in quantitative agreement with the experimental data. Values of ΔG_{form} for other silicates were predicted.[132] It was shown that the configurational entropy passes through a minimum at $B_{13} = 1602$ eV as B_{13} increases and then increases by only $\sim 0.4Nk$. Changes in entropy ΔS in a formation of one mole of a complex oxide from the simple ones depends on B_{13} in a similar way and has a minimum at $B_{13} = 3844$ eV.

Models of oxides in a binary $(Na_2O)_x(SiO_2)_{1-x}$ system composed of 500 ions with various x were constructed using the CSR and MD methods with the pair potentials (1).[134] The results of the simulation are summarised in Table 5.

The values of molar volumes were obtained with an error of several percent due to slow changes in pressure in the CSR calculations. Therefore, the molar volume changes non-monotonically as a function of composition. Nevertheless, there is a distinct minimum of the molar volume at $x = 0.2-0.3$. In general, a noticeable compression of a system occurs in the formation of binary oxides from pure non-crystalline Na_2O and SiO_2 (by 8%–9% in middle range of compositions). Comparison with the experimental data for the crystalline compounds demonstrated that the calculated volume of glass exceeds the corresponding experimental value by $\sim 10\%$ in all cases. The energy of glasses per one mole of a complex oxide depends virtually linearly on x with deviations from additivity not exceeding 1.2%. Changes in the energy ΔE_{form} are positive for $x < 0.5$ and negative for $x > 0.5$. In the case of potassium silicate at 1200 K, the transition of excess enthalpy ΔH_{form} to positive values is almost unnoticeable.[162] The error in the determination of ΔE_{form} is 15 to 20 kJ (g-ion)$^{-1}$. The experimental values for the partial enthalpy of SiO_2 at $x = 0.10-0.22$ and $T = 1200-1800$ K is ~ 0.9 kJ mol^{-1}, *i.e.* substantially less than the error of simulation.

Positions of PPCF peaks obtained in simulation are in good agreement with the experimental data (see above), especially for sodium bisilicate. The TPCF calculated for this model agrees well with the published data [165] but differs from those from another study.[164] Positions of the peaks found in Ref.[134] are in agreement with the results of calculation.[156] Longer Na–Na, Na–O and shorter Na–Si distances were obtained in a simulation with the use of three-particle potentials.[35]

Distributions of CN for the Na–O pairs appeared rather broad; for instance, at $x = 0.666$, the values of $z(Na-O)$ lie in the range from 1 to 7 and the mean CN is 3.33 ± 0.95. Distribution of O–Si–O angles lies within the range of $90-140\,^\circ$ ($114 \pm 8.4\,^\circ$). Therefore, the distribution of O^{2-} ions around Si^{4+} ions is mostly tetrahedral, though 9% of silicon ions have two, three, or five O^{2-} neighbours.

Neglecting an Ewald potential terms with a cubic symmetry (in order to save computational time) may lead to serious errors. For example, at $x = 0.5$ the Na–Na distance without taking account of the cubic contributions is 258 pm, while accounting for these terms gives 288 pm; Na–Si distances are 261 and 313 pm,

Table 5. Parameters of models of glasses in the system $(Na_2O)_x(SiO_2)_{1-x}$ at 0 K.

Parameter	x 1.0	0.8	0.67	0.5	0.33	0.2	0.1	0.0
V/N /cm^3 mol^{-1}	27.6	28.4	25.3	27.3	25.8	25.4	26.5	27.2
$r_1(ij)$ /pm for pairs								
Na–O	222	229	229	228	233	226	237	–
Si–O (exp.[164])	–	160	160	161	163	162	161	161
Na–O	–	–	–	235	236	–	–	–
Si–O	–	–	–	162	162	–	–	–
ρ_1	1.073	1.01	1.03	0.98	1.00	0.96	0.93	0.93

respectively. Thus, the simplification of the computational algorithm is not always justified.

When $T = 0$ K and $x \leqslant 0.5$, the energy of formation $\Delta E_{form} > 0$, so that a tendency for separation of components should be observed. This point was specially considered for a K_2O-SiO_2 system.[162] It was shown that K^+ ions occupy large pores of the oxygen-silicon network. Basing on analysis of diffraction data, it was proposed [165] that the melt (glass) is built up of two types of microgroups, *viz*. with high alkali metal content ($Na_2O \cdot 2SiO_2$) and with high silicon content (with composition close to silica) in the range $0.2 \leqslant x \leqslant 0.33$. These microgroups cannot exist in models with $N \simeq 500$.

The addition of Na_2O to SiO_2 leads to a rapid increase in ρ_1 and abrupt decrease in s. Therefore, the addition of Na_2O causes an effective depolymerisation of the structure, *i.e*. a decomposition of the tetrahedral network of bonds. The system is depolymerised to a noticeable degree already at $x = 0.5$. Models [35] constructed with accounting of three-particle potentials give higher values of ρ_1. For example, a calculation[35] at $x = 0.333$ gave the value of $\rho_1 = 1.056$, which is typical of dense non-crystalline systems. Results of simulation[134, 156] agree well with each other in respect of ρ_1 (for instance, at $x = 0.33$, $\rho_1 \simeq 0.96$).

The applicability of the polymer theory of slags (PTS) to the Na_2O-SiO_2 oxides was analysed.[134] The basic parameters of this theory are the degree of polymerisation α, molar ratios of different anions, and polymerisation constant K_p. Solutions of associates are usually regarded as ideal ones. To use a polymer model, the following conditions have to be met: 1) CN for the Si-O pairs has to be equal to 4 for all Si atoms; 2) the oxygen atom with two closest silicon neighbours is considered as a 'bridging' O^0 atom; 3) the oxygen atom with one closest silicon neighbour is considered as a 'terminal' O^- atom; 4) 'free' oxygen O^{2-} ion does not have any closest Si neighbours.

Further, the n_0, n_1, and n_2 will be used to denote numbers of 'bridging', 'terminal' atoms, and 'free' ions, respectively. The degree of polymerisation is given by the formula:[134]

$$\alpha = n_0 \, [2n(\mathrm{Si})]^{-1} \, ,$$

where $n(\mathrm{Si})$ is a number of silicon ions. For pure SiO_2, $\alpha = 1$ if all O particles have two Si neighbours. The polymerisation constant is defined as the equilibrium constant for the reaction $2O^- = O^0 + O^{2-}$ within the ideal solution approximation.

$$K_p = X(O^0)X(O^{2-}) \, [X(O^-)]^{-2} \, ,$$

where $X(O_k) = n_k/n(\mathrm{O})$ is a ratio of O_k particles to the total number of oxygen particles in the system. The α and K_p parameters can be calculated from the computer simulations. For models of $(Na_2O)_x(SiO_2)_{1-x}$ glasses, the following values were found:

x	0.800	0.667	0.500	0.333	0.20
α	0.197	0.336	0.542	0.715	0.87
K_p	0.104	0.064	0.027	0.044	0.051

K_p were determined approximately due to the small value of n_2 for $x \leqslant 0.5$. If the condition $z(\mathrm{Si}-\mathrm{O}) = 4.00$ (for each silicon ion), as well as the condition on the electrical neutrality of the system are met, the following expression holds:[134]

$$K_p = \frac{\alpha[x - 2(1-x)(1-\alpha)]}{8(1-x)(1-\alpha)^2} \, .$$

This expression holds satisfactorily for sodium silicate models.

In order to determine the polyanionic composition of a model in terms of the PTS, it is necessary to distinguish complex $Si_mO_n^{q-}$ anions as bound groups of particles in which each silicon atom is linked to at least one other silicon atom of the same group through a bridging oxygen atom. Distributions of the bound groups calculated for $(Na_2O)_x(SiO_2)_{1-x}$ models are shown below:

x	0.8	0.667	0.5	0.333
Group	$1^{12}2^6 4^1 5^1$	$1^{11}2^4 3^2 4^1 7^1 19^1$	$1^3 2^2 3^1 68^1$	110^1

The notation $1^{12}2^6$... means that 12 SiO_4^{4-} 'monomers', 6 $Si_2O_7^{6-}$ dimers, and so on, were found in the model. When $x \leqslant 0.333$, all oxides are completely polymerised (in accordance with the PTS). Another PTS parameter is the equilibrium K_{11} constant for the reaction

$$2SiO_4^{4-} = Si_2O_7^{6-} + O^{2-} \, .$$

Within the ideal solution approximation K_{11} is given by:

$$K_{11} = n_2 n(Si_2O_7^{6-}) \, [n(SiO_4^{4-})]^{-2} \, .$$

Values of K_{11} for models of sodium silicate vary in a wide range (from 1.56 at $x = 0.5$ to 3.46 at $x = 0.8$).

In agreement with the PTS, ionic ratios $Y(i)$ are defined as ratios of numbers of polyanions composed of i particles to the total number of all polyanions and free anions O^{2-}; the ionic ratio $Y(O^{2-})$ is defined similarly. These parameters characterising the anionic composition of silicates only slightly depend on temperature.

In terms of the theory of perfect ionic solutions, the thermodynamic activity of M_2O in M_2O-SiO_2 oxides is equal to the ionic ratio $Y(O^{2-})$. It was found [134] that in an $(Na_2O)_x(SiO_2)_{1-x}$ system $Y(O^{2-})$ is always close to x, *i.e*. the solutions should be ideal. In fact, however, strong negative deviations from the ideal state are observed for Na_2O; and the activity coefficient of Na_2O at $x = 0.6$ and $T = 2000$ K is 0.092. Nevertheless, the value of $Y(O^{2-})$ under these conditions is ~ 0.60.

Therefore, the polymer theory of slags, being self-consistent to some extent (in respect of concentrations of different types of particles and polyanions), does not predict correctly the thermodynamic activity of the components. Therefore, the PTS parameters (α, K_p) obtained from a fit to the thermodynamic properties rather than to the structural data, are only effective measures. Within this approximation, the PTS is simplified (like the model of associated solutions).

Models of $Na_2Si_2O_5$ glass were constructed using the MD method in a temperature range of 1000–2000 K (1080 ions, density of 2.5656 g cm^{-3}).[159] The potentials proposed earlier [166] included pairwise and three-particle interactions. The Coulomb terms were calculated according to Ewald. It was shown that PCF and structural factor of the model at 1000 K are in good agreement with the diffraction data and with the results of MD simulation of sodium silicate [157] with the Buckingham potentials.[167] It was found that 98% of silicon ions have CN of 4.0% and 2% have CN of 3.0. Only 5% of oxygen ions are bridging and therefore do not have neighbouring sodium ions. Sodium ions are situated in pores of the silicate network close to the terminal oxygen atoms and diffuse between site positions of the structure *via* a jumping mechanism. The value of activation energy of self-diffusion of sodium ions (54.3 kJ mol^{-1}) was close to the experimental value (66.6 kJ mol^{-1}).

The penetration of inert gases (Ne, Ar, N_2) into SiO_2, Na_2SiO_3, $Na_2Si_2O_5$, and sodium-aluminosilicate glasses was investigated using the MD method.[168] The results of the simulation demonstrated that none of the above glasses absorbs nitrogen and argon, while neon can penetrate into the first three of them.

b. Models of $MO-SiO_2$ systems

The structure of liquid FeO was investigated by X-ray anomalous scattering.[141, 169] In the simulation of the oxide, B_{ij} values for Fe–O and O–O pairs were adjusted to achieve the agreement between the simulated interionic distances and the experimental results.[170] The following values were obtained: $B_{11} = 1300$, $B_{12} = 1900$, $B_{22} = 1500$ eV (alternatively, the value of $B_{22} = 905.6$ was taken [9]). The agreement between the results of simulation and the diffraction data was good (Table 6). Using the same B_{ij} values and taking $R_{ij} = 29$ pm, reasonably good agreement with the experimental data was achieved for energy, molar volume, and compressibility of FeO crystals.

Table 6. Interionic distances and coordination numbers for liquid FeO.

Parameter	Model for FeO (see Ref. 170)	Experiment [169]
r_1 /pm for pairs		
Fe–Fe	313	315
Fe–O	207	205
O–O	317	320
z for pairs		
Fe–Fe	12.6	11.8
Fe–O	5.8	5.7
O–O	12.3	12.2

The structure of some non-crystalline oxide systems, *viz*., FeO–SiO_2, MgO–SiO_2, and CaO–SiO_2 were investigated by X-ray scattering.[51, 141, 171] Interionic distances were determined by interpretation of certain TPCF peaks. Structural analysis of $MgSiO_3$ [172] and $CaSiO_3$ [173] glasses was performed. Structure of $CaSiO_3$ glass was also studied by X-ray diffraction and Raman spectroscopy. The TPCF exhibits only three peaks at 164 pm, 243 pm, and 364 pm. The Raman spectrum for this glass was similar to the corresponding spectra of pyroxenes, which contain chains of SiO_4^{4-} tetrahedra linked through vertices as the main structural elements; the chains are linked to each other *via* Ca^{2+} ions. Ring anions, such as $Si_4O_{12}^{8-}$, $Si_5O_{15}^{10-}$, were rare. The peak at 164 pm was attributed to the Si–O pairs. The maximum at 243 pm was a result of overlapping of Ca–O and O–O contributions. A structural model of $CaSiO_3$ glass based on the pyroxene structure was proposed,[173] in this model one half of oxygen atoms were bridging.

In the case of an $MgSiO_3$ glass, the X-ray TPCF contains five peaks.[172] A peak at 163 pm was attributed to the Si–O pairs, and at 208 pm to the Mg–O pairs (the sum of the ionic radii of Mg and O is 207 pm). The mean CN for the Mg–O pairs was 4.1. A structural model of an $MgSiO_3$ glass was also constructed on the basis of the pyroxene structure. There, the main structural elements were also chains of SiO_4^{4-} tetrahedra linked through vertices. The magnesium ions are situated between the chains. Each Mg^{2+} ion has four oxygen neighbours at a distance of 208 pm and two more neighbours at a distance of 250 pm. Mg^{2+} ions occupy two types of sites: in almost ideal octahedral sites with $z = 6$ and in rather irregular sites with $z = 7$.

The Born–Meyer pair potentials were used in simulations of $2MO \cdot SiO_2$ (M = Mg, Ca, Sr, Ba, Fe),[136–139] CaO–SiO_2 (see Ref. 65), and FeO–SiO_2 (see Ref. 170) complex oxides. The following values for parameters were taken (numbering of atoms: 1 states for M, 2 for Si, 3 for O): $B_{11} = B_{12} = 0$, $B_{22} = 2055.4$ eV,[9] $B_{23} = 1729.5$,[9] $B_{33} = 1500$, and $R_{ij} = 29$ pm. Models of $(FeO)_x(SiO_2)_{1-x}$ for the whole range of compositions $0 \leqslant x \leqslant 1$ were constructed.[170] The models contained ~ 500 ions in the basic cube. Densities were taken from a reference book.[174] The Coulomb interactions were taken into account using the Ewald–Hansen method.[39] Positive deviations from the ideal state found for the energy of formation amounted to few tens kJ mol^{-1}. The experimental values of changes in energy in the formation of a complex oxide lie in the range from -6.3 kJ mol^{-1} to 2.5 kJ mol^{-1}. The heat of formation for crystalline fayalite ($2FeO \cdot SiO_2$) is 33.5 kJ mol^{-1}. The Fe–O and Si–O distances depend insignificantly on the composition of the binary oxides.[170] For other pairs, this dependence is more pronounced though also not very strong. The results of the simulation showed that the interpretation of diffraction data is not correct for complex oxides in all cases due to a possibility of attributing false TPCF peaks to the real ones.

Distributions of CN for the Fe–O pairs in $(FeO)_x(SiO_2)_{1-x}$ models are rather broad. For instance, at $x = 0.5$ and $T = 2000$ K, $2 \leqslant z(Fe–O) \leqslant 5$ (the mean value is 3.3); in the fayalite ($x = 2/3$), $2 \leqslant z(Fe–O) \leqslant 6$ and the percentage of Fe^{2+} ions in octahedral coordination is 2.1%. Measurements of the Mossbauer effect in silicate slags gave close estimates (1.1%–2.0%).[175] Most of Fe^{2+} ions in the models have three or four O^{2-} neighbours.

Distributions of O–Fe–O, Fe–O–Fe, O–Si–O, and Si–O–Si azimuthal angles for linked three-atom combinations were calculated.[170] Distributions of Fe–O–Fe and O–Fe–O angles are spread over the range of 45–180° and have a flat maximum near 90°. The diffusion corresponds to scatter of the CN values for the Fe–O and O–Fe pairs. For the O–Si–O angles, the coordination sphere radius was adjusted to obtain $z(Si–O) = 4$. In this case, the distribution of the θ(O–Si–O) angles is a Gaussian with $\theta = 108 \pm 15°$. The width of this distribution is equal to the corresponding width obtained for the model of SiO_2 at 2500 K.[55] Hence, on going from pure silica to fayalite the configuration of ions in SiO_4^{4-} groups changes insignificantly. However, the models considered [170] are closer to the tetrahedral configuration than other models.[55] The distribution of angles in fayalite generally agree with the diffraction data.[176]

The topological parameter ρ_1 for pure FeO is 1.08, *i.e*. the structure of the oxide is dense. The addition of SiO_2 is accompanied by increase in the structural looseness. The following parameters were found for a model of FeO at 2000 K:[170]

x	1.00	0.80	0.67	0.50	0.25	0
ρ_1	1.08	0.98	1.00	0.96	0.93	0.93
s	1.13	0.90	1.08	1.19	1.40	1.62

It is clearly seen that the addition of FeO to SiO_2 initially affects ρ_1 insignificantly, and for $x \leqslant 0.4$ the depolymerisation of the tetrahedral network does not take place. However, in the range $0.5 \leqslant x \leqslant 0.6$ the ρ_1 parameter increases due to the transition to a dense structure with the octahedral coordination. In fact, at $x = 0.5$ the CN $z(Fe–O) = 3.5$ and at $x = 0.667$, $z(Fe–O) = 4.0$, while for pure FeO $z(Fe–O) = 5.8$. The short-range order in FeO is analogous to that in liquid NaCl.

The adequacy of the PTS for $(FeO)_x(SiO_2)_{1-x}$ was examined.[170] The main condition of the theory, $z(Si–O) = 4$, is not met for all silicon atoms, but the number of Si ions with three or five O^{2-} neighbours is relatively small.

z(Si–O)	3	4	5
$x = 0.8$	5	35	5
0.667	7	58	6
0.5	5	89	6
0.25	15	105	15
0	4	75	3

The values of α and K_p were calculated from n_0, n_1, and n_2 (the numbers of oxygen ions), and the distributions of Si_mO_n bound groups were also found (Table 7).[170]

The bound group distribution shows that for $x \leqslant 0.5$, the system is almost completely polymerised. Cyclic anions were absent in the models.

'Polymerisation constants' K_p listed in Table 7 depend on the FeO content: they increase with increase in x (as in the Na_2O–SiO_2 system). This increase does not agree with the model of ideal polymer solution. Values of K_p obtained in different studies were summarised.[177] The value 0.08 obtained in Ref. 178 at 1573 K is

Table 7. Characteristics of models of $(FeO)_x(SiO_2)_{1-x}$ oxides.

x	α	K_p	K_{11}	Bound groups	$X(O^{2-})$
0.8	0.19	0.085	3.3	$1^{16}2^{8}3^{3}4^{1}$	0.79
0.667	0.34	0.072	0.68	$1^{15}2^{3}3^{2}6^{1}9^{1}12^{1}17^{1}$	0.68
0.5	0.56	0.039	–	$1^{1}4^{1}95^{1}$	(0.78)
0.25	0.82	(0.025)	–	135^{1}	(0.5)

Note. Values with low precision are indicated in parentheses.

the closest to data of Ref. 170, but the majority of K_p values calculated by fitting to the thermodynamic activities of components lies in the range of 0.7–2.0. As in the case of sodium silicates, these polymerisation constants are effective parameters and they do not describe the real structure. The K_{11} values also strongly depend on the composition.

The results of simulation of $(FeO)_x(SiO_2)_{1-x}$ oxides showed that for $x \leqslant 0.5$ the system is almost completely polymerised to form a spatial silicon-oxygen network.[170] A loose structure with the low mean CN is maintained there. An assumption on predominence of linear and cyclic anions[179] in the range $0.2 \leqslant x \leqslant 0.5$ was not confirmed. The relatively slight dependence of K_p on concentration is in agreement with the associated ideal solution theory. In the thermodynamic respect, the $FeO-SiO_2$ system is close to the ideal one. The calculated activity of FeO for $x \geqslant 0.667$ is in reasonable agreement with the experimental data. Therefore, the PTS model reflects correctly some substantial features of structures of $FeO-SiO_2$ melts and glasses for $x \geqslant 0.5$. However, for lower x values the model is inadequate due to virtually complete polymerisation of the system.

The proportions of oxygen particles present as 'free' O^{2-} ions or included into SiO_4^{4-} groups calculated by different authors for the $FeO-SiO_2$ melts were summarised.[180] Results of computer simulation are in good agreement with the computation.[181] For other systems (for example, sodium silicates), such agreement was not achieved.

It should be taken into consideration that the interpretation[170] of the polymerisation is purely structural, since it does not assume the formation of the valence bonds, and it is due to sum of the Coulomb forces and forces of the electron shell repulsion. Therefore, the reason for the polymerisation in ionic models is totally different from that underlying the PTS. The agreement of the results of simulation with the conclusions from PTS for $x > 0.5$ is probably due to the fact that the adequacy of the PTS is defined directly by the structure rather than by bonding type that determines the structure.

A similar study of structures and the properties of $(CaO)_x(SiO_2)_{1-x}$ oxides at 2000 K was performed.[65] The metasilicate ($x = 0.5$) is formed from simple liquid oxides with a decrease in volume by $\sim 5\%$. Changes in the energy in the formation of the metasilicate is -4.8 ± 20 kJ mol^{-1}; the experimental value is -40 kJ mol^{-1}. The reasonable agreement between the simulated characteristics and the experimental results[51,141] as regards the positions of the TPCF peaks and CN was achieved. The majority of Ca^{2+} ions have five or six oxygen neighbours, however Ca–O pairs with CN ranging from 3 to 9 are also present.

The addition of CaO to SiO_2 leads to a linear increase in ρ_1 up to 1.00 at $x = 0.5$. But the addition of FeO initially almost does not change ρ_1. The smaller Fe^{2+} ion deforms the network structure not as strongly as the Ca^{2+} ion. However, already when $x \geqslant 0.65$ the difference between the structures of these silicates becomes insignificant.

The PTS was also applied to analyse the structures of $CaO-SiO_2$ models.[65] The difference between $FeO-SiO_2$ and $CaO-SiO_2$ systems in terms of degree of polymerisation α, polymerisation constant K_p, and the bound group distribution, is rather small. When $x \leqslant 0.5$, the polymerisation is almost complete. However, the deviations from the ideal state for the $CaO-SiO_2$ system are negative and significant. Adjustment of the activity coefficients within different version of the PTS gives the value of $K_p \simeq 0.0016-0.0045$.[177] The difference between these (effective) K_p and the value found by the structural analysis is due to the inadequacy of the ideal PTS modification and probably due to an insufficient model size.

A series of models of $2MO \cdot SiO_2$ oxides was constructed using the Born–Meyer potentials ($B_{13} = 1441.4-8885.1$ eV).[137–139] Additionally, two hypothetical models with $B_{13} = 500$ eV and 800 eV were also considered.[136] Each model contained 497 ions. Figure 9 illustrates some properties of the models. The molar volume depends on non-monotonically B_{13}. It has a minimum near 800–1000 eV. The molar volume of simple MO oxides similarly depends on B_{13}. An increase in the volume at $B_{13} < 800$ eV indicates an abrupt increase in the structural looseness of the oxide. The interparticle $r_1(M-O)$ distances for the models increases gradually with an increase in B_{13}. The transition from pure MO to the silicate affects the $r_1(M-O)$ distance insignificantly. A similar effect was observed for CN of the M–O pairs. At $B_{13} = 500$ eV, the value of $z(M-O)$ in the orthosilicate is 2.00, which indicates the presence of chain structural elements. At $B_{13} = 800$ eV, $z(M-O) = 3.3$, *i.e.* the trigonal elements should dominate in the structure. For simple MO oxides, the CN for the M–O pairs with the same values of B_{13} are 2.0 and 3.5, respectively (see above). Hence, the structure of first coordination spheres of M^{2+} ions are the same in both the orthosilicate and the simple oxide. The addition of SiO_2 leads to a broadening of the O–M–O angle distributions, *i.e.* results in a certain disordering of the oxide structure.

It should be noted that the Mg–O distance behaves abnormally for magnesium orthosilicate.[139] This distance for the model at 2000 K (196 pm) is substantially shorter than the experimental value (208–216 pm). Coordination numbers for the M–O pairs are also noticeably smaller (3.7 instead of 4.7–5.0). The repulsion parameter for the Mg–O pairs was determined from the compressibility data for MgO crystals. Presumably, this characteristic has to be corrected for a non-crystalline phase.

A specific arrangement of the O–O pairs with maxima of distributions of their CN at $z = 3$ and 6 was found for models with $B_{13} = 3283-8885$ (from calcium to barium silicate). A reason for the appearance of these maxima becomes obvious on consideration of the spatial models.[136] Silicon ions are situated in almost planar parallel layers separated by ~ 0.61 nm. A layer of SiO_4^{4-} corresponds to each Si^{4+} layer. The centre of the model is occupied by a figure composed of two SiO_4 tetrahedra linked through a shared vertex to form an almost ideal trigonal prism Si_2O_7 the centre and six vertices of which are occupied by the O^{2-} ions. The central O^{2-} ions have CN for the O–O pairs equal to 6, and each O^{2-} ion in the vertices of the prism has three O neighbours. The

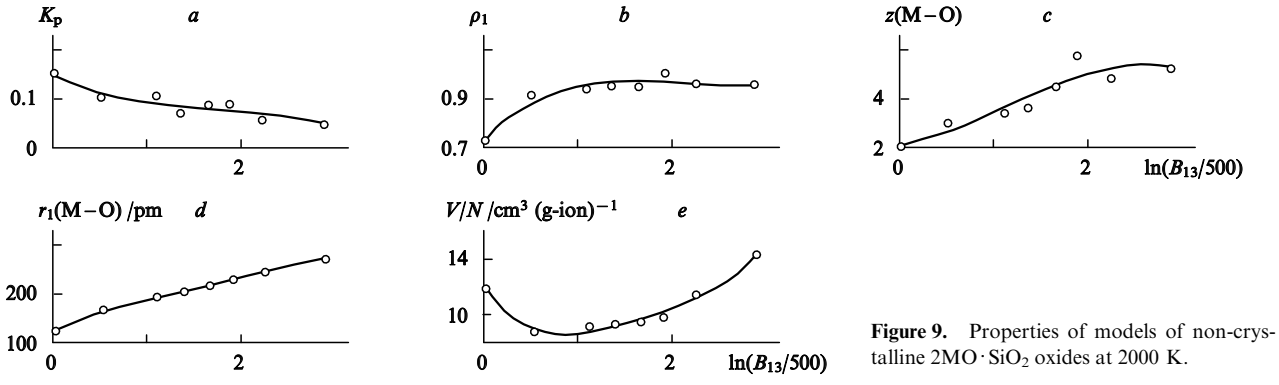


Figure 9. Properties of models of non-crystalline $2MO \cdot SiO_2$ oxides at 2000 K.

ratio of the ions with CN 3 and 6 is 6. In models of $MO \cdot SiO_2$ oxides, the similar type of ordering of O^{2-} ions was revealed.

Thus, for $2MO \cdot SiO_2$ oxides with large M^{2+} ions (such as Ba^{2+}) an association of silicate tetrahedra to form Si_2O_7 trigonal prisms with approximately layered arrangement of tetrahedra is typical. The space between layers is loosely filled with M ions and some of the O ions. A part of M ions is situated in the layers as well. Large pores with an average radius of ~ 0.44 nm (the size of ions was not taken into account) were also observed. A decrease in the size of M ions leads to their stronger interactions with oxygen ions. As a result, M ions begin to form bridges between the SiO_4^{4-} tetrahedra and between the tetrahedra and oxygen ions as well. This leads to a disordering of the structure and to its loosening. It is clearly seen from the plots of ρ_1 and s vs. B_{13} (see Fig. 9). An analysis of bound group distribution demonstrated that the increase in B_{13} is accompanied by the increase in the number of monomers and a decrease in the size of bound groups.

A series of MD models for an $(MnO)_x(SiO_2)_{1-x}$ system was constructed[162] using the potentials (1). The heat of formation for the models was negative for $x > 0.4$ and positive for the models high silica content. This corresponds to a stratification of a liquid phase in the system. The reason for the switching of the ΔH_{form} sign lies in the strong effect of small Mn^{2+} ions on the structure of the silicon-oxygen network. The smaller M^{2+} ions, the stronger the distortion of the network and the higher the energy of the system, leads to a broadening of the area of stratification of a liquid phase in the binary $MO-SiO_2$ system.[162]

The applicability of the PTS to orthosilicates at various B_{13} was examined.[136] An increase in B_{13} from 500 to 8885 eV leads to a decrease in K_p by a factor of 3 (see Fig. 9). The effective values of K_p calculated according to the thermodynamic activity of MO oxide vary over a substantially wider range: from 1.0 in iron silicates to 3×10^{-4} in barium silicates.[182] The difference from the structural data is due to the non-ideal nature of the solutions.

Calculation of the changes in configurational entropy along the $2MO \cdot SiO_2$ series showed that the transition to values $B_{13} < 1441.4$ eV leads to a decrease in the entropy.[136] When B_{13} grows in the range 1441–1900 eV, the entropy passes through a flat maximum and further remains almost constant. The entropy of simple MO oxides behaves similarly (see Fig. 4).

Changes in the Gibbs energy in the formation of orthosilicates starting from simple oxides are positive for $B_{13} \leqslant 1441$ eV. This indicates the instability of the complex oxide with respect to probable decomposition into two phases. In fact, in $BeO-SiO_2$ and $MgO-SiO_2$ systems at 2000 K the area of a monophase liquid is very narrow. However, in the $FeO-SiO_2$ system ($B_{13} = 1900$ eV) this area becomes much broader.

A model of amorphous $ZnO \cdot 3SiO_2$ using the MD method with the BMH potentials was constructed.[183] The model contained 264 ions, viz. Zn^{2+}, Si^{4+}, and O^{2-}, in the basic cube with the edge of 15.38 pm (the density is 2.87 g cm^{-3}). First, heating of the system up to 10 000 K followed by cooling to 300 K in ~ 30 ps were simulated. As a result, the first PPCF peaks appeared isolated, the Si–O, Si–Si, and Zn–O distances were 162 pm, 318 pm, and 198 pm, respectively. The mean CN for the Zn–O pairs was estimated (not very reliably) as 4.41, since coordination numbers 4 and 5 were predominant in the distribution in accordance with the diffraction data. For Zn^{2+} ions with CN of 4.0, the mean Zn–O distance was 197 pm and 204 pm for ions with CN 6. According to the shape of the PPCF for the O–O pairs, a conclusion was made on the presence in the structures of SiO_4 tetrahedra linked *via* edges. In this case, the CN of the corresponding Si ions is 5; this results in a low value of the O–Si–O angle (89°). The majority of oxygen ions adjacent to Zn ions have three neighbours. In general, the arrangement of particles in the model resembled that in $ZnSiO_3$ crystal of the pyroxene type. MD data demonstrated that Zn cannot completely substitute silicon atoms in the network and therefore destroys the silicon framework.

c. Models of $M_2O_3-SiO_2$ systems

$(B_2O_3)_x(SiO_2)_{1-x}$ melts readily form glasses, while the $(Al_2O_3)_x(SiO_2)_{1-x}$ oxides form glasses only for $x < 0.65$. Among the systems considered, only the structure of the $(Al_2O_3)_x(SiO_2)_{1-x}$ glasses (see Ref. 184) was studied experimentally. It was established that for $x = 0.061-0.469$ the position of the first TPCF peaks shifts monotonically from 162 to 179 pm with increase in x. Since this peak is a result of overlapping of Si–O and M–O contributions and the r_1(Si–O) distance is 161–162 pm, the M–O distance may be estimated as 199 pm. The O–O distance is 260 pm.

It is usually assumed that the amorphous Al_2O_3 oxide may act both as a modifier and a network-forming component, *i.e.* aluminium particles can either occupy cavities between the SiO_4^{4-} tetrahedra or substitute the silicon atoms in the silicon-oxygen network. The CN for the Al–O pairs are usually 4 or 6.

The following oxide systems were studied by the computer simulation methods: $B_2O_3-SiO_2$,[64] $Al_2O_3-SiO_2$,[66] $Fe_2O_3-SiO_2$,[104] and the $M_2O_3 \cdot SiO_2$ series (see Refs 185, 186). The potentials (1) were used in these studies, the potential parameters were taken from the corresponding models of pure M_2O_3 oxides. The Coulomb interactions were taken into account using the Ewald–Hansen method.[39] Each model contained ~ 500 ions in the basic cube.

It was demonstrated that the molar volume of $(B_2O_3)_x(SiO_2)_{1-x}$ oxides decreases substantially in the formation of a complex oxide from the simple non-crystalline ones (by 12% for $x = 0.667$). The energy of the complex oxide formation appeared very small for $x \geqslant 0.7$, for the lower x and $T = 0$ K it is positive and reaches the value 42 kJ mol^{-1}; however, this energy is negative at 2000 K. Hence, cooling of the system results in destabilisation of the oxide thermodynamically.

First TPCF peaks are split into two narrow subpeaks that represent contributions of the B–O and Si–O pairs. The height of the left subpeak (at 134–139 pm) increases and the height of the right one (at 161–162 pm) decreases as x decreases. Most of B ions have three oxygen neighbours and Si ions have four oxygen neighbours. Spatial arrangement of neighbours around the boron and silicon ions are almost independent of each other. The structure of all oxides is loose, the ρ_1 parameter increases from 0.79–0.83 in B_2O_3 to 0.93 in SiO_2 (with a small minimum at $x = 0.5$). It was concluded[64] that the $B_2O_3-SiO_2$ oxide are copolymers of two B_2O_3 and SiO_2 polymers. The BO_3^{3-} and SiO_4^{4-} are linked through shared vertices as a result of random combination of the two figures.

Models of the $Al_2O_3-SiO_2$ oxides at 0 K and 2000 K were constructed using the MD and CSR methods.[66] Each model contained ~ 500 ions. The potentials (1) were used. The increase in the molar volume in the formation of a complex oxide from the simple ones at 0 K was 10% for $x = 0.5$, and ΔE_{form} was 70–100 kJ mol^{-1} for $x = 0.2-0.667$. Therefore, the system exhibits positive deviations from the ideal state. The addition of small amounts of Al_2O_3 to SiO_2 results in an abrupt increase in energy, and therefore the amorphous phase appears thermodynamically unstable at 0 K. The positive ΔV_{form} remains at $T = 2000$ K, but ΔE_{form} changes the sign, which means that liquid oxides are formed from the simple oxides with the liberation of heat. The experimental values of ΔE_{form} are very small (of the order of several kJ mol^{-1}).

The Al ions with z(Al–O) = 4 dominate in the models. The portion of these ions increases from 51% for $x = 1.0$ to 76% for $x = 0.2$. These values are in agreement with the estimates based on viscosity of the melts. A decrease in x favours the transition of Al^{3+} ions into the coordination state with the CN 4 and their inclusion into the tetrahedral network. Therefore, for $x < 0.4$ the value of ρ_1 is almost constant. The coordination number 6 is rather rare ($< 6\%$). After 4, the most typical value of CN is 5. It was shown[66] that the PTS can be applied to the $Al_2O_3-SiO_2$ oxides if the inclusion of the ions into the tetrahedral network is

taken into consideration. The K_p constant varies from 0.21 ($x = 1$) to 0.15 ($x = 0.2$).

2. Simulation of borate systems

The results of simulation of $Na_2O-B_2O_3-SiO_2$ ionic glasses using the MD method have been published.[84] An addition of sodium oxide leads to the increase in CN for the B–O pairs from 3 to 4, and sodium atoms occupy the nearest pores of the structure. The changes in the CN of boron atoms was confirmed by the NMR data.[187]

The structure of $B_2O_3-Li_2O$ glasses with 0%, 10%, and 20% of Li_2O were studied[188] using the X-ray scattering and MD-simulation. The potentials (1) were applied. The models contained from 1656 to 1728 ions in the basic cube. It appeared that the B–B and Li–O distances did not depend on the concentration, and the structure is built of the randomly linked BO_3 and BO_4 groups. The lithium ions are weakly bound with the boron ions and are located mostly in pores of the boron-oxygen network. The vibrational spectra of the glasses were also calculated. They resembled the IR-absorption spectra, but differ from the Raman spectra.

Models of B_2O_3 and $Na_2O \cdot 2B_2O_3$ were constructed using the MD method with the mixed ion-covalent potentials.[189] The Born–Meyer potentials (1) were applied for all pairs of atoms; additionally, the three-particle potentials were used for O–B–O and O–B–B combinations. For the $Na_2O \cdot 2B_2O_3$ oxide the value of 3.4 for z(B–O) was obtained, which is in agreement with the results for lithium borate.[188]

Nanoscale structural inhomogenities for the alkali-borate glasses both in liquid and glassy states were revealed by the small angle X-ray scattering.[82] In order to reproduce this effect in MD-models, the size of the models has to be enlarged substantially.

Simulation of the crystallisation process of liquid $2MgO \cdot B_2O_3$ using the MC method was performed.[190]

3. Simulation of phosphate and vanadate glasses

Structures of the metaphosphate glasses containing Zn, Mg, Ca, Sr, Ba, and Na were studied by X-ray diffraction methods.[191] The following values of CN for the M–O pairs were found:

M	Zn	Mg	Ca	Sr	Ba	Na
z(M–O)	4.1	4.6	6.8	7.0	7.8	5.7

For Ca, Sr, Ba, and Na the CN are close to those in crystalline compounds, but the values for Zn and Mg are abnormal.

Models of $(CaO)_x(P_2O_5)_{1-x}$ oxides with $x = 0.8$, 0.667, 0.5, 0.333, and 0.2 were constructed[117] using the Born–Meyer potentials with the charge of phosphorus atoms equal to +5. The Coulomb interactions were taken into account using the Ewald–Hansen method.[39] Such characteristics of the metaphosphates, as r_1(P–O) = 155 pm and the molar volume of 8.40 cm^3 (g-ion)$^{-1}$ were reproduced with high accuracy. The values of ΔE_{form} reached −66 kJ mol^{-1}, which is extremely small compared to the total molar energies of the oxides (from −3405 for CaO to −36 930 kJ mol^{-1} for P_2O_5 at 2000 K). However, these values are significant if compared with the RT = 16.6 kJ mol^{-1}. Thus, the negative deviations from the ideal state should be expected. Changes in the volume of the system in the formation of one mole of a complex oxide are always positive and equal to 5.26 cm^3 mol^{-1} for the metaphosphate at 2000 K.

The calculated TPCF for X-rays has only three distinct maxima. The first one is attributed to the P–O pairs, the second one is a result of overlapping of Ca–O and O–O contributions. The third maximum is a result of overlapping of Ca–Ca, Ca–P, and P–O contributions. Therefore a reliable interpretation of the experimental diffraction data for these complex oxides is very difficult. The r_1(P–O) distance depends slightly on the CaO concentration (it changes from 150 pm for $x = 0.80$ to 159 pm for $x = 0$). For the metaphosphate, r_1(P–O) = 153–156 pm. For the phosphorus ions with z(P–O) = 5, the distance is slightly longer than for the ions with z(P–O) = 4.

The distributions of CN for the P–O pairs are given below:

z(P–O)	$x = 0.8$	0.667	0.5	0.333	$x = 0.0$
4	33	40	30	18	19
5	31	46	71	94	105
6	2	4	9	12	18

The tetrahedral coordination of the phosphorus ions dominates (50%) for $x = 0.8$; with a decrease in x, the maximum of the distribution shifts to $x = 5$. In pure P_2O_5, the CN varies in the range 4–6: *ca.* 13%–14% of P^{5+} ions in the oxide have z(P–O) = 4 or 6. The less the P_2O_5 concentration in the model, the greater the portion of the phosphorus ions having z(P–O) = 4. Diffraction data usually give the values of CN for the P–O pairs close to 4 and even less (to 3.8).[192] Therefore, the Born–Meyer potentials with charge of the phosphorus ions equal to +5 do not allow one to obtain purely tetrahedral coordination of the phosphorus ions in the models. Presumably, this fact is indicative of the substantial contribution of the covalent bonding in phosphates.

For the Ca–O pairs, the following values of CN were found: 5.6 in pure CaO, 4.7 for the model with $x = 0.5$; for $x = 0.333$, the CN increases up to 6.5.[117] The diffraction data[193] reveal a minimum of the CN values at $x = 0.333$; usually, the CN values given by the diffraction exceed the simulation data by ~ 1.5. This difference is due to different schemes used for calculation of the CN.

The distributions of CN for the O–O pairs have specific features. For pure P_2O_5, the distribution has a usual form, *i.e.* a curve with a broad maximum at CN $z = 7$. The same shape is maintained at $x = 0.333$, but an additional maximum appears at the CN of 4. In the range $0.500 < x < 0.800$, the distributions of z(O–O) exhibit two maxima: z(O–O) = 3 and 6–7. A similar effect was observed earlier for the computer models of complex oxides, such as $2MO \cdot SiO_2$ and $M_2O \cdot 2SiO_2$ (see above). This is due to the formation of rather rigid coordination spheres composed of O^{2-} ions surrounding the central metal ions (like SiO_4^{4-}) and fusion of these groups through a shared vertex. If z(P–O) = 4, then in such a distorted tetrahedron each O^{2-} ion has three O^{2-} neighbours, *i.e.* z(O–O) = 3. In the case of z(P–O) = 5, the coordination sphere of the P^{5+} ion is a trigonal bipyramid and two out of five O^{2-} ions have z(O–O) = 3 and three O^{2-} ions have z(O–O) = 4. In the fusion of two groups with z(P–O) = 4, the common O^{2-} ion has z(O–O) = 6. For the fusion of two groups with z(P–O) = 4 and 5 or 5 and 5, the common O^{2-} ion may have z(O–O) from 6 to 8.

At $x = 0$, the model almost does not contain O^{2-} ions with z(O–O) = 3. Hence, each O^{2-} ion has two P^{5+} neighbours and is shared between two PO_5 groups. It is clearly seen from the distributions of CN for the P–O pairs. For $x = 0.333$, *ca.* 20% of O^{2-} ions have z(O–P) = 1 and for these ions z(O–O) = 3–4. However, O^{2-} ions with z(O–P) = 2 should have z(O–O) = 6–7. Therefore, the distribution of z(O–O) exhibits two maxima, *viz.*, a small peak at CN $z = 4$ and a high one at CN $z = 7$. When $x \geqslant 0.500$, the two maxima are maintained in the z(O–O) distribution but the height of the peak at z(O–O) = 6 decreases with growth of x due to decrease in the number of O^{2-} ions which have two P^{5+} neighbours.

The distributions of the O–P–O azimuthal angles are very broad for all compositions and do not indicate the presence of any specific configurations of ions. This is caused by the rather broad distributions of z(P–O). With a decrease in x, the proportion of large bound groups increases, and at $x \leqslant 0.500$ the complete polymerisation of the structure occurs.

A probable contribution of a ring component to the structure was also analysed. Rings with a minimum size more than eight members were totally absent. A decrease in x results in an increase in the number of rings, and the six- and eight-membered rings predominate in the structure. The four-membered rings are almost absent due to the high energy of the corresponding spatial figure.

For all values of $x < 0.8$, the structure of oxides appeared loose. According to the ρ_1 values (from 0.96 for $x = 0.8$ to 0.93 for $x = 0$), the $CaO-P_2O_5$ oxides should readily form glasses when $x < 0.8$. But in practice for the $CaO-P_2O_5$ system it is possible to obtain glass by rapid cooling only at $x < 0.57$.[118] The difference between these limits is noticeable; it indicates that several additional effects leading to the crystallisation of real calcium phosphates with high CaO content, exist.

A model of $AlPO_4$ glass (192 particles in the basic cube) was built by MD method with the Born–Meyer potentials.[194] A total time for one run was 24 ps (2 ps at 20 000 K, 2 ps at 10 000 K, and 20 ps at 1500 K). It was established that the structure is a network of AlO_4 and PO_4 tetrahedra fused to each other through vertices like in silica. However, a proportion of oxygen ions are terminal. The calculated TPCF are in reasonable agreement with the experimental data:[195]

Pair	P–O	Al–O	O–O	P–P	Al–P	Al–Al
$r_1(ij)$ /pm						
calculation	150	180	245	320	325	330
experiment[195]	160	160	260	310	310	310

The distributions of CN are as follows: $z(P-O) = 4$ (96.7%) and 5 (3.3%), $z(Al-O) = 3$ (10%) and 4 (90%). The mean P–O–P angle is 164°. The network of bonds in the model is not perfect, but it is generally more ordered than in silica. It is possible that the structure of aluminium phosphate contains clusters linked by bridging oxygen ions.

Models of $2ZnO \cdot P_2O_5$ and $2Na_2O \cdot P_2O_5$ glasses containing 407 and 481 ions in the basic cube were constructed.[196] The Born–Meyer potentials were used. The PO_4 tetrahedra were the main structural elements of the models obtained, they can aggregate to form larger polymeric groups. The degree of polymerisation and the portion of long chains are less in sodium phosphate. Fragments with branching points are totally absent. The sodium and zinc ions occupy randomly the cavities of the tetrahedral network. The coordination numbers for the Na–O pairs lie in the range from 3 to 6 and from 4 to 6 for Zn–O.

A model of $Pb(PO_3)_2$ was also constructed[197] using the MD method. The force functions (6) were applied (the functions were assumed to be zero for distances $r > 0.55$ nm). The interaction parameters were adjusted so as to achieve agreement between peak positions for the calculated and experimental TPCF.

Ion	O	P	Pb
r_i /pm	120	15	99
Z_i	−1.136	2.840	1.136

The Coulomb interactions were taken into account approximately. The model contained 630 ions in the basic cube. Cooling of the system from 15000 K to 300 K was performed at an average rate of 1.23×10^{13} K s^{-1}. The final density of the glass was taken equal to the actual value (4.74 g cm^{-3}).

It was shown that the models of crystalline metaphosphate contain chains of the PO_4 tetrahedra linked through their vertices. The chains are linked to each other via Pb^{2+} ions, which are attracted to non-bridging oxygen ions. The following distances were found in the crystal: 156 and 146 pm (P–O), 235 and 261 pm (O–O), 289 and 301 pm (P–P), and 382 pm (Pb–Pb). For models of the glass, the first PPCF peak for the P–O pairs was isolated with positions of 145 pm and CN equal to 4.0. This distance is shorter than the value found in amorphous iron-lead metaphosphate (155–158 pm, see Ref. 198) and in nickel-copper pyrophosphate (154.3–154.5 pm, see Ref. 192) using the X-ray diffraction methods, but it is close to the value (150 pm) obtained in Ref. 199. The distributions of the O–P–O and P–O–P azimuthal angles (from 95 to 125° and from 130 to 180°, respectively) demonstrate that the orientation of the neighbouring PO_4 tetrahedra is random. No fusion of the tetrahedra via their edges or faces was found. The following values were obtained for the interatomic distances and the coordination numbers:

Pair	O–O	O–Pb	P–Pb	O–P	P–P	Pb–Pb
$r_1(ij)$ /pm	245	243	371	151	304	390
CN	5.82	6.94	5.50	4.00	2.00	5.00

Therefore, only distances for the P–P and Pb–Pb pairs change noticeably upon amorphisation.

An analysis of the bound groups distribution in the model revealed linear chains comprising from one to eleven PO_4 tetrahedra, rings of 5–10 tetrahedra, and larger associates.[197] A secondary network, which is formed by the lead ions bound to non-bridging oxygen ions, was also found.

A structural model for a $Ba(PO_3)_2$ glass with the phosphate network composed of the PO_4 tetrahedra was constructed by the MC method based on the neutron scattering and NMR data.[200]

One of the possible reasons for the non-coincidence of the results of different simulations of non-crystalline phosphates is the use of different density values. If the density is chosen to be equal to that of the real glass, the calculated pressure may appear strongly negative or positive. Since it is for the phosphate systems that the most substantial differences were observed, this indicates again the insufficient accuracy of the Born–Meyer potentials due to the neglecting of the covalent contribution.

Models of the $(CaO)_x(V_2O_5)_{1-x}$ oxides were constructed using the MD method.[201] The Born–Meyer potentials (1) were applied. The value of B_{ij} for the V–O pairs was selected to be 2970 eV. The charges were +2, +5, and −2 for calcium, vanadium, and oxygen ions, respectively. Changes in the energy in the formation of a complex oxide from the simple ones was negative in all cases reaching the value −43 kJ mol^{-1} for $x = 0.5$. The V–V and V–O distances were virtually the same (350 and 180 pm) for all the compositions. It was demonstrated that the increase in the CaO content leads to a gradual transition from a loose network structure to a dense one. At $x = 0.333$ and 0.5, the network is built up of oxygen polyhedra arranged around the vanadium ions and linked through their vertices. The coordination numbers of the vanadium ions for such compositions are close to 5.

4. Simulation of tungstate glasses

Models of Na_2O-WO_3 (see Ref. 127) and $CaO-WO_3$ (see Ref. 128) systems were studied by the MD and CSR methods. The Born–Meyer potentials (1) were used; the value for the $B(W-O)$ parameter was chosen to be 3400 eV. The models with 100 mol.%, 80 mol.%, 60 mol.%, 40 mol.%, 20 mol.%, and 0 mol.% of WO_3 were considered. An increase in the molar volume (by 10%) was found for the Na_2O-WO_3 in the formation of a complex oxide from the simple ones. The value of ΔE_{form} for 60% of Na_2O at 2000 K was −102 kJ mol^{-1}. It was shown that the distributions of $z(W-O)$ are rather narrow and have the centres near 6. The mean CN values depend insignificantly on the composition (varying from 5.7 to 6). However, the distribution of the O–W–O azimuthal angles is rather broad (90±10°). Hence, for the preferred octahedral coordination of the W^{6+} ions the arrangement of oxygen ions around the W^{6+} may differ substantially for different ions. In general, W^{6+} ions form their closest coordination sphere not so rigidly as Si^{4+} ions in silicates.

In pure WO_3 and in oxides with the WO_3 content more than 50%, almost all the oxygen ions have CN equal to 2, *i.e.* they are bridging particles (in terms of the PTS). The addition of Na_2O results in a decrease in the number of such ions, *i.e.* the depolymerisation of the network of the W–O bonds occurs. The distribution of the W–O–W azimuthal angles is very broad, and the mean values decrease from 150 to 135° with an increase in Na_2O concentration. The distributions of CN for the Na–O pairs are broad, this is due to the fact that relatively large sodium ions cannot form a stable coordination sphere. In the topological sense, all the models containing WO_3 were loose with values of ρ_1 in the range from 0.98 to 0.96; the *s* factor varied in the range from 1.06 to 1.55.

For the molar volume of the $(CaO)_x(WO_3)_{1-x}$ system positive deviations from the additivity (up to 2.35 $cm^3\ mol^{-1}$ for $x = 0.8$) were observed; for the energy, negative deviations were observed (up to -101 kJ mol^{-1} for $x = 0.6$) similar to the Na_2O-WO_3 system. Presumably, this type of deviation is typical of systems including cations with strongly different charges. The negative deviations for the energy could be anticipated, since stable compounds are formed in the $CaO-WO_3$ system.

Positions of the first TPCF peaks for the Ca–W, W–W, Ca–O, and W–O pairs depend insignificantly on the concentration. For pairs of oppositely charged ions (Ca–O, W–O) it is not surprising, but for the Ca–W and W–W pairs such behaviour is anomalous. This may be due to strong indirect interactions of these ions via intermediate O^{2-} ions. The value of $r_1(W-O) = 177-179$ pm is close to the corresponding value for real Na_2O-WO_3 glasses (~ 180 pm) and for models of these oxides (172–180 pm). In the $CaO-WO_3$ models, the $r_1(W-O)$ distances depend on the WO_3 concentration weaker than in the sodium tungstenate models.

The mean CN for the Ca–O pairs decrease noticeably with a decrease in x. To the contrary, for ions with a high charge, such as W^{6+}, the mean $z(W-O)$ is virtually constant over the whole range of the concentrations and very close to 6. The tungsten particles form rather stable octahedral WO_6 groups with the neighbouring oxygen atoms. For the Na_2O-WO_3 system at 2000 K, the mean $z(W-O) = 5.52-5.93$, *i.e.* the addition of Na_2O distorts the octahedral structure more than that of CaO. In the ideal octahedron, the $r_1(O-O)$ distance should be equal to $\sqrt{2}r_1(W-O)$. This expression holds with good accuracy. The distribution of the O–W–O azimuthal angles for the complex oxide has two maxima with the most probable values of ~ 90 and 173°. These angles are typical of a distorted octahedron with the tungsten ion in its centre and oxygen ions in the vertices.

The distributions of CN for different pairs of ions have specific features. For the W–O pairs, these distributions are very narrow, especially when $x \geqslant 0.4$. For $x = 0.8$, only 2.5% of the W ions have five oxygen neighbours. When $x \leqslant 0.2$, the distribution becomes slightly broader and the percentage of the 'oddly' coordinated tungsten ions reaches $\sim 14\%$. The distributions of $z(O-O)$ for $x \leqslant 0.4$ have two maxima, *viz.*, at CN equal to 4 and 8. The value of 4 corresponds to the oxygen ions in one of the vertices of an isolated WO_6 octahedron. The value $z = 8$ corresponds to the oxygen ions that are common for two fused octahedra. The decrease in x from 0.8 to 0 is accompanied by a gradual decrease in the portion of oxygen ions with $z(W-O) = 4$; and these ions are totally absent in pure WO_3 oxide. This is caused by the aggregation of the WO_6 octahedra into the united polymer network.

In the case of models of the $3CaO \cdot 2WO_3$ oxide at 2000 K, the first TPCF peaks for the Ca–Ca, Ca–W, Ca–O, and O–O pairs are relatively small, while peaks for the W–W and W–O pairs are much higher. For the W–O pairs, this behaviour is not surprising, since it is a result of strong attraction of oppositely charged tungsten and oxygen ions. However, for the W–W pairs this effect had not been observed earlier. The first PPCF peak for the W–W pairs is almost completely isolated, which indicates the highly ordered mutual arrangement of the tungsten ions. Since these ions repel, the reason for the ordering should be their indirect interactions via intermediate oxygen ions. If W–O distance is strictly fixed and the angle formed by vectors from an oxygen atom to two closest W neighbours is close to 180°, then the W–W distance should be close to $2r_1(W-O)$, *i.e.* 354 pm. The actual value of $r_1(W-W)$ is 358 pm. The data show that the octahedral WO_6 groups linked via a shared vertex are ordered in such a way that their spatial diagonals passing through this vertex have a tendency to be arranged along certain direction. The W–O–W azimuthal angles in the models vary from 135 to 178°, and their mean value is 151.8 ± 15.9°.

The analysis of the Voronoi polyhedra[43, 44] constructed for the central tungsten ions demonstrates that the dominant polyhedra (from 92.5% for $x = 0.8$ to 63% for $x = 0.2$) have the form 0–6–0–0, which corresponds to the cube, that is the Voronoi polyhedron for an ideal octahedron (the notation 0–6–0–0 means the numbers of triangular, rectangular, *etc.* faces of the polyhedron). There are 59 polyhedra of the 0–6–0–0 type and 29 polyhedra of the 1–3–3–0 type (the cube with truncated vertex) in pure WO_3. Overall, they constitute 70% of all polyhedra for the model considered. The volume of the polyhedron with a tungsten atom increases with a decrease in x, and the distribution of the volumes broadens. For instance, at $x = 0.8$ the volumes of the polyhedra are equal to 5928 ± 231 pm^3, and at $x = 0$ they are 6506 ± 458 pm^3. The degree of sphericity also decreases from 0.511 to 0.488. The mean face areas depend only slightly on the concentration x but the width of their distribution increases as x decreases. Therefore, the increase in the WO_3 content results in disordering of the Voronoi polyhedra constructed around the tungsten atoms.

A study of the 'polymerisation' in the $CaO-WO_3$ oxides was performed by analysis of the W_mO_n bound groups. The tungsten atoms with a common oxygen neighbour at a distance shorter than 200 pm were considered as a group. For this distance, $z(W-O) \simeq 6.0$, and in addition no O–O pairs were found, *i.e.* all the oxygen atoms have only W neighbours. The following bound groups were found in the models:

x	0.8	0.6	0.4	0.2	0.0
Group	$1^5 2^3 5^5 18^1$	$17^1 21^1 51^1$	93^1	108^1	125^1

The notation $1^5 2^3$... means that five WO_6^{6-} monomers, three $W_2O_{11}^{10-}$ dimers, and so on were found in the model. When $x \leqslant 0.4$, the system is completely polymerised, for $x = 0.6$ and 0.8 there exist isolated monomers surrounded only by CaO matrix. The models of Na_2O-WO_3 oxides behave similarly.

For $x = 0.8$, only one eight-membered ring was found in the model. The distribution of the bound groups demonstrates that this ring is a part of a bound group of 18 tungsten ions. For $x = 0.6$, 21 rings were found that included about 60 tungsten ions. Since the model contained only 70 ions altogether, the most of them were included into the ring. A comparison with the bound group distribution showed that these rings are not isolated but they are incorporated into two 12^1 and 51^1 groups. Attempts to account all these sophisticated 'polyanions' would result in a substantial complication of the polymer theory.

Finally, all rings found in the models with $x \leqslant 0.4$ belong to one bound group containing all tungsten ions of the models, since the oxides are completely polymerised for such concentration.

5. Simulation of other binary oxide systems

Models of binary $(CaO)_x(Fe_2O_3)_{1-x}$ systems and oxides of the $CaO \cdot M_2O_3$ series were constructed [202, 203] using the MD and CSR methods. The Born–Meyer potentials (1) were applied. The change in the molar volume in the formation of a complex oxide in the $CaO-Fe_2O_3$ system at 2000 K was small, this parameter is positive for $x = 0.5$-0.7 and negative for $x = 0.333$. The value of ΔE_{form} does not exceed 45 kJ mol^{-1}. According to the values of the heats of formation, the oxides in this system are close to the ideal ones. At 0 K, the values of ΔE_{form} are positive, so the oxides should readily decompose. It was shown that Ca^{2+} and Fe^{3+} ions form their first coordination spheres virtually independent of the value of x. The mean CN for the Ca–O pairs is 5.0–5.2, and $z(Fe-O)$ is 4.7–5.3. The topological characteristics point to the dense structures.

Models of oxides in the $CaO \cdot M_2O_3$ series at 2000 K were constructed using the potentials (1).[203] The B_{23} parameter for the M–O pairs (numbering of atoms as follows: 1 for Ca, 2 for M, and 3 for O) varied in the range of 800–5000 eV. It was demonstrated that the molar volume has a minimum at $B_{23} = 1480$ eV, which corresponds to the $CaO \cdot Al_2O_3$ system. The coordination numbers for the Ca–O pairs were close to 6 in all cases, and $z(M-O)$ increases gradually from 3.3 ($B_{23} = 800$ eV) to 5.9 ($B_{23} = 5000$ eV). For $B_{23} = 1470$ eV, most

M^{3+} ions have four O^{2-} neighbours; a distorted octahedral packing dominates. At higher B_{23} values, the structure is dense. When B_{23} increases from 800 to 2453 eV the configurational entropy of the oxides initially increases slightly and then again decreases slightly. A decrease in the size of M^{3+} can result in an increase in the negative deviations from the ideal state (as regards thermodynamics).

Models of oxides in the $FeO-Fe_2O_3$ system with 0 mol.%, 25 mol.%, 50 mol.%, 75 mol.%, and 100 mol.% of FeO at 0 K and 2000 K were constructed using the MD and CSR methods.[105] Change in the molar volume in the formation of complex oxides from the simple ones was positive (up to 4.3 $cm^3\ mol^{-1}$), the value of ΔE_{form} was also positive and did not exceed 27 $kJ\ mol^{-1}$. It was established that the structure of the coordination spheres of Fe^{2+} and Fe^{3+} in glasses and melts almost was not changed with variation of the FeO content. The topological parameter ρ_1 has a minimum (1.02) at 60% of FeO, which indicates small looseness of these oxides. The results of computer simulation [105] allowed one to estimate the equilibrium oxygen pressure over the $FeO-Fe_2O_3$ oxides. It was possible to predict the decomposition of magnetite Fe_3O_4 on heating, but the accuracy in determination of the decomposition temperature was not very high.

Solutions of oxygen in Fe_2O_3 at 0 K and 2000 K were studied by the MD and CSR methods.[106] In order to determine the preferred form of existence of the oxygen particles, the solutions of the atomic oxygen (O^0), as well as O^- and O^{2-} ions were considered. A possible reaction $2O^- = O^0 + O^{2-}$ was also taken into account, *i.e.* it was assumed that the dissolution of O_2 in the oxide, which dissociates according to the scheme $O^2 \rightarrow 2O^0$, should be accompanied by an increase in O^- concentration and a decrease in O^{2-} concentration. Charges of iron ions were not changed in this case. The heat of dissolution of oxygen as O^0 (ΔH) was estimated as ~ 1000 kJ $(mol\ O_2)^{-1}$ at 0 K and 768 kJ $(mol\ O_2)^{-1}$ at 2000 K. The heat of dissolution of oxygen as O^- was 428 kJ $(mol\ O_2)^{-1}$. Since that the dissolution as O^- is preferable. The solubility of O_2 at 1700 K may be described by the expression $X(O^-) = 1.3 \times 10^{-10} p_{O_2}^{1/4}$, where X is the ionic portion of O^- in the oxide and p_{O_2} is the partial pressure of the oxygen expressed in atm. units. The solubility decreases rapidly as temperature decreases.

VII. Simulation of multi-component systems

It was shown by NMR,[204] that the aluminium ions in multi-component silicate glasses have tetrahedral coordination at any Al_2O_3 content, while silicon ions have one or two terminal oxygen neighbours. The coordination number for the B—O pairs is mainly 4. In lead-fluoride-silicate glasses, the silicon ions always have two terminal O^{2-} neighbours.

Several complex oxides in $K_2O-Na_2O-SiO_2$, $CaO-Na_2O-SiO_2$, and $B_2O_3-Na_2O-SiO_2$ systems were investigated using the MD method.[84, 205, 206] It was shown that the inclusion of Na^+ ions leads to destruction of Si—O—Si bonds; Na^+ ions occupy the cavities between 3–8 non-bridging oxygen ions. Small rings are formed and the number of silicon ions with five oxygen neighbours increases. However, when the volume or temperature are increased, the Si ions with $z(Si-O) = 5$ disappear.

A 'poly-alkali effect' caused by a mutual influence of different ions of alkali metals was studied for silicate glasses using the MD method.[207] The calculated values of electrical conductivity for the glasses indicate the presence of the effect (a minimum on the plot of conductivity *vs.* composition). Heating of the system results in a weakening of the effect due to easier relaxation of anions. Preferable ways of diffusion of alkali metal ions in the glass were determined. The application of NMR to structural studies of the alkali- and alumino-silicates including the analysis of the poly-alkali effect were reviewed.[208] Alkali metal ion transfer was also studied.[209]

Models of aluminosilicates, such as $7CaO \cdot Al_2O_3 \cdot 2SiO_2$, $5CaO \cdot Al_2O_3 \cdot 2SiO_2$, $3CaO \cdot Al_2O_3 \cdot 2SiO_2$, $CaO \cdot Al_2O_3 \cdot 2SiO_2$, were constricted using the MD method at 400 K.[210] Comparison of the CN values calculated from the PPCF and the characteristics of the Voronoi polyhedra showed that for all pairs, except Ca—O, reasonably good agreement was achieved. The deviations for the Ca—O pairs were due to the formation of clusters of admixturing atoms around the oxygen anions.[211] Structures of $CaO \cdot Al_2O_3 \cdot 2SiO_2$ were studied using the X-ray diffraction and the MD method. It was established that the structures include a framework of fused SiO_4 and AlO_4 tetrahedra and Ca^{2+} ions. The framework contains four- and six-membered rings. The main structural defects resulting in disordering are three- and five-membered rings.

A series of models (1300 atoms in the basic cube) for melts with 10 different compositions in the $NaAlSiO_4-SiO_2$ system at 2500–4500 K and 2–5 GPa was constructed using the MD method.[212] The run duration was 0.1 ns. The Coulomb interactions were taken into account according to the Ewald method. It appeared that more than 90% of silicon and aluminium ions have CN = 4, and more than 90% of oxygen ions have two neighbouring cations. These results insignificantly depend on temperature. It was established that the T—T coordination (T = Al or Si) depends more on the composition than the T—O coordination. If a model contains more than 1000 ions, the self-diffusion coefficients and conductivity no longer depend on the size of a model; for $N = 400-600$, these characteristics are overestimated by 10%–100%. A cut-off of the Ewald sums additionally distorts the model. The dependence of structure on the number of particles in the model is not so pronounced. The replacement of silicon ions by Al + Na pairs leads to a decrease in the mean T—O—T angle, which is due to the increase in the number of Al—O—Al bridges and the broadening of the azimuthal angle distributions. The PCF oscillations are virtually absent at distances exceeding 500 pm.

MD-models of sodium aluminosilicates with the ratio $a = Al_2O_3/Na_2O = 0.25-2.0$ were constructed.[213] At $a = 1$, an extremum of the sodium ion self-diffusion coefficient and its activation energy was observed, it was analogous to that for the viscosity and conductivity. When $a < 1$, the size of rings in the structure decreases, and a minimum concentration of terminal oxygen ions was observed for $a = 1$. When $a > 1$, the groups of neighbouring oxygen particles with $z(O-O) = 3$ appear.

Models of glassy pyrope ($Mg_3Al_2Si_3O_{12}$) and grossular ($Ca_3Al_2Si_3O_{12}$) were constructed using the MD method at 300 K.[214] Good agreement with the X-ray data on their structure was achieved. The first PPCF peaks for the Si—O and Al—O pairs in pyrope appeared broader than those in grossular. It was found that Al–O–Al combinations were present in the structure, *i.e.* Al ions do not avoid close proximity to each other. A proportion of Al ions act to modify the network.

Two series of ionic models of MO and MO_2 solutions in non-crystalline $(CaO)_x(SiO_2)_{1-x}$ oxides with $x = 1, 2/3, 1/2, 1/4$, at 0 and 2000 K were constructed using the MD method.[215] The models corresponded to real and hypothetical oxides. The ratios of the activity coefficients γ_{MO}/γ_{CaO} and $\gamma_{MO_2}/\gamma_{SiO_2}$ were calculated for various x. It was demonstrated that for the MO series the γ_{MO}/γ_{CaO} ratio increases with the increase in the size of M ion for $x > 0.8$ and decreases for $x < 0.8$. This means that for $x > 0.8$ the $CaO-SiO_2$ oxides behave as the basic and for $x < 0.8$ as the acidic ones. However, this rule does not hold for admixtures of the MO type; and neither oxide of the $CaO-SiO_2$ system is neutral in respect of these admixtures. Therefore, the thermodynamic scale of basicity for simple oxides, and hence the meaning of the neutral oxide may be established only for admixtures of a certain type (such as MO) in the $CaO-SiO_2$ system. These scales may differ for different types of admixtures.

Models of an amorphous $(AgI)_x(AgPO_3)_{1-x}$ system for $x = 0-0.5$ were constructed using the Reverse MC method and data on neutron and X-ray diffraction together with X-ray absorption fine structure (EXAFS).[216, 217] For the initial configuration, it was assumed that PO_4 tetrahedra are linked in a chain via two bridging oxygen ions of each tetrahedron and the chains

are linked through the silver ion and two terminal oxygen ions. The number of ions in the basic cube was 3840 – 5376. Reasonably good agreement between the experimental and simulated structural factors and EXAFS spectra was achieved. No AgI microcrystals were found in the models. It was established that the iodide admixtures are situated in the pores of the phosphate network. The size of pores decreases with a decrease in the AgI concentration. It was shown that the first distinct peak in the total structural factor is due to density correlations of the phosphate network, which increase with the addition of iodide, rather than due to the distribution of the AgI admixtures. The concentration of the tunnel-shaped pores passes the percolation threshold in the range $0.2 < x < 0.3$, that provides rapid diffusion of Ag^+ ions, and the structure acquires the superionic conductivity.

A model of $(AgI)_x(Ag_2O \cdot 2B_2O_3)_{1-x}$ glass (960 particles in the basic cube, $x = 0.1$ and 0.6) was constructed using the BMH pair potentials.[218] It was demonstrated that the calculated structural factor of the model has a peak in the small angle region at 9 nm^{-1} (detected earlier by the neutron scattering), which is due to correlations in arrangement of AgI clusters embedded into the boron-oxygen network. Addition of AgI up to $x = 0.6$ does not affect the structure of the boron-oxygen framework.[219] In the case of $(LiCl)_x(Li_2O \cdot 2B_2O_3)_{1-x}$ glass ($x = 0$ and 0.6), the addition of chloride leads to a decrease in $z(B-O)$, which finally results in a more open boron-oxygen framework and lower structural ordering. The boron-oxygen network is composed mainly of statistically linked BO_3 and BO_4 groups. Glasses with overall composition $Na_2O-B_2O_3-NaCl$ were investigated by the MD method.[220] The effects of separation of phases in the glass were successfully reproduced within the atomic model.

VIII. Simulation of ion transfer processes

A parameter such as electrical conductivity, which is sensitive to the bonding type, is a useful tool to examine the adequacy of the ionic model. In the case of covalent bonding, the oxide should be a dielectric. For the cases of mixed ionic/covalent bonding, it is very difficult to use the computational methods to estimate the electrical conductivity while this can be easily estimated within the ionic model. To this end, it is necessary to consider the forces of external field given by the eEZ_i term, where E is the external electric field in the summation of all forces applied to an atom. In MD-simulation, it is necessary to calculate the charge flows for each type of ion in the direction of E and their sum, which is the current. Reliable averaging of the data is needed due to strong fluctuations of the flows. Another point is that the ion transfer cannot be examined in rather weak fields comparable with those normally used in practice. The electric field of the order of $10^8 - 10^9$ V m^{-1} corresponds to the electric force making a noticeable drifting flow. Substantial structural distortions of the melt occur in stronger electric fields. Nevertheless, calculations of the conductivity for models of oxide systems are a good test for the adequacy of the ionic concept.

The study of processes of the ion transfer in electric fields at 2000 K for oxides in the $CaO-SiO_2$ system showed that the mechanism of ion transfer is drifting.[221] The values of the calculated conductivity are in good agreement with the experimental data for melts with conductivity higher than 50 $(Ohm\ m)^{-1}$ (for CaO concentration exceeding 65 mol.%). For systems with the conductivity below 10 – 20 $(Ohm\ m)^{-1}$ the accuracy of the computational methods is not sufficient. The effect of 'removal' of Si^{4+} ions by surrounding O^{2-} ions was found. Therefore, the Si^{4+} ions give a negative contribution to the total conductivity. The reason for this effect is the high stability of the complex SiO_4^{4-} ions.

IX. Conclusion

All data considered above show that for many oxide systems (except for phosphate and several other) the ionic model allows one to obtain results that are in reasonably good agreement with the experimental data on the thermodynamic, structural, diffusion, and electrochemical (mobility in the electric field) properties. Good results were obtained even using such simple interparticle potentials, as the Born – Meyer potential. Complicated modifications of the potential describe certain objects with higher precision, but make the prediction of properties of complex systems based on data for the simpler ones more difficult.

The prediction of the vibrational spectra on the basis of simple ionic model is not so confident. The agreement with the experimental IR and Raman spectra is more difficult to achieve. Therefore, these properties were not considered here. Further investigations are needed in this field. Nevertheless, the results discussed show that clear understanding of the structural features and properties of non-crystalline oxide systems may be achieved by a combination of experimental and computer simulation methods.[222]

References

1. L V Woodcock, in *Advances in Molten Salt Chemistry* Vol. 1 (New York: Plenum Press, 1971) p. 1
2. V A Polukhin, V F Ukhov, M M Dzugutov *Komp'yuternoe Modelirovanie Dinamiki i Struktury Zhidkikh Metallov* (Computer Modelling of the Dynamics and Structure of Liquid Metals) (Moscow: Nauka, 1981)
3. C A Angell, J H R Clarke, L V Woodcock *Adv. Chem. Phys.* **48** 397 (1981)
4. D K Belashchenko *Struktura Zhidkikh i Amorfnykh Metallov* (the Structure of Liquid and Amorphous Metals) (Moscow: Metallurgiya, 1985)
5. M Rovere, M P Tosi *Rep. Progr. Phys.* **49** 1001 (1986)
6. M J L Sangster, M Dixon *Adv. Phys.* **25** 247 (1976)
7. D W Heerman *Computer Simulation Methods in Theoretical Physics* (Berlin: Springer, 1986)
8. H J C Berendsen, W F van Gunsteren, in *Molecular Liquids — Dynamics and Interactions* (Derdrecht: D. Reidel Publ., 1984) p. 475
9. L V Woodcock, C A Angell, P Cheeseman *J. Chem. Phys.* **65** 1565 (1976)
10. F G Fumi, M P Tosi *J. Phys. Chem. Solids* **25** 31 (1964)
11. D K Belashchenko *Zh. Fiz. Khim.* **67** 5 (1993) [a]
12. M P Tosi, F G Fumi *J. Phys. Chem. Solids* **25** 45 (1964)
13. L V Woodcock, K Singer *Trans. Faraday Soc.* **67** 12 (1971)
14. M J L Sangster, A M Stoneham *Philos. Mag. B* **43** 597 (1981)
15. C R A Catlow, C M Freeman, M S Islam, R A Jackson , M Leslie, S M Tomlinson *Philos. Mag. A* **58** 123 (1988)
16. A M Stoneham, M J L Sangster *Philos. Mag. B* **43** 609 (1981)
17. K Kawamura, in *Molecular Dynamics Simulations. Springer Series in Solid-State Sciences* Vol. 103 (Ed. F Yonezawa) (Berlin: Springer, 1990) p. 88
18. M Amini, S K Mitra, R W Hockney *J. Phys. C, Solid State Phys.* **14** 3689 (1981)
19. S Tsueyuki, M Tsukada, H Aoki *Phys. Rev. Lett.* **61** 869 (1988)
20. L I Voronova, B M Lepinskikh, O I Bukhtoyarov, S P Kurlov *Fiz. Khim. Stekla* **13** 112 (1987) [b]
21. R S Mulliken *J. Phys. Chem.* **56** 295 (1952)
22. L I Voronova, O I Bukhtoyarov, G P Vyatkin *Rasplavy* (6) 50 (1994)
23. L I Voronova, O I Bukhtoyarov, G P Vyatkin *Rasplavy* (6) 58 (1994)
24. L I Voronova, O I Bukhtoyarov, G P Vyatkin *Rasplavy* (1) 65 (1995)
25. L I Voronova, O I Bukhtoyarov, G P Vyatkin *Rasplavy* (4) 65 (1995)
26. B S Vorontsov *Fiz. Khim. Stekla* **19** 403 (1993) [b]
27. S L Chaplot, K R Rao *J. Phys. C, Solid State Phys.* **13** 747 (1980)
28. W Soppe, C van der Marel, H W den Hartog *J. Non-Cryst. Solids* **101** 101 (1988)
29. P N Keating *Phys. Rev.* **145** 637 (1966)
30. F Wooten, D Weaire *Solid State Phys.* **40** 1 (1987)
31. Lee Chongmu *J. Phys. C, Solid State Phys.* **19** 5555 (1986)
32. E A Moelwyn-Hughes *Physical Chemistry* (London: Pergamon Press, 1961)
33. B M Axilrod, E Teller *J. Chem. Phys.* **11** 299 (1943)
34. J D Kubicki, A C Lasaga *Am. J. Sci.* **292** 159 (1992)
35. R A Murray, L W Song, W Y Ching *J. Non-Cryst. Solids* **94** 133 (1987)
36. H Inoue, N Aoki, I Yasui *J. Am. Ceram. Soc.* **70** 622 (1987)

37. D J Adams, I R McDonald *J. Phys. C, Solid State Phys.* **7** 2761 (1974)
38. F Lantelme, P Turq, B Quentrec, J W E Lewis *Mol. Phys.* **28** 1537 (1974)
39. J P Hansen *Phys. Rev. A, Gen. Phys., Ser. 3* **8** 3096 (1973)
40. J H R Clarke, W Smith, L V Woodcock *J. Chem. Phys.* **84** 2290 (1986)
41. P Linse, H C Andersen *J. Chem. Phys.* **85** 3027 (1986)
42. D K Belashchenko *Fiz. Met. Metalloved.* **60** 1076 (1985) [c]
43. C A Rogers *Packing and Coverings* (Cambridge: University Press, 1964)
44. G F Voronoi *Z. Reine Angew. Math.* **133** 97 (1908); **134** 198 (1908)
45. D K Belashchenko *Metally* (1) 166 (1990)
46. D Beeman, J Silverman, R Lynds, M R Anderson *Phys. Rev. B, Condens. Matter.* **30** 544 (1984)
47. F Lantelme, P Turq *J. Chem. Phys.* **81** 5046 (1984)
48. D K Belashchenko *Zh. Fiz. Khim.* **67** 2359 (1993) [a]
49. L I Tatarinova *Struktura Tverdykh Amorfnykh i Zhidkikh Veshchestv* (The Structure of Solid Amorphous and Liquid Substances) (Moscow: Nauka, 1983)
50. R L Mozzi, B E Warren *J. Appl. Cryst.* **2** 164 (1969); **3** 251 (1970)
51. N A Vatolin, E A Pastukhov *Difraktsionnye Issledovaniya Stroeniya Vysokotemperaturnykh Rasplavov* (Diffraction Studies on the Structure of High-Temperature Melts) (Moscow: Nauka, 1980)
52. W L Warren, E H Poindexter, M Offenberg, W Müller-Warmuth *J. Electrochem. Soc.* **139** 872 (1992)
53. D K Belashchenko *Zh. Fiz. Khim.* **67** 1330 (1993) [a]
54. S K Mitra, M Amini, D Fincham, R W Hockney *Philos. Mag. B* **43** 365 (1981)
55. S K Mitra *Philos. Mag. B* **45** 529 (1982)
56. L Guttman, S Rahman *J. Non-Cryst. Solids* **75** 419 (1985)
57. R G Della Valle, E Venuti *Chem. Phys.* **179** 411 (1994)
58. Y Benino, N Soga, K Hirao, in *Proceedings of the 16th International Congress on Glass, Madrid, 1992* Vol. 3
59. S L Chan, S R Elliott *Phys. Rev. B, Condens. Matter* **43** 4423 (1991)
60. S N Taraskin, S R Elliott, M I Klinger *J. Non-Cryst. Solids* **192 – 193** 263 (1995)
61. S R Elliott *J. Phys., Condens. Matter* **4** 7661 (1992)
62. J H Lee, S R Elliott *J. Non-Cryst. Solids* **192 – 193** 133 (1995)
63. D K Belashchenko *Neorg. Mater.* **26** 172 (1990) [d]
64. D K Belashchenko, A D Fed'ko *Neorg. Mater.* **28** 1682 (1992) [d]
65. D K Belashchenko, A B Gritsenko, O I Ostrovskii *Metally* (3) 47 (1991)
66. D K Belashchenko, A D Fed'ko *Neorg. Mater.* **28** 108 (1992) [d]
67. R G Della Valle, H C Andersen *J. Chem. Phys.* **97** 2682 (1992)
68. M Ya Frenkel', E A Vasserman *Rasplavy* (1) 52 (1993)
69. B Vessal, M Amini, H Akbarzadeh *J. Chem. Phys.* **101** 7823 (1994)
70. L Stixrude, M S T Bukowinski *Phys. Rev. B, Condens. Matter* **44** 2523 (1991)
71. A Nakano, R K Kalia, P Vashishta *J. Non-Cryst. Solids* **171** 157 (1994)
72. F H Stillinger, T A Weber *Phys. Rev. B, Condens. Matter* **31** 5262 (1985).
73. P Vashishta, R K Kalia, G A Antonio, J P Rino, H Iyetomi, I Ebbsio *Solid State Ion. Pt. 1* **40 – 41** 175 (1990)
74. J H Simmons, Tsaj Yueh-Long, J J Mecholsky, T P Swiler, in *Proceedings of the 17th International Congress on Glass, Beijing, 1995* Vol. 2, p. 93
75. A Monteil, A Bouajaj, G Cormier, J A Copabianco *J. Phys., Condens. Matter* **6** 9881 (1994)
76. F Herre, H Richter *Z. Naturforsch. A, Phys. Sci.* **12** 545 (1957)
77. K V Tkachev, Yu S Plyshevskii *Tekhnologiya Neorganicheskikh Soedinenii Bora* (Technology of Inorganic Compounds of Boron) (Leningrad: Khimiya, 1983)
78. R E Youngman, J W Zwanziger *J. Non-Cryst. Solids* **168** 293 (1994)
79. A C Wright, N M Vedishcheva, B A Shakhmatkin *J. Non-Cryst. Solids* **192 – 193** 92 (1995)
80. P J Bray *J. Non-Cryst. Solids* **75** 29 (1985)
81. V V Golubkov *J. Non-Cryst. Solids* **192 – 193** 463 (1995)
82. V V Golubkov *Fiz. Khim. Stekla* **18** 14 (1992) [b]
83. T Soules *J. Chem. Phys.* **73** 4032 (1980)
84. T Soules *J. Non-Cryst. Solids.* **49** 29 (1982)
85. W Soppe, C van der Marel, W F van Gunsteren, H W den Hartog *J. Non-Cryst. Solids.* **103** 201 (1988)
86. L I Voronova, O I Bukhtoyarov *Fiz. Khim. Stekla* **13** 818 (1987) [b]
87. W Soppe, H W den Hartog *J. Phys. C, Solid State Phys.* **21** L689 (1988)
88. D K Belashchenko *Neorg. Mater.* **27** 2127 (1991) [d]
89. U D Veryatin, V P Mashirev, N G Ryabtsev, V I Tarasov, B D Rogozkin, I V Korobov *Termodinamicheskie Svoistva Neorganicheskikh Veshchestv. Spravochnik* (Thermodynamic Properties of Inorganic Substances. Handbook) (Ed. A P Zefirov) (Moscow: Atomizdat, 1965)
90. A Takada, C R A Catlow, G D Price *J. Phys., Condens. Matter* **7** 8659 (1995)
91. A Takada, C R A Catlow, G D Price *J. Phys., Condens. Matter* **7** 8693 (1995)
92. A H Verhoef, H W den Hartog *J. Non-Cryst. Solids.* **146** 267 (1992)
93. M S Meikhail *J. Phys., Condens. Matter* **5** 2679 (1993)
94. I Prigogine, R Defay *Chemical Thermodynamics* (London: Longman, 1966)
95. A M Jones *Phys. Chem. Glasses* **16** 992 (1975)
96. I A Popova *Neorg. Mater.* **14** 1934 (1978) [d]
97. N M Yakovleva, A D Fofanov *Neorg. Mater.* **21** 48 (1985) [d]
98. P Brand, W Gβener, D Müller *Wiss. Z. Tech. Univ. Karl-Marx-Stadt* (7) 185 (1990)
99. V M Kozlov, I A Popova, T A Shabalina *Izv. Akad. Nauk Latv. SSR, Ser. Fiz. Tekhn. Nauk* (3) 73 (1982)
100. I A Popova, Ya A Ugai, Yu K Timoshenko, in *Tez. Dokl. 15-go Mezhdunarodnogo Kongressa "Steklo-89", Leningrad, 1989* (Abstracts of Reports of the 15th International Congress 'Glass-89', Leningrad, 1989) Vol. 1b, p. 114
101. O I Bukhtoyarov, L I Voronova *Rasplavy* (4) 60 (1989)
102. J F Elliott, M Gleiser, V Ramakrishna *Thermochemistry for Steelmaking* (London, 1969)
103. D K Belashchenko *Neorg. Mater.* **28** 1672 (1992) [d]
104. D K Belashchenko *Neorg. Mater.* **28** 2156 (1992) [d]
105. D K Belashchenko *Metally* (3) 46 (1993)
106. D K Belashchenko *Neorg. Mater.* **29** 70 (1993) [d]
107. N Iwamoto, N Umesaki, T Atsumi *J. Mater. Sci. Lett.* **6** 271 (1987)
108. I-K Suh, K Sugiyama, Y Waseda, J M Toguri *Z. Naturforsch., B Chem. Sci.* **44** 580 (1989)
109. P Sindzingre, M J Gillan *J. Phys. C, Solid State Phys.* **21** 4017 (1988)
110. A Feltz *Amorphe und Glasartige Anorganische Festkörper* (Berlin: Academie Verlag, 1983)
111. J R Van Wazer *Phosphorus and Its Compounds* Vols 1, 2 (New York: Interscience, 1958, 1961)
112. A E R Westman, in *Modern Aspects of the Vitreous State* (Ed. J D Mackenzie) (London: Butterworths, 1960) p. 63
113. P K Shufflebotham *J. Non-Cryst. Solids* **92** 183 (1987)
114. G W Brady *J. Chem. Phys.* **28** 48 (1958)
115. L Cervinka, J Bergerova, M Trojan *J. Non-Cryst. Solids* **192 – 193** 121 (1995)
116. W Matz, D Stachel, E A Goremychkin *J. Non-Cryst. Solids* **101** 80 (1988)
117. D K Belashchenko *Neorg. Mater.* **33** 565 (1997) [á]
118. O V Mazurin, M V Strel'tsina, T P Shvaiko-Shvaikovskaya *Svoistva Stekol i Stekloobrazuyushchikh Rasplavov. Spravochnik* (Properties of Glasses and Glass-Forming Melts. Handbook) (Leningrad: Nauka, 1980, 1981, 1987)
119. S Takeda, M Inui, Y Kawakita, K Maruyama, Sh Tamaki, K Sugiyama *Physica B* **213 – 214** 499 (1995)
120. P A V Johnson, A C Wright, C A Yarker *J. Non-Cryst. Solids* **81** 163 (1986)
121. L I Voronova, B M Lepinskikh, O I Bukhtoyarov *Fiz. Khim. Stekla* **13** 287 (1987) [b]
122. V S Perel'muter, A B Gritsenko, D K Belashchenko *Izv. Vyssh. Uchebn. Zaved., Chern.* Metall. (7) 1 (1992)
123. D K Belashchenko *Zh. Fiz. Khim.* **68** 1171 (1994) [b]
124. A M Solodukha, O K Zhukov, M V Lesovoi, N N Makeeva *Neorg. Mater.* **25** 777 (1989) [d]
125. S Laruelle, M Figlarz, B Bouchet-Fabre *J. Non-Cryst. Solids* **192 – 193** 116 (1995)
126. Sh Kobayashi, M Misawa, K Suzuki *J. Non-Cryst. Solids* **91** 180 (1987)
127. D K Belashchenko *Neorg. Mater.* **30** 948 (1994) [d]
128. D K Belashchenko *Neorg. Mater.* **32** 336 (1996) [d]
129. *Khimicheskaya Entsiklopediya* (Chemical Encyclopedia) (Moscow: Izd. Sovetskaya Entsiklopediya, 1988)
130. D K Belashchenko *Neorg. Mater.* **29** 1263 (1993) [d]
131. P T Sarjeant, Rustum Roy *J. Am. Ceram. Soc.* **50** 500 (1967)
132. D K Belashchenko *Neorg. Mater.* **30** 1046 (1994) [d]

133. J O M Bockris, J W Tomlinson, J L White *Trans. Faraday Soc.* **52** 299 (1956)
134. D K Belashchenko, A D Fed'ko *Rasplavy* (5) 40 (1992)
135. D K Belashchenko *Zh. Fiz. Khim.* **68** 1390 (1994) [a]
136. D K Belashchenko *Metally* (1) 46 (1994)
137. D K Belashchenko, I E Gopengauz, A B Grytsenko, O I Ostrovskij *Iron Steel Inst. Jpn. Int.* **39** 990 (1992)
138. D K Belashchenko, I E Gopengauz, O I Ostrovskii *Zh. Fiz. Khim.* **66** 1753 (1992) [a]
139. D K Belashchenko, I E Gopengauz, A B Gritsenko, O I Ostrovskii *Metally* (6) 29 (1992)
140. R D Shannon, C T Prewitt *Acta Crystallogr., Sect. B* **25** 925 (1969)
141. Y Waseda *The Structure of Non-Crystalline Materials. Liquids and Amorphous Solids* (New York: McGraw-Hill, 1980)
142. D K Belashchenko *Neorg. Mater.* **29** 941 (1993) [d]
143. H Scholze *Glass* (Berlin: Springer, 1977)
144. P Bondot *Acta Crystallogr., Sect. A* **30** 470 (1974)
145. A J Leadbetter, A C Wright *J. Non-Cryst. Solids* **7** 23 (1972)
146. H Morikawa, T Osuka, F Marumo, A Yasumori, M Yamane, M Momura *J. Non-Cryst. Solids* **82** 97 (1986)
147. Wang Zhongcai, Sui Bingkai, Wang Shizhuo, Liu Hanxing *J. Non-Cryst. Solids* **80** 160 (1986)
148. K Matusita, M Tashiro *J. Non-Cryst. Solids* **11** 471 (1973)
149. J Biscoe, M A A Druesne, B E Warren *J. Am. Ceram. Soc.* **24** 100 (1941)
150. B E Warren, J Biscoe *J. Am. Ceram. Soc.* **21** 259 (1938)
151. M Misava, D Price, K Suzuki *J. Non-Cryst. Solids* **37** 85 (1980)
152. N Iwamoto, N Umesaki, M Takahashi, M Tatsumisago, T Minami, Y Matsui *J. Non-Cryst. Solids* **95 – 96** (1) 233 (1987)
153. K Hirao, N Soga *J. Non-Cryst. Solids* **84** 61 (1986)
154. A A Tesar, A K Varshneya *J. Chem. Phys.* **87** 2986 (1987)
155. N Umesaki, N Iwamoto, M Takahashi, M Tatsumisago, T Minami, Y Matsui *Trans. Iron Steel Inst. Jpn.* **28** 852 (1988)
156. S K Mitra, R W Hockney *Philos. Mag. B* **48** 151 (1983)
157. C Huang, A N Cormack *J. Chem. Phys.* **93** 8180 (1990)
158. G Cormier, J A Capobianco, A Monteil *J. Non-Cryst. Solids* **152** 225 (1993)
159. W Smith, G N Greaves, M J Gillan *J. Chem. Phys.* **103** 3091 (1995)
160. H Melman, S H Garofalini *J. Non-Cryst. Solids* **134** 107 (1991)
161. C Huang, A N Cormack *J. Chem. Phys.* **95** 3634 (1991)
162. J Kieffer, C A Angell *J. Chem. Phys.* **90** 4982 (1989)
163. K Hirao, N Soga *J. Non-Cryst. Solids* **95 – 96** 577 (1987)
164. Y Waseda, J M Toguri *Trans. Iron Steel Inst. Jpn.* **17** 82 (1977)
165. V E Sokol'skii, V I Galinich, V P Kazimirov, G I Batalin, V A Shovskii *Rasplavy* (2) 47 (1989)
166. B Vessal, A Amini, D Fincham, C R A Catlow *Philos. Mag. B* **60** 753 (1989)
167. B Vessal, M Leslie, C R A Catlow *Inf. Quart. MD MC Simul.* **28** 39 (1988)
168. A E Kohler, S H Garofalini, in *Extended Abstracts of Reports of Fall Meeting on Glass and Optical Materials Division, Columbus, OH, 1994* p. 51
169. Y Waseda, Y Shiraishi *Trans. Iron Steel Inst. Jpn.* **18** 783 (1978)
170. D K Belashchenko, I E Gopengauz, A B Gritsenko, O I Ostrovskii *Metally* (5) 47 (1991)
171. V E Sokol'skii, N N Potapov, V A Shovskii, N M Koval', in *V Vsesoyuz. Konf. "Stroenie i Svoistva Metallicheskikh i Shlakovykh Rasplavov" (Tez. Dokl.) Sverdlovsk, 1983* [The Fifth All-Union Conference 'The Structure and Properties of Metallic and Slag Melts' (Abstracts of Reports)] Sverdlovsk, 1983, p. 97
172. C D Yin, M Okuno, H Morikawa, F Marumo *J. Non-Cryst. Solids* **55** 131 (1983)
173. C D Yin, M Okuno, H Morikawa, F Marumo, T Yamanaka *J. Non-Cryst. Solids* **80** 167 (1986)
174. *Schlackenatlas* (Slag Atlas) (Düsseldorf: Stahleisen Verlag, 1981)
175. J P Bowker, C H P Lupis, P A Flinn *Can. Metall. Q.* **20** 69 (1981)
176. R L Mozzi, B E Warren *J. Appl. Cryst.* **2** 164 (1969)
177. V K Novikov *Rasplavy* (2) 124 (1989)
178. I B Bobylev, V N Anfilogov *Izv. Akad. Nauk SSSR, Metally* (2) 23 (1986)
179. O A Esin, P V Gel'd *Fizicheskaya Khimiya Pirometallurgicheskikh Protsessov* Ch. 2 (Physical Chemistry of Pyrometallurgical Processes, Part 2) (Moscow: Metallurgiya, 1966)
180. C Borgianni, P Granati *Met. Trans.* **10B** 21 (1979)
181. C R Masson, I B Smith, S G Whiteway *Can. J. Chem.* **48** 201 (1970).
182. V K Novikov, in *VII Vsesoyuz. Konf. "Stroenie i Svoistva Metallicheskikh i Shlakovykh Rasplavov" (Tez. Dokl.)* [The Seventh All-Union Conference 'The Structure and Properties of Metallic and Slag Melts' (Abstracts of Reports)] (Chelyabinsk: Institute of Metallurgy, Ural Division of the Academy of Sciences of the USSR, 1990) p. 4
183. A B Rosenthal, S H Garofalini *J. Non-Cryst. Solids* **87** 254 (1986)
184. H Morikawa, S Miwa, M Miyake, F Marumoto, T Sata *J. Am. Ceram. Soc.* **65** 78 (1982)
185. D K Belashchenko *Metally* (6) 39 (1993)
186. D K Belashchenko *Zh. Fiz. Khim.* **67** 1104 (1993) [a]
187. Y H Yun, P J Bray *J. Non-Cryst. Solids* **27** 363 (1978)
188. W Soppe, C van der Marel, H W den Hartog *J. Non-Cryst. Solids* **101** 101 (1988)
189. H Inoue, N Aoki, I Yasui *J. Am. Ceram. Soc.* **70** 622 (1987)
190. Zhang Peixin, Lin Hong, Guo Zhengzhong, Sui Zhitong *J. Chin. Ceram. Soc.* **23** 555 (1995)
191. U Hoppe, G Walter, D Stachel *Phys. Chem. Glasses* **33** 216 (1992)
192. A Musinu, G Piccaluga *J. Non-Cryst. Solids* **192 – 193** 32 (1995)
193. U Hoppe, W Günter, R Kranold, D Stachel, A Barz *J. Non-Cryst. Solids* **192 – 193** 28 (1995)
194. A K Varshneya, R F Busbey, T F Soules *J. Non-Cryst. Solids* **69** 381 (1985)
195. G D Wignall, R N Rothon, G W Longman, G R Woodard *Mater. Sci.* **12** 1039 (1977)
196. G G Boiko, A V Parkachev, in *"Komp'yuternoe Modelirovanie Fiziko-khimicheskikh Svoistv Stekol i Rasplavov" (Tez. Dokl.) Kurgan, 1994* [Computer Modelling of Physicochemical Properties of Glasses and Melts (Abstracts of Reports) Kurgan, 1994] p. 6
197. G Cormier, J A Capobianco, A Monteil *J. Non-Cryst. Solids* **168** 115 (1994)
198. A Musinu, G Piccaluga, G Pinna *J. Non-Cryst. Solids* **122** 52 (1990)
199. A Musinu, G Piccaluga, G Pinna *J. Chem. Phys.* **89** 1074 (1988)
200. M Dubiel, U Barenwald, in *Proceedings of the 7th International Conference on Physics of Non-Crystalline Solids, Cambridge, 1991* (London 1992) p. 751
201. V S Perel'muter, A B Gritsenko, D K Belashchenko *Izv. Vyssh. Uchebn. Zaved., Chern. Metall.* (6) 84 (1993)
202. D K Belashchenko *Neorg. Mater.* **29** 961 (1993) [d]
203. D K Belashchenko *Neorg. Mater.* **29** 1046 (1993) [d]
204. S Prabakar, K J Rao *Philos. Mag. B* **64** 401 (1991)
205. T Soules *J. Chem. Phys.* **71** 4570 (1979)
206. T Soules *J. Chem. Phys.* **72** 6314 (1980)
207. S Balasubramanian, K J Rao *J. Phys. Chem.* **97** 8835 (1993)
208. J F Stebbins, S Sen, A M George *J. Non-Cryst. Solids* **192 – 193** 298 (1995)
209. C Huang, A N Cormack, in *Proceedings of the 7th International Conference on Physics of Non-Crystalline Solids, Cambridge, 1991* (London 1992) p. 31
210. M Liska, P Perichta, B Hatalova *J. Non-Cryst. Solids* **192 – 193** 249 (1995)
211. B Himmel, J Weigelt, Th Gerber, M Nofz *J. Non-Cryst. Solids* **136** 27 (1991)
212. D J Stein, F J Spera *Am. Mineral.* **80** 417 (1995)
213. D M Zirl, S H Garofalini *J. Am. Ceram. Soc.* **73** 2848 (1990)
214. M Okuno, K Kawamura *J. Non-Cryst. Solids* **191** 249 (1995)
215. D K Belashchenko *Zh. Fiz. Khim.* **70** 1764 (1996) [a]
216. J D Wicks, R L McGreevy *J. Non-Cryst. Solids* **192 – 193** 23 (1995)
217. L Blrjesson, R L McGreevy, W S Howells *Philos. Mag. B* **65** 261 (1992)
218. M C Abramo, C Caccamo, G Pizzimenti *J. Phys., Condens. Matter* **5** 397 (1993)
219. M C Abramo, G Pizzimenti, A Consolo *Philos. Mag. B* **64** 495 (1991)
220. N Savaguti, K Kavamura, T Iokokava *Fiz. Khim. Stekla* **18** 34 (1992) [b]
221. D K Belashchenko *Neorg. Mater.* **32** 160 (1997) [d]
222. A C Wright *J. Non-Cryst. Solids* **123** 129 (1990)

[a] — *Russ. J. Phys. Chem. (Engl. Transl.)*
[b] — *Glass Phys. Chem. (Engl. Transl.)*
[c] — *Phys. Met. Metallogr. (Engl. Transl.)*
[d] — *Inorg. Matter. (Engl. Transl.)*